

High-Precision $^{40}\text{Ar}/^{39}\text{Ar}$ Dating of
Major Ash-Flow Tuff Sheets
Socorro, New Mexico

by

Laura L. Kedzie

Submitted in Partial Fulfillment
of the Requirements for the Degree
of Master of Science in Geology



New Mexico Institute of Mining and Technology
Socorro, New Mexico

December, 1984

ABSTRACT

Five major ash-flow tuff sheets in the area of Socorro, New Mexico were dated by a high-precision variation of the $^{40}\text{Ar}/^{39}\text{Ar}$ method. These ash-flow tuffs are closely spaced temporally and conventional K-Ar dates were not sufficiently precise to differentiate the units or correlate them with their source cauldrons. In addition, the conventional K-Ar ages exhibit a discrepancy between cogenetic biotite and Na-sanidine analyses.

The high-precision $^{40}\text{Ar}/^{39}\text{Ar}$ analyses yielded the following ages for the ash-flow tuffs: Hells Mesa Tuff = 32.18 ± 0.04 Ma; La Jencia Tuff = 28.76 ± 0.06 Ma; Vicks Peak Tuff = 28.76 ± 0.06 Ma; Lemitar Tuff = 28.37 ± 0.06 Ma; South Canyon Tuff = 27.76 ± 0.09 Ma. The $^{40}\text{Ar}/^{39}\text{Ar}$ analyses yielded no discrepancy between cogenetic biotite and Na-sanidine ages, so the conventional K-Ar age discrepancy was credited to incomplete degassing of the Na-sanidine samples which lead to anomalously young K-Ar ages.

The $^{40}\text{Ar}/^{39}\text{Ar}$ ages showed a 3.4 Ma hiatus between the eruptions of the Hells Mesa Tuff and the La Jencia Tuff. This hiatus has important implications for the petrogenesis of the volcanic rock suites and to initiation of the Rio Grande rift.

ACKNOWLEDGMENTS

Many people contributed to the success of this thesis study and I would like to thank everyone who offered me their advice and insight. I especially wish to thank my thesis committee, Charles Chapin, Philip Kyle, and John Sutter, for making this project a reality. Their advice, support, and encouragement were essential to the completion of this study. I thank the New Mexico Bureau of Mines and Mineral Resources for their generous funding, the United States Geological Survey for the cooperative use of their laboratory facilities, and the United States Fish and Wildlife Service for providing access to the Sevilleta National Wildlife Refuge. I also wish to acknowledge the contributions of the following individuals: Mick Kunk, Jim Moore, Dr. Jacques Renault, Dr. Allen Gutjahr, and Bob Osburn. Lastly, thank you Eric Haas for all your proof-reading and emotional support.

TABLE OF CONTENTS

	Page
Abstract	i
Acknowledgments	ii
List of Figures	vii
List of Tables	x
Introduction	1
Objectives of Study	2
Geologic Setting	5
Introduction	5
Stratigraphy	7
Hells Mesa Tuff	7
Description	7
Extent	10
Previous Radiometric Dating	11
La Jencia Tuff	11
Description	11
Extent	13
Previous Radiometric Dating	13
Vicks Peak Tuff	15
Description	15
Extent	15

	Page
Previous Radiometric Dating	16
Lemitar Tuff	16
Description	16
Extent	17
Previous Radiometric Dating	17
South Canyon Tuff	18
Description	18
Extent	18
Previous Radiometric Dating	19
Methods and Techniques of Investigation	20
Introduction	20
Sampling	21
Sample Preparation	22
$^{40}\text{Ar}/^{39}\text{Ar}$ Dating Technique	23
Analytical Results	26
Introduction	26
Hells Mesa Tuff	30
Na-sanidine	31
K-JH-26	31
K-D-1	31
K-BM-3	33
K-CM-2	36
SU-4-77	38

	Page
Biotite	39
K-JH-26	39
K-BM-3	39
K-CM-2	42
SU-4-77	44
SU-5-77	44
Hornblende	47
K-JH-26	48
K-D-1	48
La Jencia Tuff	48
K-JH-4	49
K-JH-5	49
Vicks Peak Tuff	52
K-BM-1	52
K-JH-10	55
Lemitar Tuff	55
Na-sanidine	57
K-TS-1	57
Biotite	57
K-JH-24	57
K-TS-1	60
South Canyon Tuff	60
K-JH-22	61

	Page
Interpretation of Data	63
Mineral Reliability	63
Assignment of Ages	67
Hells Mesa Tuff	67
La Jencia Tuff	69
Vicks Peak Tuff	69
Lemitar Tuff	69
South Canyon Tuff	74
Evaluation of Unit Ages	74
Discussion	77
Thesis Problem	77
High-Precision Dating	77
Na-sanidine-Biotite Conventional	77
K-Ar Age Discrepancy	78
Cauldron Correlation	80
Geologic Context	84
Stratigraphic Order	85
Volcanic Field	87
Rio Grande Rift	90
Suitability of Method	91
Conclusions	93
Summary	93
Suggestions for Further Research	94
Appendix I : The Critical Value Test	96

Appendix II : Conventional Potassium-Argon Ages	98
Appendix III : Sample Locations	102
Appendix IV : Measured Sections and Chemical Data	105
Appendix V : Mineral Separation	125
Appendix VI : The $^{40}\text{Ar}/^{39}\text{Ar}$ Dating Method	133
Appendix VII : Tabular $^{40}\text{Ar}/^{39}\text{Ar}$ Data	166
References Cited	185

LIST OF FIGURES

Figure	Page
1. Location of the study area	6
2. Composite stratigraphic column of the northeastern Mogollon-Datil volcanic field	8
3. Conventional potassium-argon dates	14
4. J-value curves	
a.	27
b.	28
5. K-JH-26 Na-sanidine age spectrum	32
6. K-D-1 Na-sanidine age spectrum	34
7. K-BM-3 Na-sanidine age spectrum	35
8. K-CM-2 Na-sanidine age spectrum	37
9. SU-4-77 Na-sanidine age spectrum	38
10. K-JH-26 biotite age spectrum	40
11. K-BM-3 biotite age spectrum	41
12. K-CM-2 biotite age spectrum	43
13. SU-4-77 biotite age spectrum	45
14. SU-5-77 biotite age spectrum	46
15. K-JH-4 Na-sanidine age spectrum	50
16. K-JH-5 Na-sanidine age spectrum	51
17. K-BM-1 Na-sanidine age spectrum	53

Figure	Page
18. K-JH-10 Na-sanidine age spectrum	54
19. K-TS-1 Na-sanidine age spectrum	56
20. K-JH-24 biotite age spectrum	58
21. K-TS-1 biotite age spectrum	59
22. K-JH-22 Na-sanidine age spectrum	62
23. $^{40}\text{Ar}/^{39}\text{Ar}$ dates	86
24. Sturtevant Jaw Crusher	126
25. Denver Crushing Rolls	127
26. Frantz isodynamic magnetic separator	129
27. Heavy liquid mineral separation	131
28. Branching decay of ^{40}K	134
29. Packaging a mineral separate	
a.	139
b.	140
c.	141
30. Closure of an irradiation vial	142
31. Components of an irradiation package	144
32. Argon extraction sample bottle	
a.	147
b.	149
33. Argon gas purification line	150
34. The VG-Micromass 1200B mass spectrometer	152

LIST OF TABLES

Table	Page
1. Description of the ash-flow tuff units	9
2. Conventional potassium-argon ages	12
3. $^{40}\text{Ar}/^{39}\text{Ar}$ constants and correction factors	25
4. Hells Mesa Tuff and Lemitar Tuff mineral data	64
5. Ash-flow tuff $^{40}\text{Ar}/^{39}\text{Ar}$ unit ages	75
6. Joyita Hills geochronologic reference section	88
7. Interfering nuclear reactions	154

INTRODUCTION

The area surrounding Socorro, New Mexico contains a stratigraphic sequence of five major ash-flow tuff sheets. An ash-flow is a " turbulent mixture of gas and pyroclastic materials of high temperature ejected explosively from a crater or fissure. . . " (Ross and Smith, 1961). Ash-flow tuff is an inclusive general term for welded and non-welded, consolidated deposits of an ash flow . The units discussed in this study are welded ash-flow tuffs, also known as welded ignimbrites (Ross and Smith, 1961) and pyroclastic- flow deposits (Fisher and Schmincke, 1984).

Ash-flow tuffs have many characteristics similar to volcanic ash or tephra layers which have been employed successfully around the world as regional time-stratigraphic marker beds. The field of tephrochronology combines precise characterization of the tephra beds with radiometric age determinations to correlate widespread marker horizons. This technique can aid in the resolution of many problems including: 1) timing and rates of fault motions; 2) rates of sedimentation; 3) calibration of paleomagnetic chronologies; 4) identification of tephra provenance; and 5) frequency of ash-producing eruptions (Izett, 1981). Porter (1981) has utilized tephra studies in the estimation of eruption magnitudes and paleo-wind directions for the western United States. Tephra, often preserved in deep-sea sediments, can indicate the volcanic history of surrounding islands and mid-ocean spreading centers (Sigurdsson and Loebner, 1981; Ledbetter, 1981; Kyle and Seward, 1984).

Both tephra beds and ash-flow tuff units are ideally suited to solving stratigraphic problems. Ash-flow eruptions produce widespread horizons of silicic volcanic rock, which cool instantaneously in the context of geologic time. As a result, they provide excellent stratigraphic markers and time planes. Many ash-flow tuffs are erupted at moderately high temperatures, greater than 600°C (Williams and McBirney, 1979), and either partially or totally weld upon emplacement.

The explosive nature of ash-flow eruptions indicates that the source magma chambers are situated at relatively shallow depths. As the chamber empties during the eruption, the overlying strata sag and collapse into the void, forming a caldera or cauldron (Smith and Bailey, 1968). This collapse, which occurs during the eruption, causes ponding of the erupting material in the subsiding depression. The thick accumulation of intracaldera material is used to identify calderas and cauldrons and should correlate with some portion of the outflow material (Fisher and Schmincke, 1984).

Objectives of Study

This study has three objectives: 1) to obtain precise ages for the five ash-flow tuff units; 2) to resolve a sanidine-biotite apparent age discrepancy shown by conventional potassium-argon data; and 3) to correlate outflow sheets with the source cauldrons.

Many of the units have been previously dated by the conventional potassium-argon and fission-track methods, but have yielded imprecise ages. The dates produced by these methods (Table 2, Appendix II) vary significantly within each unit and between laboratories. As a result, the ages of the units can only be approximated.

The dates are limited by the overall precision associated with each method. The precision of the potassium-argon method is controlled by: sample homogeneity, precision of the potassium analyses, calibration of the argon spike, and measurement of the ^{40}Ar released by the sample. The fission-track method is limited by: the irradiation monitor, the uncertainty in the ^{238}U fission half-life, and human judgement in identification and counting of the tracks. Both methods are less precise than the $^{40}\text{Ar}/^{39}\text{Ar}$ dating technique.

Precise ages are needed to differentiate the five ash-flow tuff units and to correlate these units with those in the other areas of the volcanic field. The individual units are so numerous and closely spaced temporally, that high precision is mandatory for success.

Many cogenetic sanidine-biotite pairs, dated by the conventional potassium-argon method, yield discordant ages (Foland, 1974; McDowell, 1983). The following theories may explain the discrepancy between the biotite ages and the consistently younger potassium feldspar ages. The difference in crystal structure between sanidine and biotite may produce variations in argon retention (Foland, 1974). Low-temperature ground water alteration and weathering may have affected only the feldspar

grains (Clauer, 1981). Excess argon trapped in the biotite may cause an anomalously old age (Foland, 1983; Lanphere and Dalrymple, 1976). Impurities in the mineral separates may have lost radiogenic argon or inherited excess argon. Insufficient heating in the laboratory may not extract all of the argon trapped in the feldspar (McDowell, 1983). Feldspars yield a more viscous melt than biotites; consequently, higher temperatures and longer heatings are required for complete argon extraction.

Identification of source cauldrons is currently based mainly upon stratigraphic and structural relationships combined with correlations of cauldron-fill and outflow units by petrographic and whole-rock chemical compositions. However, it is possible for two different units to appear similar in petrographic and chemical characteristics. Precise ages from outflow sheets and intracaldera tuffs may be a valuable tool for testing correlations. If the ages of intracaldera tuffs are reliable, then any disagreement with the ages of outflow sheets may indicate postemplacement alteration, correlation problems, or discrepancies in the current model for ash-flow tuff emplacement and caldera formation.

GEOLOGIC SETTING

Introduction

This study was centered around the city of Socorro in central New Mexico (fig. 1). Socorro is located on the northeastern edge of the Mogollon-Datil volcanic field where the field is transected by the Rio Grande rift. The volcanic field was most active between late Eocene and early Miocene time.

The composite stratigraphy of the northeastern Mogollon-Datil volcanic field is shown in Figure 2. Five ash-flow tuff units, Hells Mesa, La Jencia, Vicks Peak, Lemitar and South Canyon, form an orderly stratigraphic sequence interbedded with basaltic andesite flows. No attempt was made to date the basaltic andesites since they contain very few phenocrysts and would have to be dated as whole-rock samples. Whole-rock $^{40}\text{Ar}/^{39}\text{Ar}$ dating often gives more ambiguous data than single mineral phases (Harrison, 1983).

A recently published compilation of the geologic mapping and stratigraphic data available for the Cenozoic rocks of the northeastern Mogollon-Datil volcanic field (Osburn and Chapin, 1983a) is the source of all nomenclature utilized in this study. The following studies have significance to this investigation. The northern Bear Mountains, the location of the Hells Mesa type section, was mapped by Tonking (1957) and Massingill (1979). The southern Bear Mountains area was mapped by

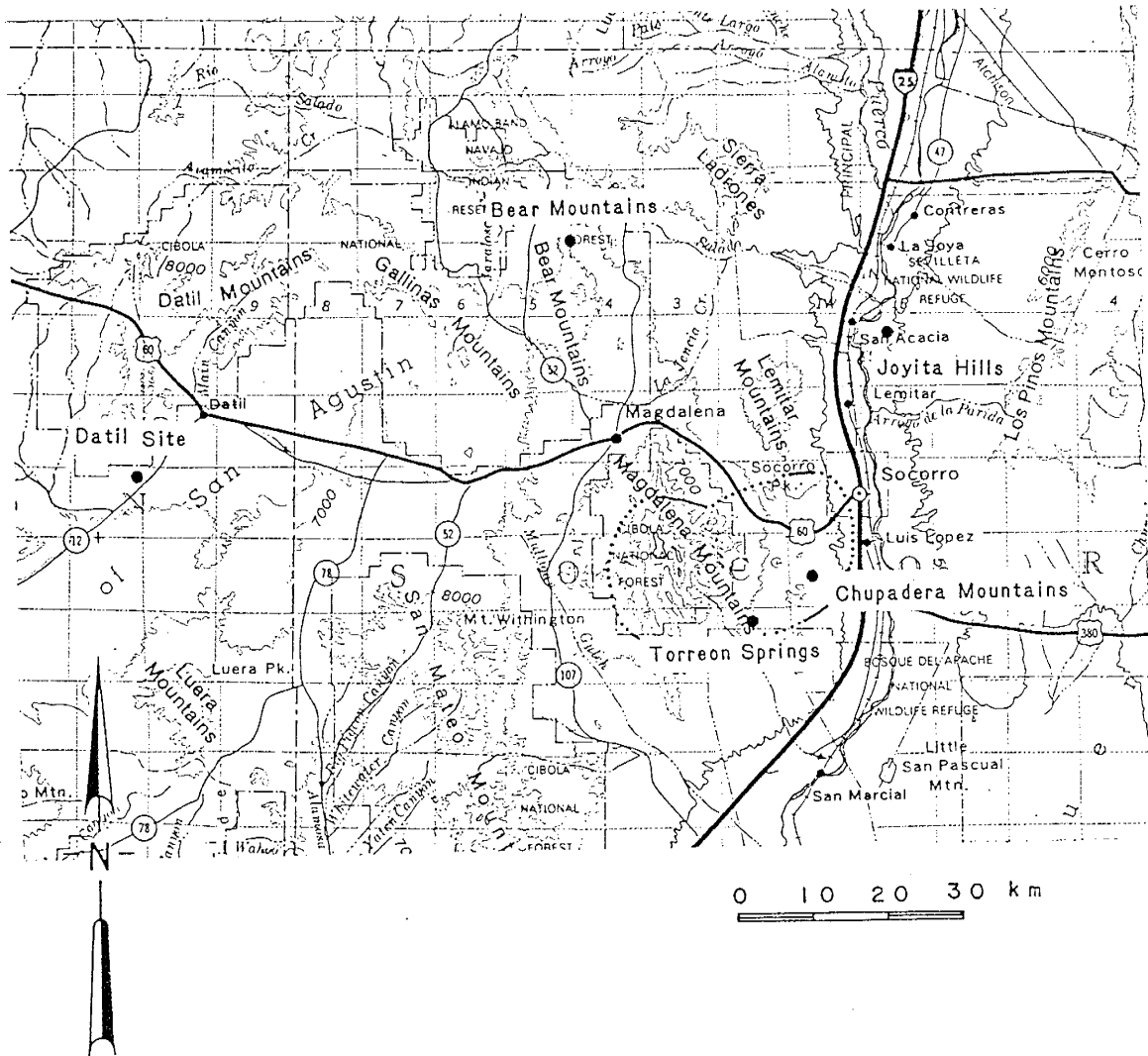


Figure 1. Location of the study area. Sample locations are shown by the large black dots. The approximate boundaries of the Socorro cauldron are shown by the dashed line (Osburn and Chapin, 1983a). Base map is Topographic Map of New Mexico, 1983, scale 1:1,000,000.

Brown (1972) and his measured sections of the La Jencia and Vicks Peak tuffs are considered the type sections for these units. The mapping in the Joyita Hills area was done by Spradlin (1976), in the Datil area by Lopez and Bornhorst (1979), and in the Torreon Springs area by Osburn and others, (1981). The type section of the Lemitar Tuff is located in the Lemitar Mountains, north of Socorro (Chamberlin, 1980), and the principle reference section is near Torreon Springs. The Chupadera Mountains, which contain exposures of cauldron-fill Hells Mesa Tuff, were mapped by Eggleston (1982).

Stratigraphy

HELLS MESA TUFF

Description

The Hells Mesa Tuff is the basal, crystal-rich, quartz-rich ash-flow unit of Tonking's (1957) Hells Mesa Member (Osburn and Chapin, 1983a). The Hells Mesa Tuff (Table 1) is a pink to reddish-brown, moderately to densely welded, multiple-flow, simple-cooling unit. It is zoned chemically from basal quartz latite through rhyolite. The lower portion contains approximately 35% phenocrysts and rests locally upon a

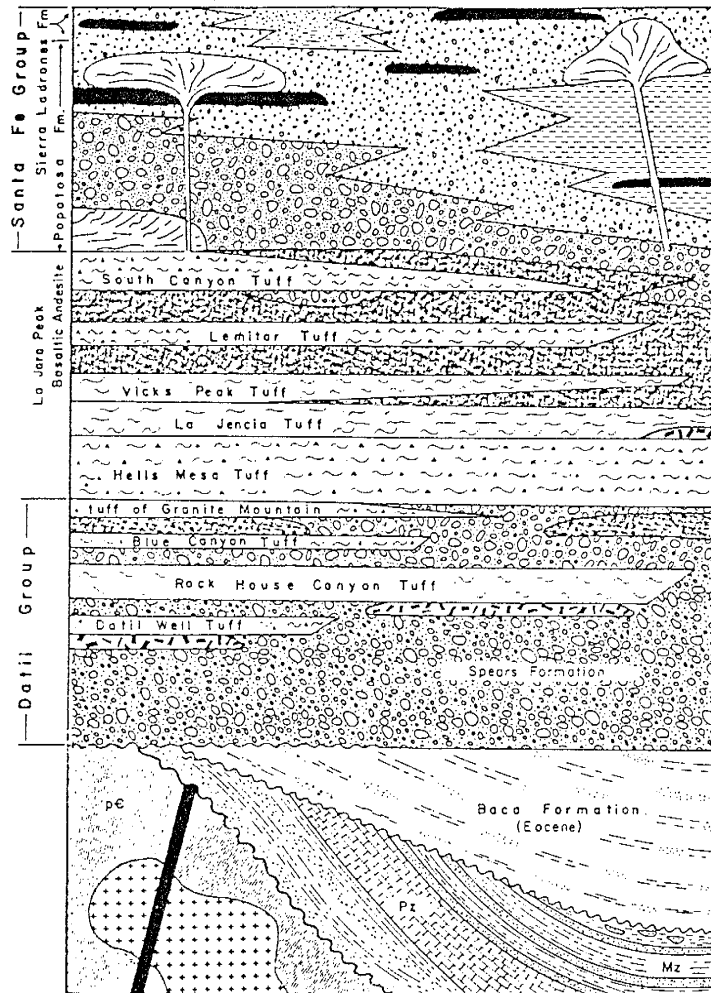


Figure 2. Composite stratigraphic column of the northeastern Mogollon-Datil volcanic field (Osburn and Chapin, 1983a).

TABLE 1
Description of the Ash-Flow Tuff Units

Unit	Thickness	Cooling	Welding	Phenocryst Mineralogy		
				Total Phenocrysts	Major	Trace
South Canyon Tuff	outflow: 0-200 m	multiple-flow, simple to compound cooling unit	upper: moderate lower: dense	upper: 15 % lower: 3 %	quartz: 7% Na-sanidine: 8%	plagioclase biotite sphene biotite plagioclase
		multiple-flow, simple to compound cooling unit	dense	upper: 45 % lower: 12 %	quartz: 15% Na-sanidine: 15% plagioclase: 10% biotite: 2%	hornblende sphene zircon zircon sphene biotite plagioclase
Vicks Peak Tuff	outflow: 0-250 m	multiple-flow, simple cooling unit	dense	3 %	Na-sanidine: 3%	biotite plagioclase
		multiple-flow, simple cooling unit	upper: dense lower: moderate	7 %	Na-sanidine: 4% quartz: minor	plagioclase biotite clinopyroxene
Hells Mesa Tuff	outflow: 0-245 m cauldron: 900 m	multiple-flow, simple cooling unit	moderate to dense	upper: 50 % lower: 35 %	quartz: 15% Na-sanidine: 25% plagioclase: 10% biotite: 1%	sphene zircon clinopyroxene hornblende clinopyroxene
		multiple-flow, simple cooling unit	dense		quartz: 15% Na-sanidine: 15% plagioclase: 15% biotite: 2-3%	hornblende clinopyroxene clinopyroxene biotite

thin, basal, black vitrophyre. The phenocrysts are predominantly Na-sanidine and plagioclase, with minor amounts of biotite, quartz, hornblende, and clinopyroxene. The upper portion contains approximately 50% phenocrysts of Na-sanidine, quartz, and plagioclase, with minor amounts of biotite, clinopyroxene, sphene, and zircon.

The potassium feldspar phenocrysts in all the outflow sheets have been previously identified petrographically as sanidine. Recent x-ray and microprobe analyses (J.I. Lindley, 1984, written commun.) have shown that the feldspars contain appreciable sodium, and should be called Na-sanidine cryptoperthites (Smith, 1974).

Extent

The Hells Mesa Tuff was erupted from the Socorro cauldron (fig.1; Eggleston, 1982). The well-documented correlation is based upon field evidence of thick intracauldron facies tuff and moat-fill deposits. This unit is among the thickest and most extensive ash-flow tuffs in the Socorro area. The outflow sheets attain a thickness of 245m; while the cauldron-fill tuff is greater than 900m in thickness. It is distributed throughout the northeastern Mogollon-Datil volcanic field with the exception of the southern Chupadera Mountains and the northern Jornada del Muerto.

Previous Radiometric Dating

The Hells Mesa Tuff has been dated repeatedly by the conventional potassium-argon and fission-track methods (Table 2). Many of the samples were collected from the Datil area and analyzed at the U.S. Geological Survey laboratory in Denver, Colorado. The dates vary more than five million years and have large uncertainties associated with them (fig. 3). The dates form two distinct groups, the Na-sanidine potassium-argon and fission-track dates, which are significantly younger, and the biotite potassium-argon dates (Appendix II). The average of the dates, weighted by the inverses of the variances, is 31.59 ± 0.44 Ma.

LA JENCIA TUFF

Description

This unit, formerly called the lower member of A-L Peak Tuff, is a multiple-flow, compound-cooling unit of crystal-poor, rhyolite, ash-flow tuff (Table 1). The unit contains approximately 7% phenocrysts, primarily Na-sanidine, with minor quartz and traces of plagioclase, and biotite. The lower portion of the unit is a moderately welded,

TABLE 2

		Conventional Potassium-Argon Ages			
Unit	Mineral	Method	Age \pm 1 (Ma)	Sample Location	Reference
South Canyon Tuff	Na-sanidine	K-Ar	26.5 \pm 1.0	Joyita Hills	Bachman and Mehner, 1978
	Na-sanidine	K-Ar	24.5 \pm 0.9	Joyita Hills	Chapin and others, 1975
	Na-sanidine	K-Ar	24.5 \pm 1.0	Joyita Hills	Chapin and others, 1975
	Biotite	K-Ar	26.9 \pm 1.0	Joyita Hills	Chapin and others, 1975
Lemitar Tuff	Biotite	K-Ar	27.0 \pm 1.0	Lemitar Mtns.	Chapin and others, 1975
	Biotite	K-Ar	27.7 \pm 1.1	San Mateo Mtns.	Chapin and others, 1975
	Biotite	K-Ar	28.3 \pm 1.1	Joyita Hills	Chapin and others, 1975
	Biotite	K-Ar	28.8 \pm 1.2	Joyita Hills	Chapin and others, 1975
	Biotite	K-Ar	28.8 \pm 0.7	Joyita Hills	Chapin and others, 1975
	Whole Rock	K-Ar	22.9 \pm 0.6	Joyita Hills	Chapin and others, 1975
Vicks Peak Tuff	Zircon	F-T	31.3 \pm 2.6		Bornhorst and others, 1982
La Jencia Tuff	Na-sanidine	K-Ar	28.1 \pm 1.2	Lemitar Mtns.	Chapin and others, 1975
	Na-sanidine	K-Ar	22.0 \pm 0.8	Joyita Hills	Chapin and others, 1975
	Na-sanidine	K-Ar	25.0 \pm 0.6	Joyita Hills	Chapin and others, 1975
	Na-sanidine	K-Ar	24.8 \pm 1.0	Joyita Hills	Chapin and others, 1975
	Whole Rock	K-Ar	24.7 \pm 0.7	Joyita Hills	Chapin and others, 1975
Hells Mesa Tuff	Na-sanidine	K-Ar	30.9 \pm 1.1	Datil	Chapin and others, 1975
	Na-sanidine	K-Ar	28.6 \pm 1.0	Datil	Chapin and others, 1975
	Na-sanidine	K-Ar	32.1 \pm 0.7	Crosby Mtns.	Bornhorst and others, 1982
	Biotite	K-Ar	34.0 \pm 1.3	Joyita Hills	Chapin and others, 1975
	Biotite	K-Ar	33.2 \pm 1.1	Datil	Chapin and others, 1975
	Biotite	K-Ar	33.0 \pm 1.1	Datil	Chapin and others, 1975
	Biotite	K-Ar	32.3 \pm 1.5	Datil	Chapin and others, 1975
	Biotite	K-Ar	30.6 \pm 2.8*	Bear Mtns.	Weber and Bassett, 1963
	Biotite	K-Ar	32.1 \pm 1.5*	Gallinas Mtns.	Burke and others, 1963; Weber, 1971
	Biotite	K-Ar	32.4 \pm 1.5*	Joyita Hills	Burke and others, 1963; Weber, 1971
Zircon	Plagioclase	K-Ar	31.1 \pm 1.9	Datil	Chapin and others, 1975
	Zircon	F-T	31.4 \pm 1.4	Datil	Chapin and others, 1975
	Zircon	F-T	29.3 \pm 1.6	Datil	Chapin and others, 1975

All ages (except *) corrected with IUGS constants using Dalrymple (1979)

medium-gray tuff. The upper portion is a densely welded, light pink to pink-and-white banded tuff. This upper member contains regions of severely compressed and lineated pumice as well as flow structures.

Extent

The La Jencia Tuff was erupted from the interconnected Sawmill Canyon and Magdalena cauldrons (Osburn and Chapin, 1983b). The outflow sheets attain a thickness of 150m, while the cauldron-fill tuff is greater than 750m in thickness. The tuff is present throughout the northeastern Mogollon-Datil volcanic field.

Previous Radiometric Dating

Five La Jencia Tuff Na-sanidine and whole-rock samples were dated by the conventional potassium-argon method (Table 2). The dates vary by more than six million years, due in part to interlaboratory variations. The average age for the unit, weighted by the inverse of the variances, is 25.2 ± 0.45 Ma.

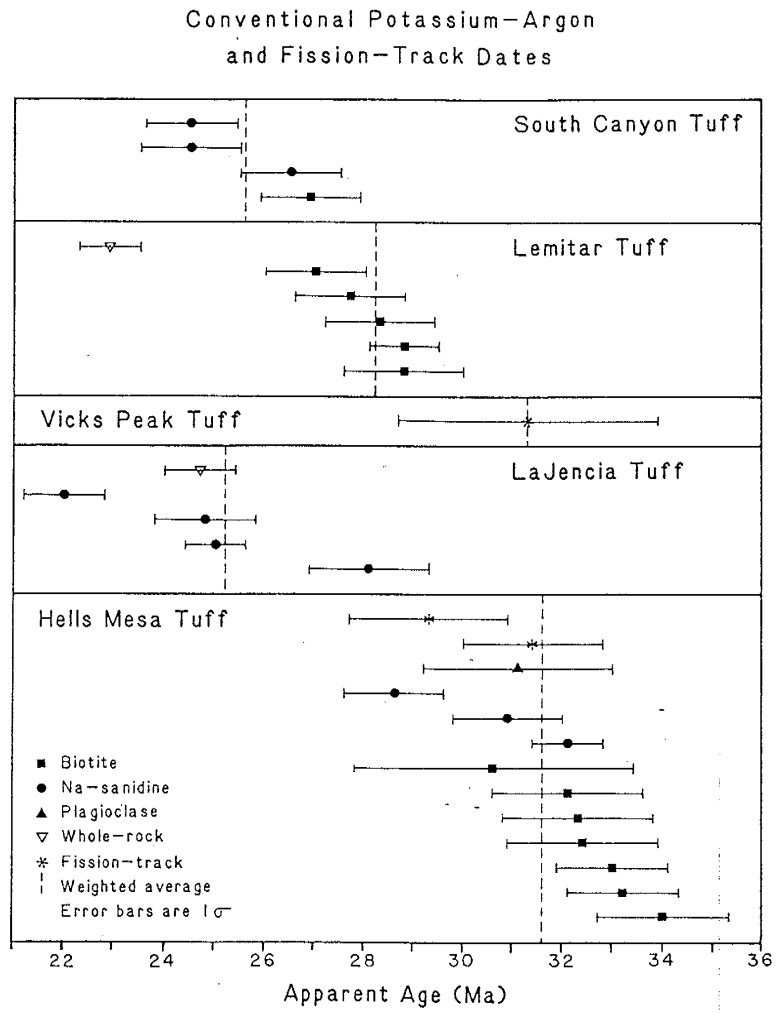


Figure 3. Conventional potassium-argon dates.

References are listed in Table 2.

VICKS PEAK TUFF

Description

This unit is a multiple-flow, simple-cooling unit composed of densely welded, gray, rhyolite, ash-flow tuff (Table 1). It is crystal-poor, containing approximately 1% to 3% phenocrysts of Na-sanidine and traces of quartz, plagioclase, and biotite. The cauldron-fill tuff contains abundant lithophysal cavities, while the outflow sheet contains large pumice filled with vapor-phase minerals.

Extent

The Vicks Peak Tuff has been tentatively correlated with the Nogal Canyon cauldron (Deal and Rhodes, 1976). Additional mapping will be required to confirm this correlation. The outflow sheet attains a maximum thickness of 250m and is found throughout the northeastern Mogollon-Datil volcanic field.

Previous Radiometric Dating

The Vicks Peak Tuff was difficult to date due to the paucity of phenocrysts. Only one fission-track date, 31.30 ± 2.6 Ma (Table 2, fig. 3), was available prior to the study and it contained a very large uncertainty.

LEMITAR TUFF

Description

This unit is a multiple-flow, simple to compound cooling-unit composed of densely welded ash-flow tuff (Table 1). It is zoned chemically from basal quartz latite to rhyolite. The lower light-gray to pale-red member is relatively crystal-poor, containing approximately 12% phenocrysts of Na-sanidine and quartz, and locally overlies a basal, black vitrophyre. The upper member contains approximately 45% phenocrysts of quartz, Na-sanidine, plagioclase, and biotite in a reddish-brown to light-yellowish-gray matrix.

Extent

The Lemitar Tuff is believed to have erupted from a cauldron in the northern San Mateo Mountains (Deal, 1973). Additional investigation of this area will be required to confirm this source. The tuff attains a thickness of 125m on the outflow sheet and thickens to 600m in the area of the proposed cauldron. It is present throughout the northeastern Mogollon-Datil volcanic field except for the Bear, Gallinas, and Datil mountains.

Previous Radiometric Dating

Six Lemitar Tuff samples, dated by the conventional potassium-argon method, vary in age by more than five million years (Table 2, fig. 3). The variation in age is reduced by the elimination of an anomalous whole-rock date and that of an altered sample. The average of the remaining four dates is 28.22 ± 0.46 Ma.

SOUTH CANYON TUFF

Description

This unit is a multiple-flow, simple to compound cooling-unit composed of rhyolite ash-flow tuff (Table 1). The lower portion, a light-gray to brownish-gray, densely welded tuff, contains approximately 3% phenocrysts of quartz and Na-sanidine. The upper portion, a medium-gray to purple-gray, moderately welded tuff, contains approximately 15% phenocrysts of chatoyant Na-sanidine and quartz.

Extent

The South Canyon Tuff has not been correlated to a source cauldron, but is thought to have been erupted from a cauldron in the northern San Mateo Mountains (Deal, 1973). Additional investigation will be required to locate the source. The unit attains a thickness of 200m in the outflow sheet, which is found throughout the northeastern Mogollon-Datil volcanic field except for the Datil area and the Bear and northern Gallinas mountains.

Previous Radiometric Dating

Four tuff sample have been dated by the conventional potassium-argon method (Table 2, fig. 3). The dates vary by more than two million years and give a weighted average of 25.54 ± 0.49 Ma for the unit.

METHODS AND TECHNIQUES OF INVESTIGATION

Introduction

In this study, the five ash-flow tuff units were dated by a high-precision variation of the $^{40}\text{Ar}/^{39}\text{Ar}$ age-spectrum method. To provide a foundation for the age comparisons, one unit, the Hells Mesa Tuff, was chosen as a data base. The Hells Mesa Tuff is areally extensive and easily identified in the field. It also contains datable amounts of three minerals, Na-sanidine, biotite and hornblende.

To assess the probability of success with this study, some preliminary samples were analyzed. Hells Mesa Tuff samples were collected near Datil by J.C. Ratte of the U.S. Geological Survey (1983, written commun.). Three mineral separates from these samples, which had been analyzed by the conventional potassium-argon method, were purified by hand-picking and packaged as part of Reston-Denver irradiation package number 16 (RD-16). Following irradiation in the central thimble of the U.S. Geological Survey TRIGA reactor for 20 hours at a power level of 1 megawatt, the samples were analyzed by J.F. Sutter of the U.S. Geological Survey in the same manner as proposed for this investigation. The successful results of the preliminary study led to this expanded investigation

with a greater number of samples.

Sampling

Sample locations, chosen primarily on the basis of stratigraphic control and the absence of alteration, contained most or all of the tuff sequence. Positive identification of the units was insured by mineralogy chemical analyses, and field relationships. Locations were chosen from recently mapped areas and localities containing previously dated samples. In addition, type and reference sections of the units were sampled when possible. Areas of known mineralization and hydrothermal alteration were avoided.

All five units were sampled in the Joyita Hills, where a complete and unaltered section of the units is exposed. Each unit was also sampled in one other location, geographically removed from the Joyita Hills, to assess the reproducibility of ages from separate outcrops within the same unit. The Hells Mesa, La Jencia, and Vicks Peak tuffs were collected from the northern Bear Mountains. The Lemitar Tuff was sampled near Torreon Springs in the southeastern foothills of the Magdalena Mountains. In addition, the Hells Mesa Tuff was sampled near the town of

Datil, and within the source cauldron in the Chupadera Mountains. The sample locations are shown in Figure 1 and listed in Appendix III.

In the Joyita Hills and the Bear Mountains, where several units occur, samples were taken at regular intervals during measurement of a stratigraphic section through the tuff sequence. The measured sections (Appendix IV) aid in the characterization of the units and define the level sampled for dating.

Sample Preparation

The samples for dating were selected by hand-sample inspection and examined for signs of alteration. Thin sections of these samples were examined for phenocryst alteration and compared with published petrographic descriptions to confirm unit identification. Each sample was analyzed for whole-rock major element chemical composition by x-ray fluorescence spectrometry (Norrish and Hutton, 1969). The chemical analyses (Appendix IV) provided information concerning chemical zonation in the units and helped to confirm unit identification. In addition, the chemical analyses were scrutinized for mild potassium metasomatism, which might not have been noticed in the

thin-section examination. If either chemical or thin-section examination revealed sample alteration, another sample was collected.

Mineral separates were prepared from each sample, because the $^{40}\text{Ar}/^{39}\text{Ar}$ method is more accurate when applied to single mineral phases (Harrison, 1983). To isolate the mineral phases, each sample was crushed, sieved, passed through various heavy liquids and a Frantz isodynamic magnetic separator, hand picked, and ultrasonically cleaned (Appendix V). Each separate was evaluated under a microscope for greater than 99% purity. Samples of Hells Mesa and Lemitar tuffs produced separates of both Na-sanidine and biotite. In addition, Hells Mesa Tuff produced hornblende separates from two samples. The La Jencia, Vicks Peak, and South Canyon tuffs each produced only Na-sanidine separates.

$^{40}\text{Ar}/^{39}\text{Ar}$ Dating Technique

The theories and analytical procedures comprising the $^{40}\text{Ar}/^{39}\text{Ar}$ dating method are detailed in Appendix VI. The samples in this study were analyzed by a high-precision variation of this dating method. The variation employed detailed monitoring of the constant J portion of the

irradiation canister (see Analytical Results). Hornblende standard MMhb-1 (Alexander and others, 1978), which has an accepted conventional potassium-argon age of 519.4 Ma (Dalrymple and others, 1981), was used as the monitor standard. The irradiation package, RD-20, contained 100-milligram Na-sanidine and biotite samples, 400-milligram hornblende samples, and fourteen monitor standards. The package was irradiated incrementally in the central thimble facility of the U.S. Geological Survey TRIGA reactor for twenty hours at 1 megawatt. All samples in this study were placed in the constant J portion of the irradiation canister and therefore received equivalent neutron dosages, within the estimated analytical uncertainty. This increased the level of precision at which these samples could be compared. The argon was then extracted in an ultra-high vacuum system by heating the standards and samples with a radio-frequency (RF) induction coil. The temperatures, accurate to 25° to 50°C, were set with a radio-frequency power output versus temperature curve, calibrated with an optical pyrometer, and checked with the melting point of aluminum. The samples were degassed, beginning at intermediate temperatures, to minimize the effects of argon released at low temperatures on the age-spectrum plateaus. The argon isotopes were analyzed with a computer controlled VG-Micromass 1200B mass spectrometer operated in the static mode. The apparent ages were calculated from the equations listed in Appendix VI and the constants from Steiger and Jager (1977; Table 3).

TABLE 3
Constants and Correction Factors

Element	Isotope	Abundance	Half-Life	Decay Constant
Ar	³⁶ Ar	0.00337		
	³⁷ Ar		35.1 d	$1.975 \times 10^{-2} \text{ d}^{-1}$
	³⁸ Ar	0.00063		
	³⁹ Ar		259 d	$2.58 \times 10^{-3} \text{ y}^{-1}$
	⁴⁰ Ar	0.99600		
K	³⁹ K	0.932581		
	⁴⁰ K	0.0001167	$1.25 \times 10^9 \text{ y}$	$= 0.581 \times 10^{-10} \text{ y}^{-1}$
				$= 4.963 \times 10^{-10} \text{ y}^{-1}$
	⁴¹ K	0.067302		
Ca	⁴⁰ Ca	0.96947		
	⁴² Ca	0.00646		
	⁴³ Ca	0.00135		
	⁴⁴ Ca	0.02083		
	⁴⁶ Ca	0.00186		
	⁴⁸ Ca	0.0018		
Monitor	Mineral	K ₂ O (%)	⁴⁰ Ar* (mole/g)	Age (Ma)
MMhb-1	hornblende	1.874	1.624×10^{-9}	519.4×10^6
Correction Factors				
$(^{36}\text{Ar}/^{37}\text{Ar})_{\text{Ca}} = 2.64 \times 10^{-4}$				
$(^{39}\text{Ar}/^{37}\text{Ar})_{\text{Ca}} = 6.73 \times 10^{-4}$				
$(^{40}\text{Ar}/^{39}\text{Ar})_{\text{K}} = 0.594 \times 10^{-2}$				

from Dalrymple and others, 1981

ANALYTICAL RESULTS

Introduction

Fourteen aliquots of MMhb-1 were used to monitor the fast-neutron irradiation. The conventional potassium-argon age of MMhb-1 is 519.4 Ma (Dalrymple and others, 1981). The monitors were used to calculate the J-values for the package using the equation:

$$J = (e^{\lambda t_m} - 1) / ({}^{40}\text{Ar}^* / {}^{39}\text{Ar}_K)_m$$

${}^{40}\text{Ar}^*$ is the amount of radiogenic argon in the monitor, ${}^{39}\text{Ar}_K$ is the amount of potassium-produced argon in the monitor, λ is the ${}^{40}\text{K}$ total decay constant, and t_m is the age of the monitor. The J-values are proportional to the neutron dosage at different levels in the irradiation canister (Appendix VI). Plots of J versus distance above the base of the canister for the irradiation packages RD-16 and RD-20 are shown in Figure 4 (a,b). The uncertainty in the J-value was estimated from the run-to-run, long-term reproducibility in the ${}^{40}\text{Ar}^* / {}^{39}\text{Ar}_K$ ratio (denoted F) of the MMhb-1 standard as measured by the mass spectrometer. This uncertainty was estimated at 0.25% (J.F. Sutter, 1984, oral commun.). As shown in Figure 4 (a,b), the J-curves reached constant values, within the estimated 0.25% uncertainty, near the centers of the canisters, which is characteristic of the U.S. Geological Survey TRIGA reactor. The individual J-values

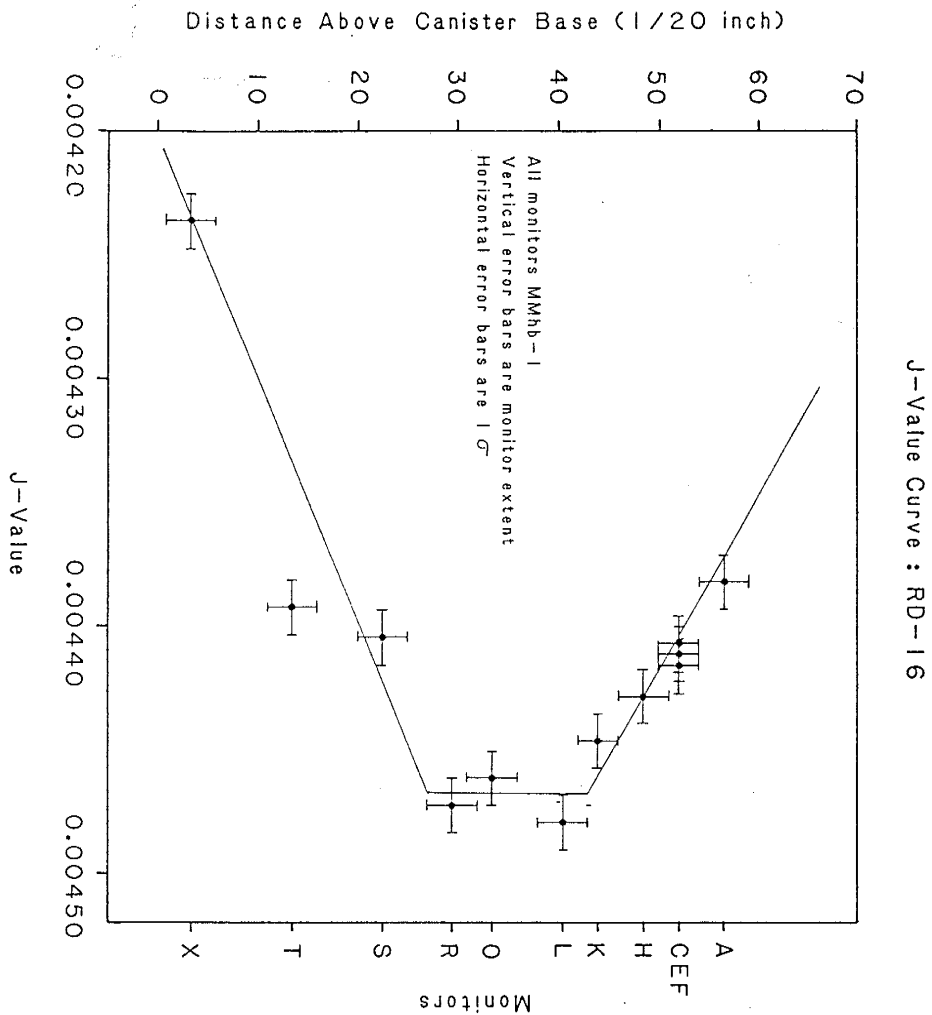


Figure 4. J-value curves

a. J-value curve: RD-16

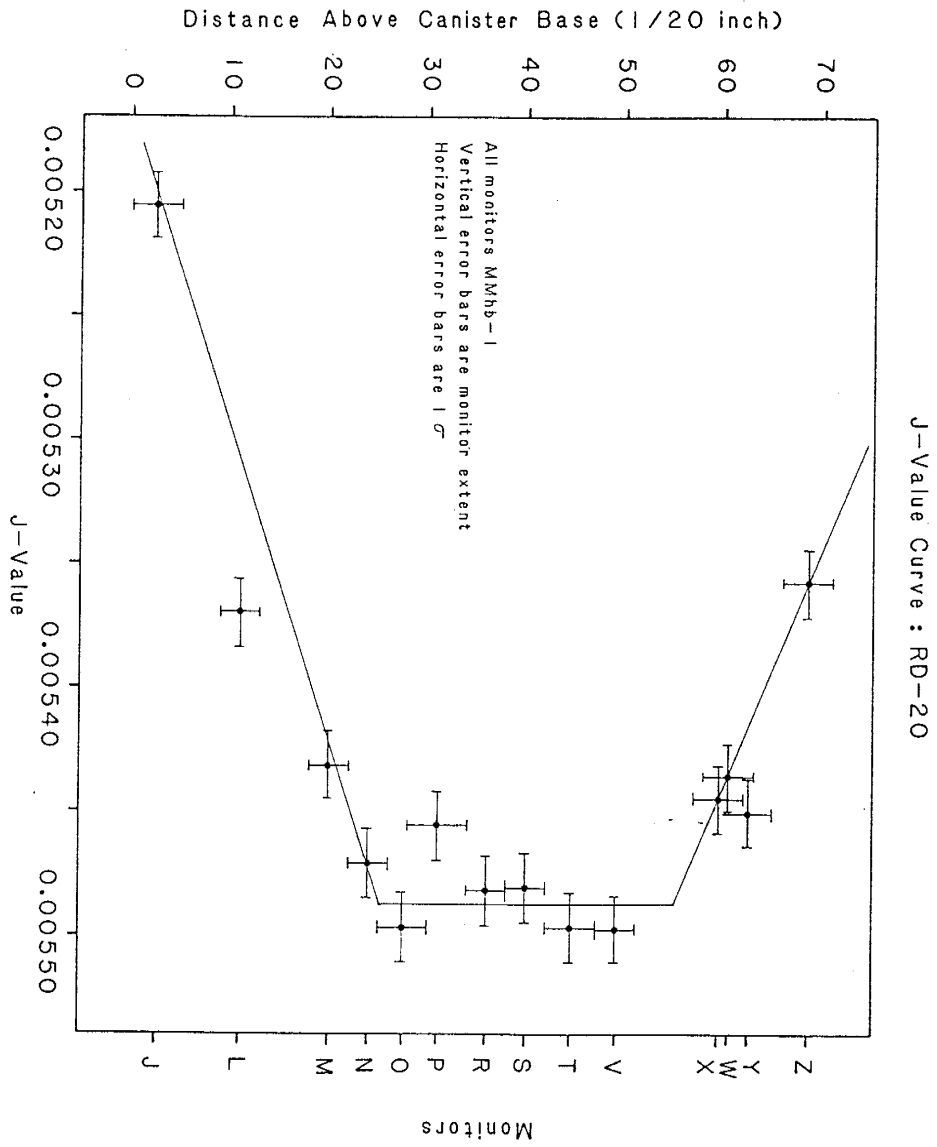


Figure 4. J-value curves

b. J-value curve: RD-20

in the central portion of the canisters were tested for inclusion in the constant J-value area by the critical value test (Appendix I; Dalrymple and Lanphere, 1969, page 120).

Evaluation of the monitor data from RD-16 showed that the area of constant J consisted of monitors L, O, and R (fig. 4a). The value for the area of constant J, 0.004468 ± 16 , is the mean of these data points, with the uncertainty equal to the population standard deviation.

Testing the monitor data from RD-20 eliminated monitor P from the area of constant J (fig. 4b). The value for the area of constant J, the mean of the remaining data points (monitors O, R, S, T, and V), is 0.005488 ± 11 .

All analytical data has been corrected for reactor-produced interfering isotopes. The correction factors used were: $(^{36}\text{Ar}/^{37}\text{Ar})_{\text{Ca}} = 2.64 \times 10^{-4}$, $(^{39}\text{Ar}/^{37}\text{Ar})_{\text{Ca}} = 6.73 \times 10^{-4}$, and $(^{40}\text{Ar}/^{39}\text{Ar})_{\text{K}} = (0.594) \times 10^{-2}$ (Dalrymple and others, 1981). These reactor constants are also used to calculate the apparent K/Ca ratios of the samples. The resulting relationship is:

$$\text{K/Ca} = 0.52 \left(^{39}\text{Ar}_{\text{K}} / ^{37}\text{Ar} \right) \text{ mol/mol}$$

(Fleck, and others, 1977).

The quality of age-spectrum data was measured by the presence or absence of an age plateau. The definition of a plateau employed in this study (Fleck and others, 1977) was that a plateau was formed by two or more contiguous gas fractions which totaled 50% or more of the total $^{39}\text{Ar}_{\text{K}}$ released, and which were all statistically the same at the 95% confidence level. The critical value test (Appendix I) was used to test

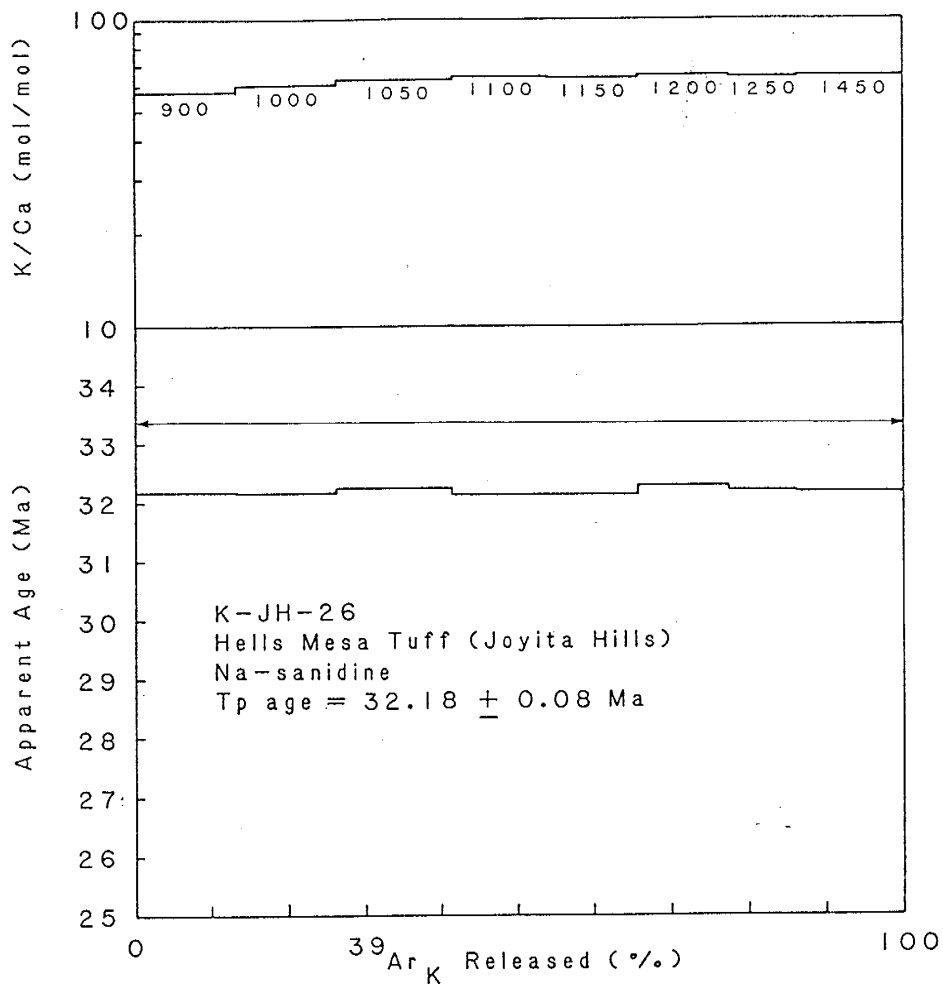


Figure 5. K-JH-26 Na-sanidine age spectrum

age plateau (fig. 6). The total-gas age of the sample before the re-regression was 32.10 Ma. The plateau formed by the 1050° and 1150°C steps includes 54.2% of the total $^{39}\text{Ar}_K$ released and yields a plateau age of 32.05 ± 0.10 Ma which is statistically indistinguishable from the total-gas age, but more precise. The K/Ca ratio remained nearly constant over all of the gas fractions at approximately 60.

K-BM-3

This sample was degassed in eight temperature steps from 900° to 1450°C. It did not produce a plateau due to an anomalously low F value for the 1150°C gas fraction. This low value is not a true characteristic of this sample but is an artifact of the analytical procedure. The analysis was interrupted overnight, and the 1150°C fraction was the first gas fraction analyzed the next day. The mass spectrometer experienced stability problems on this first run. The spectrometer magnetic field intensity drifted substantially during the analysis. This affected all the data, but the ^{39}Ar data was especially poor with a large uncertainty. For these reasons, the 1150°C fraction was treated as a lost fraction and the analytical data was ignored. The age spectrum with the 1150°C fraction omitted forms a plateau from the 1000° to the 1450°C fractions, encompassing 71.4% of the total $^{39}\text{Ar}_K$ released (fig. 7). The plateau age equals 32.25 ± 0.09 Ma, statistically the same as the total-gas age (32.16 Ma) which includes the 1150°C fraction. This shows that the age of the sample was not

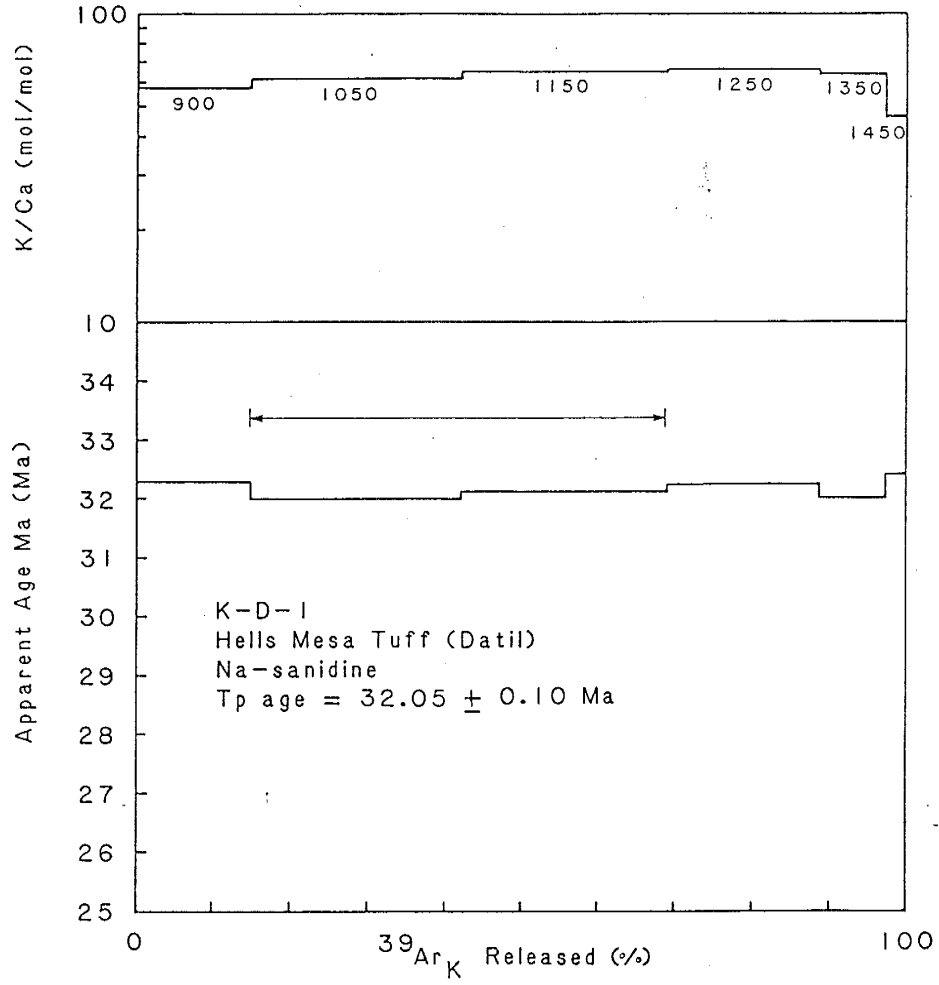


Figure 6. K-D-1 Na-sanidine age spectrum

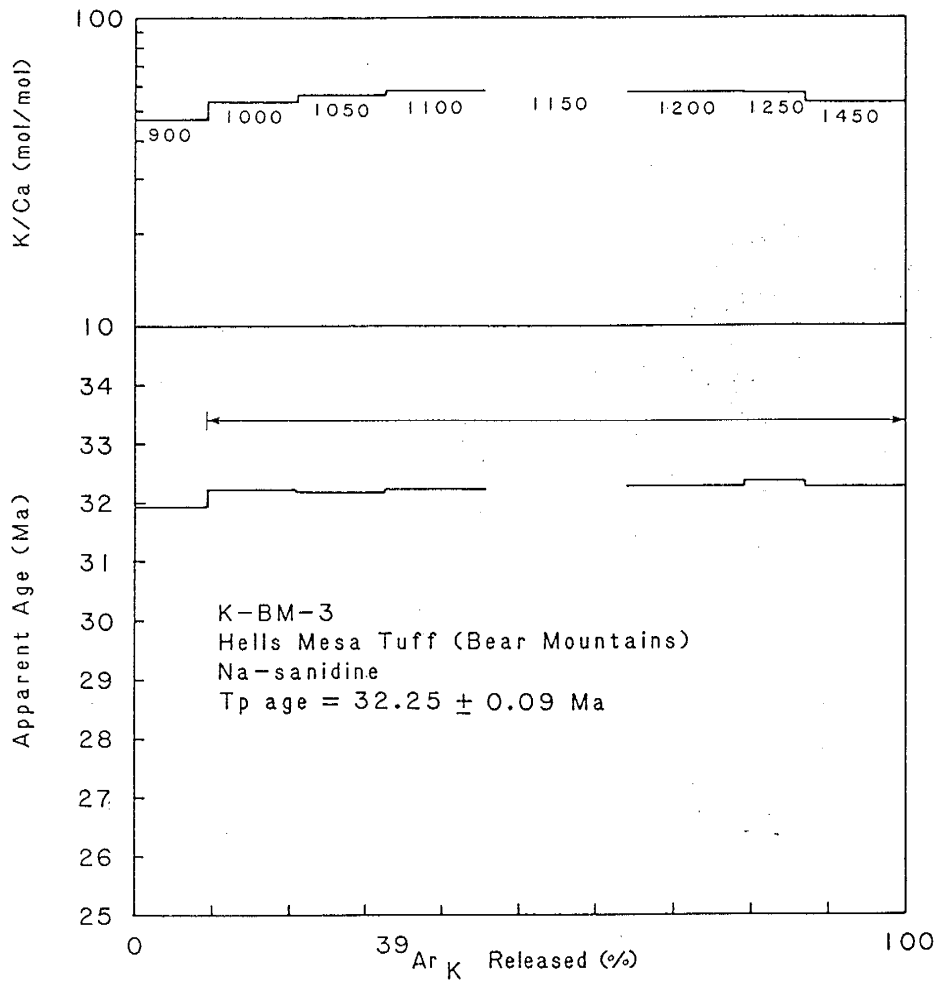


Figure 7. K-BM-3 Na-sanidine age spectrum

affected by omission of the one gas fraction. The K/Ca ratio remained nearly constant over all gas fractions at approximately 55.

K-CM-2

This Na-sanidine sample was degassed in eight temperature steps from 900° to 1350°C and yielded an age-spectrum plateau (fig. 8). The plateau includes the gas fractions from 1150° to 1350°C, which contain 67.6% of the total $^{39}\text{Ar}_K$ released. The plateau age is 31.77 ± 0.09 Ma which is statistically identical to the total-gas age of 31.79 Ma. The K/Ca ratio began at a low value but stabilized at approximately 60 for most of the gas fractions.

SU-4-77

This Na-sanidine sample was one of three preliminary samples irradiated in package RD-16. The sample was degassed in seven temperature steps from 750° to 1200°C. The age spectrum yields a plateau from the 1000° to 1200°C gas fractions, which contain 93.5% of the total $^{39}\text{Ar}_K$ released (fig. 9). The plateau age equals 31.87 ± 0.11 Ma, statistically the same as the total-gas age of 31.91 Ma. The K/Ca ratio began low for the low-temperature gas fractions and stepped up slowly to approximately 50.

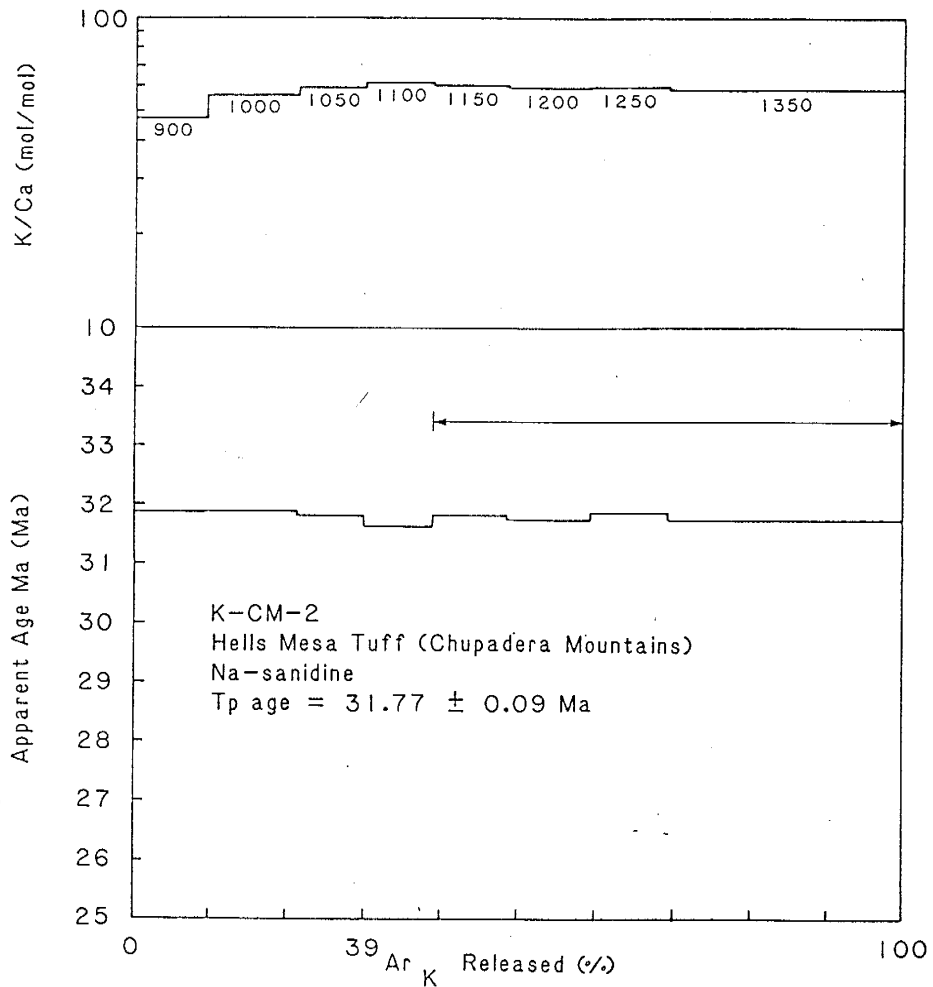


Figure 8. K-CM-2 Na-sanidine age spectrum

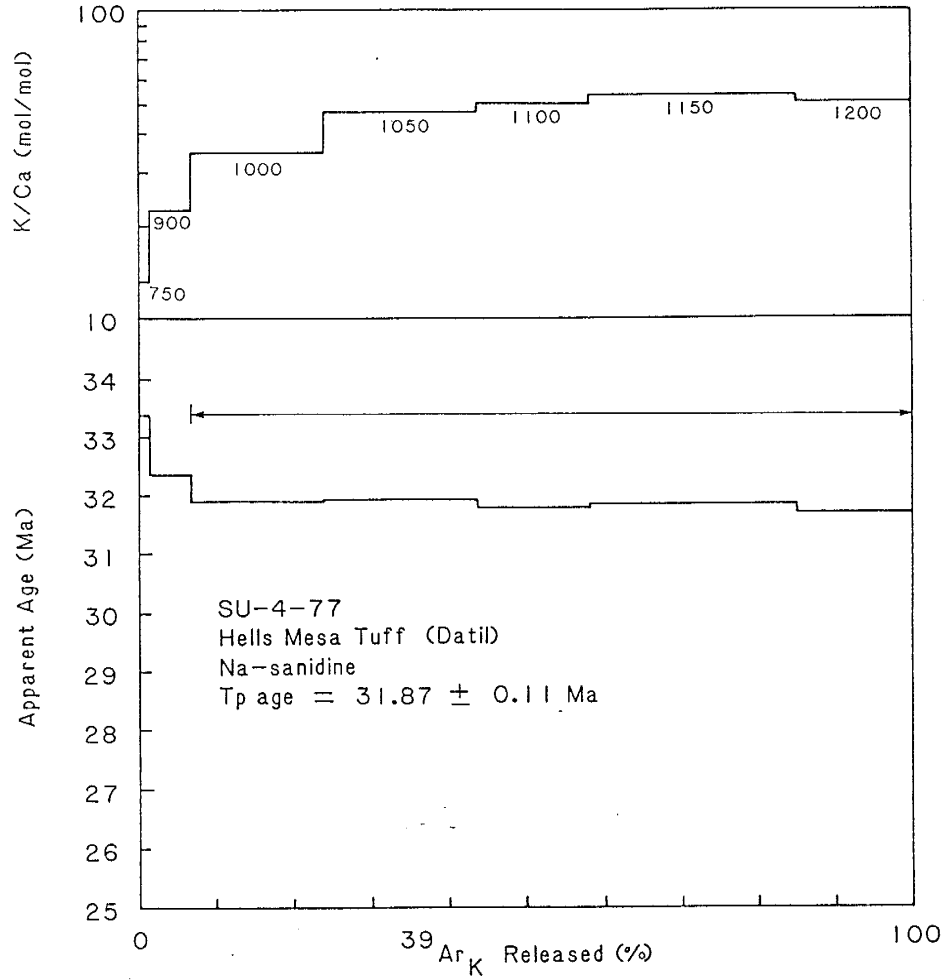


Figure 9. SU-4-77 Na-sanidine age spectrum

BIOTITE

K-JH-26

This sample was degassed in eight temperature steps from 850° to 1500°C. Initially, no plateau was formed from the data due to an anomalously high F value for the 1150°C gas fraction. When this data was re-regressed to reduce the uncertainty, the spectrum formed a plateau from the 1100° to 1250°C gas fractions, which contain 52.8% of the total $^{39}\text{Ar}_K$ released (fig. 10). The plateau age is 32.28 ± 0.10 Ma, which is statistically the same as the total-gas age before re-regression of 32.56 ± 0.53 Ma. This shows that the re-regression did not alter the data but only improved the precision. The K/Ca ratio began at very low values, stepped up to a maximum value of 100, and then slowly decreased to approximately 70.

K-BM-3

This biotite sample was degassed in eight temperature steps from 850° to 1500°C. The sample does not form a plateau. The age spectrum begins anomalously high and gradually decreases with increasing temperature (fig. 11). The total-gas age for K-BM-3 biotite equals 32.54 ± 0.61 Ma. The pattern of the age spectrum indicates that the sample's potassium-argon system has been disturbed. For this reason,

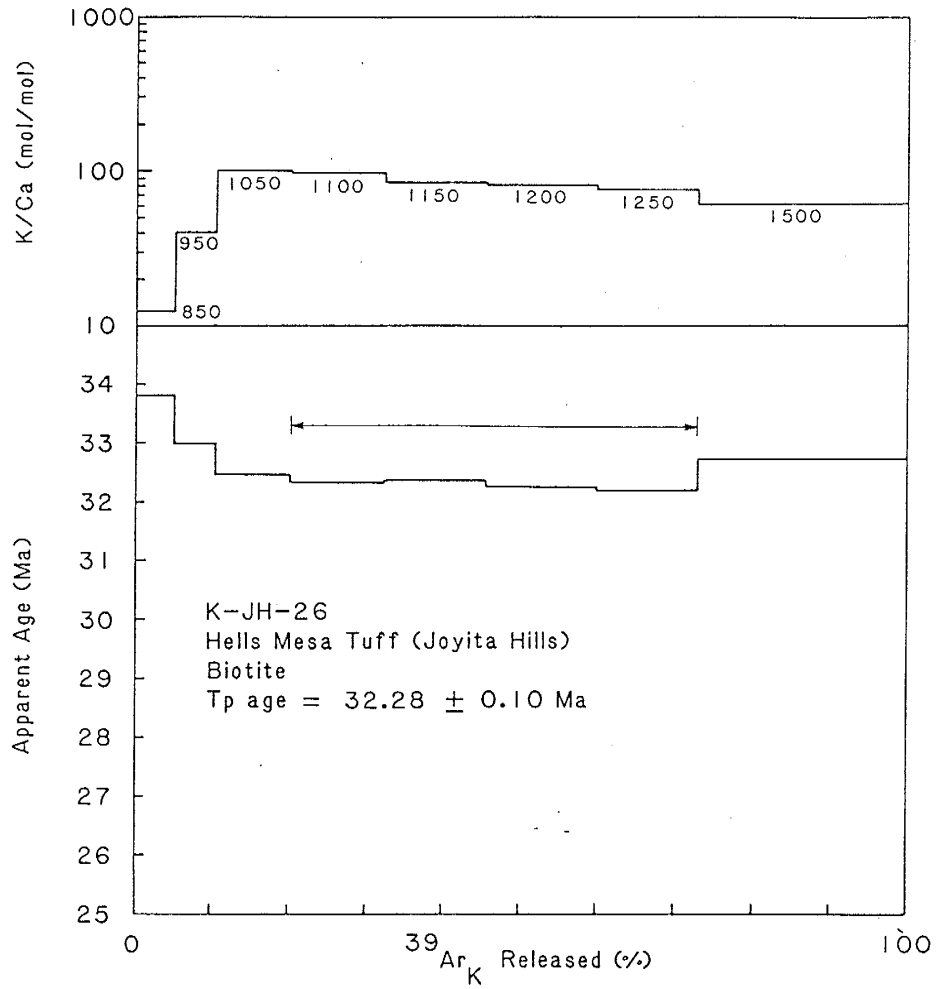


Figure 10. K-JH-26 biotite age spectrum

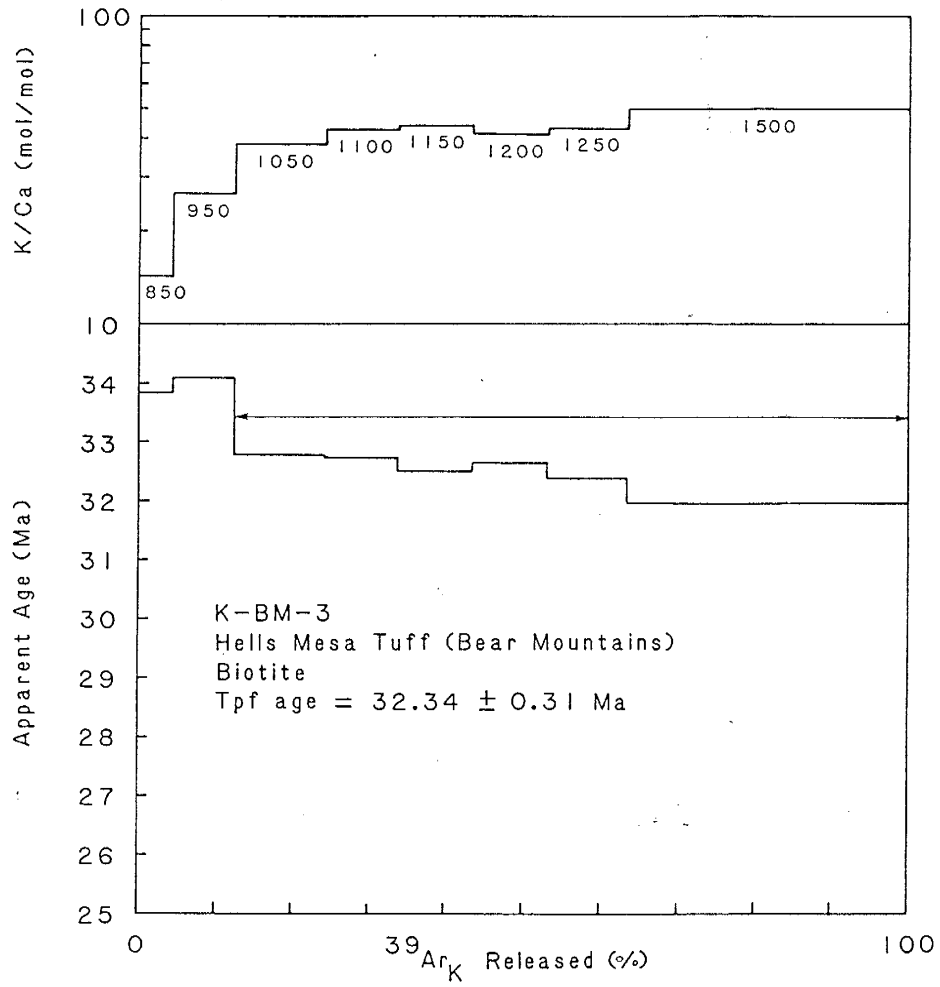


Figure 11. K-BM-3 biotite age spectrum

the high-temperature steps are considered to yield the most reliable data. The high-temperature fractions from 1050° to 1500°C contain 87.5% of the total $^{39}\text{Ar}_K$ released, and yield a preferred age of 32.34 ± 0.31 Ma. This preferred age is statistically the same as the total-gas age, but is more precise. The K/Ca ratio began at anomalously low values and increased steadily with each temperature step to a maximum value of 50.

K-CM-2

This biotite sample, degassed in six temperature steps from 950° to 1450°C, did not form a plateau. The age-spectrum diagram begins anomalously low and gradually increases with increasing temperature (fig. 12). The total gas age equals 32.13 ± 0.23 Ma. The age spectrum pattern suggests that the sample's potassium-argon system has been disturbed, so the high-temperature data is the most reliable. The high-temperature fractions from 1050° to 1450°C contain 65.2% of the total $^{39}\text{Ar}_K$ released, and yield a preferred age of 32.30 ± 0.17 Ma. This preferred age is statistically the same as the total-gas age but is much more precise. The K/Ca ratio began at a value greater than 150 and decreased with each subsequent temperature step to end at approximately 80.

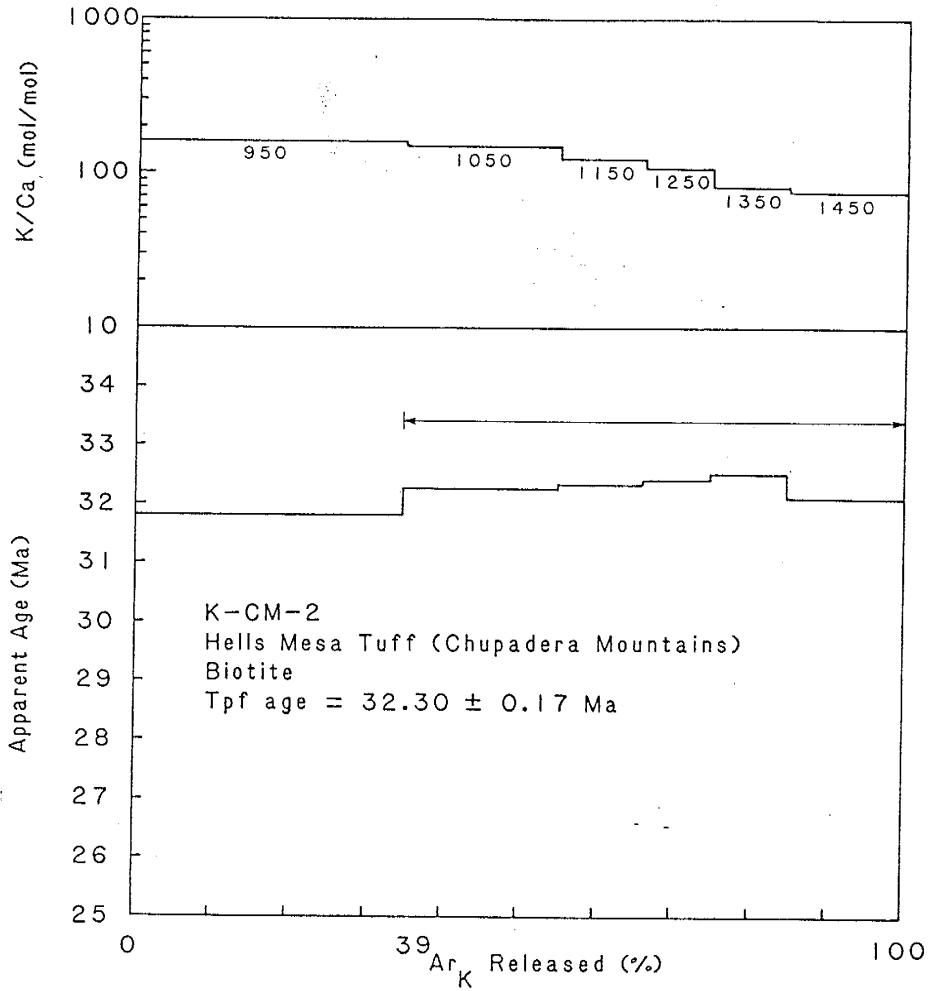


Figure 12. K-CM-2 biotite age spectrum

SU-4-77

Two Hells Mesa Tuff biotite samples were irradiated in package RD-16. Sample SU-4-77 was degassed in eleven temperature steps from 550° to 1300°C. The first four temperature steps combined released only 1.1% of the total $^{39}\text{Ar}_K$ released and were disregarded. The sample did not form a plateau. The 1200° and 1250°C gas fractions approximate a plateau and contain 58.1% of the total $^{39}\text{Ar}_K$ released (fig. 13). The 1200° and 1250°C fractions yield a preferred age of 32.11 ± 0.19 Ma, which is statistically the same as the total-gas age of 32.03 Ma. The K/Ca ratio began at approximately 5, increased sharply to approximately 30, then decreased with increasing temperature to approximately 7.

SU-5-77

This sample was degassed in ten temperature steps from 550° to 1250°C. The first four temperature steps each yielded less than 1% of the total $^{39}\text{Ar}_K$ released by the sample and were disregarded. This sample formed a plateau from the 1050° to the 1150°C gas fractions which contain 57.1% of the $^{39}\text{Ar}_K$ released (fig. 14). The plateau age equals 32.09 ± 0.10 Ma which is statistically the same as the total-gas age of 32.55 Ma. The K/Ca ratio began at approximately 3, increased to approximately 20, then decreased with increasing temperature to approximately 6.

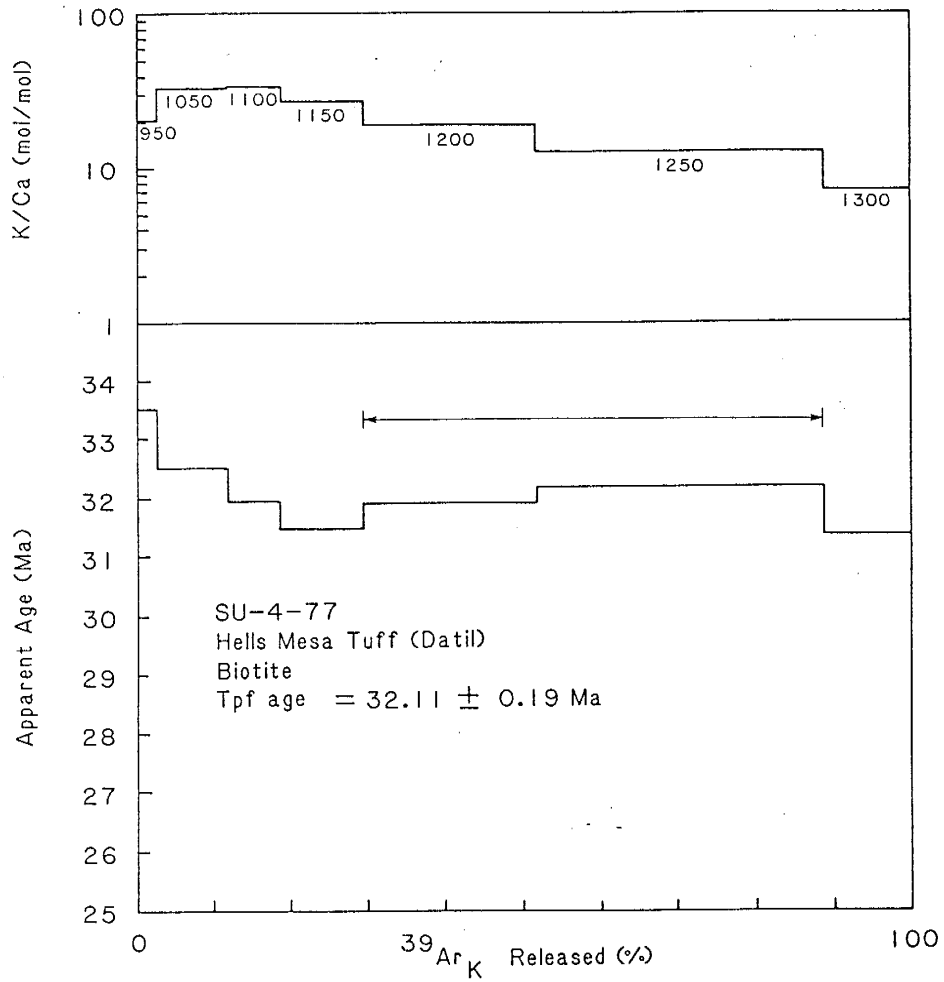


Figure 13. SU-4-77 biotite age spectrum

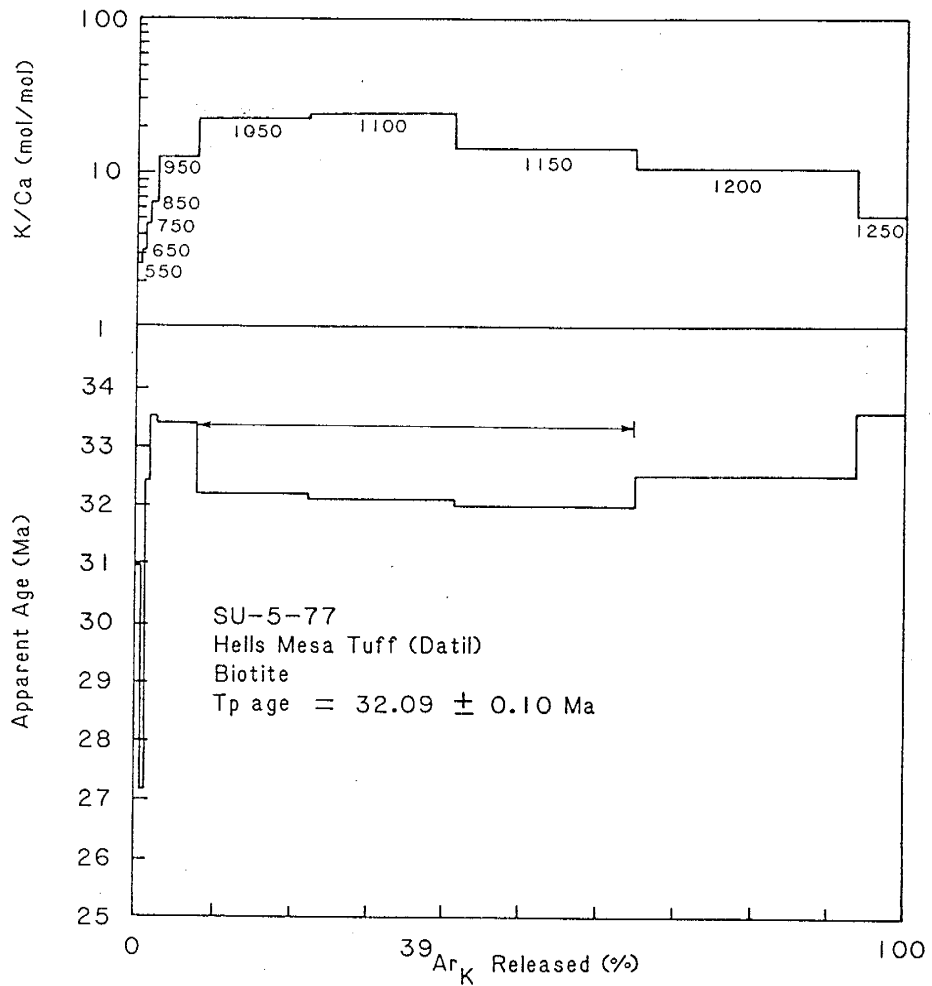


Figure 14. SU-5-77 biotite age spectrum

HORNBLLENDE

The two samples of hornblende were analyzed differently than the Na-sanidine and the biotite samples. The hornblendes were analyzed in three-step fusions. The first temperature step is at intermediate temperature, about 1000°C, to release the atmospheric argon component. The second step is at the melting temperature of hornblende, approximately 1400°C, in order to release the majority of the argon gas present in the sample. The final temperature step is at very high temperature, approximately 1500°C, to insure that the sample is completely degassed. This type of analysis does not yield an age spectrum diagram.

The necessity of the three-step fusion procedure was dictated by the small sample size of the hornblende samples obtained. There was insufficient material to generate a standard multi-increment age spectrum. The three-step fusion procedure was designed to maximize the argon isotope signal sizes, enhance the radiogenic yield, and increase the precision of the analysis over that of a total fusion analysis. It has also been demonstrated (J.F. Sutter and M.J. Kunk, 1984, oral commun.) that complete age spectra on unaltered hornblende from simple cooling units are not strictly necessary. If the mineral separates were carefully prepared and hand-picked, homogeneous, volcanic hornblendes generally yield plateau age spectra.

K-JH-4

This sample was degassed in eight temperature steps from 900° to 1450°C. The age spectrum yielded a plateau from the 1000° to the 1200°C gas fractions, which contain 71.0% of the total $^{39}\text{Ar}_K$ released by the sample (fig. 15). The plateau age equals 28.77 ± 0.07 Ma, equivalent to the total-gas age of 28.85 ± 0.19 Ma. The K/Ca ratio was uniform at approximately 28 to 30.

K-JH-5

This Na-sanidine sample was degassed in eight temperature steps from 900° to 1450°C. This sample produced a plateau from the 1050° to the 1200°C gas fractions, encompassing 59.8% of the total $^{39}\text{Ar}_K$ released from the sample (fig. 16). The plateau age is 28.75 ± 0.09 Ma, statistically the same as the total-gas age of 28.72 ± 0.23 Ma. The K/Ca ratio was constant at approximately 28.

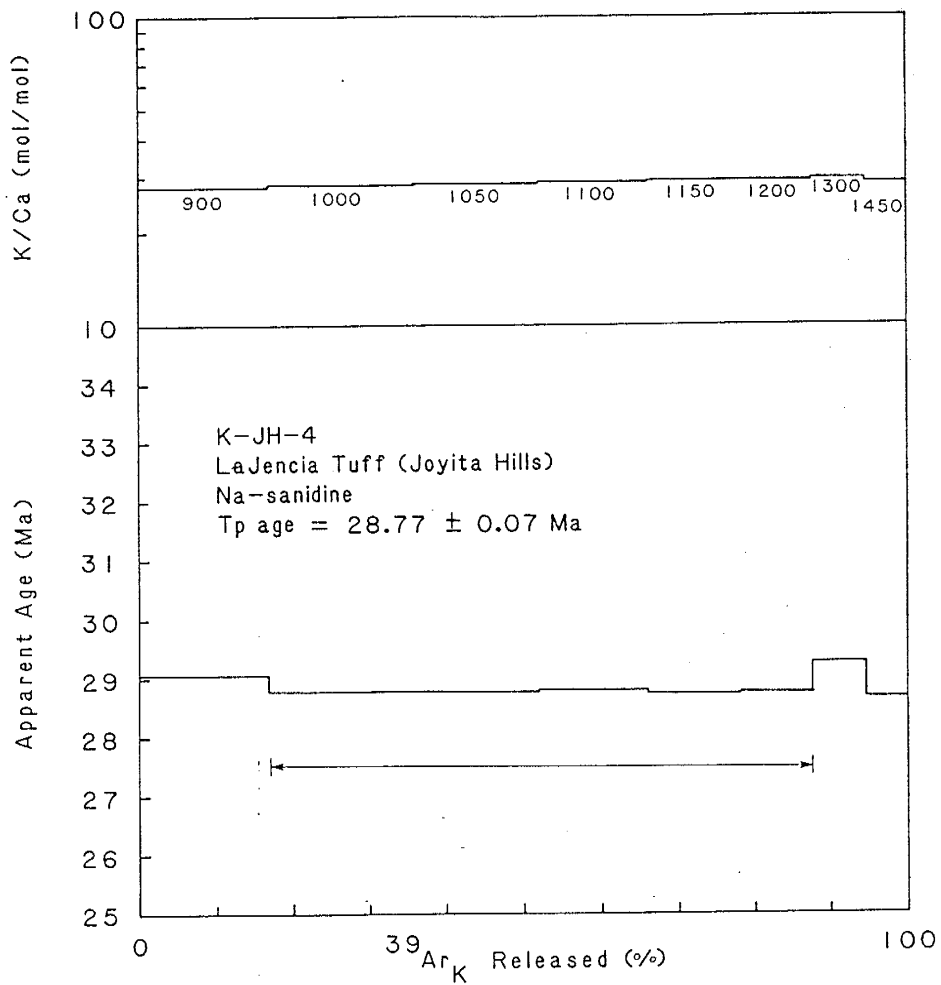


Figure 15. K-JH-4 Na-sanidine age spectrum

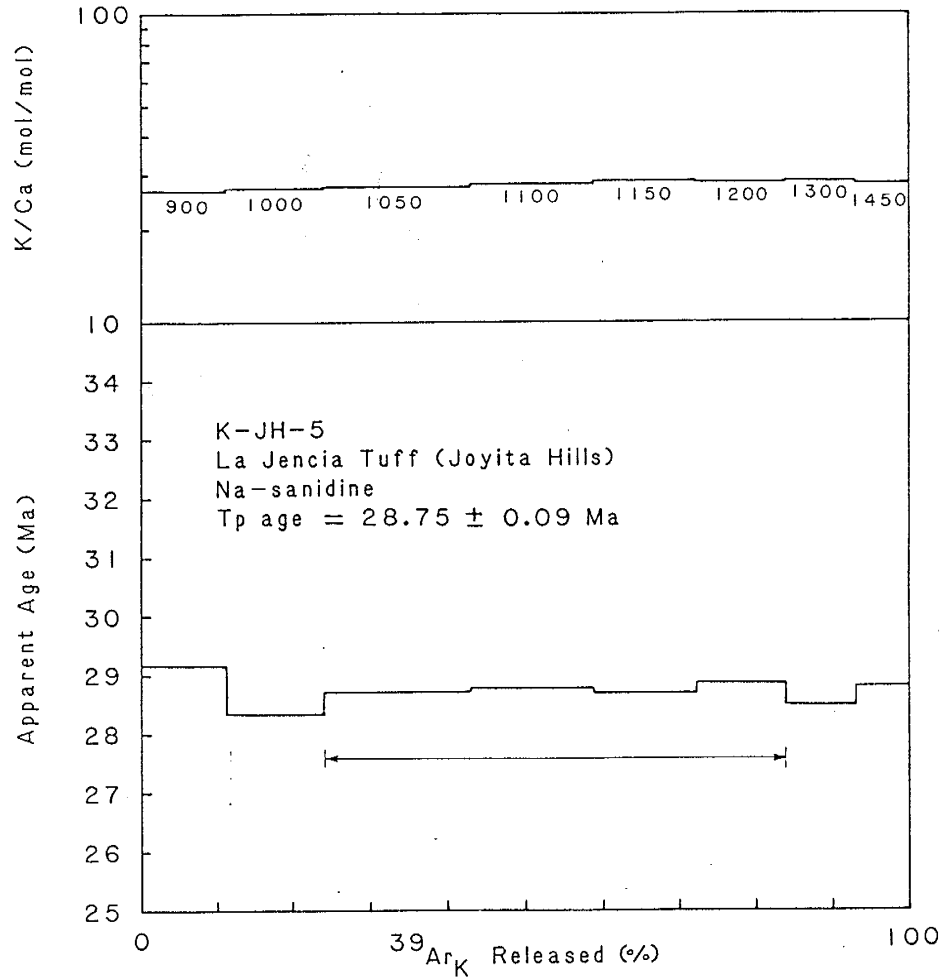


Figure 16. K-JH-5 Na-sanidine age spectrum

Vicks Peak Tuff

Two samples of the Vicks Peak Tuff were collected from different locations and each yielded a pure Na-sanidine separate. Sample K-BM-1, collected in the Bear Mountains, and sample K-JH-10, collected in the Joyita Hills, are both grey, densely welded tuff containing abundant large pumice.

K-BM-1

This sample was degassed in eight temperature steps from 900° to 1450°C. The age spectrum yielded a plateau from the 900° to the 1150°C gas fractions which contain 63.2% of the total $^{39}\text{Ar}_K$ released (fig. 17). The plateau age is 28.83 ± 0.09 Ma, which is the same as the total-gas age. The K/Ca ratio began at approximately 50, increased in the intermediate temperature steps to 65, then decreased to approximately 40.

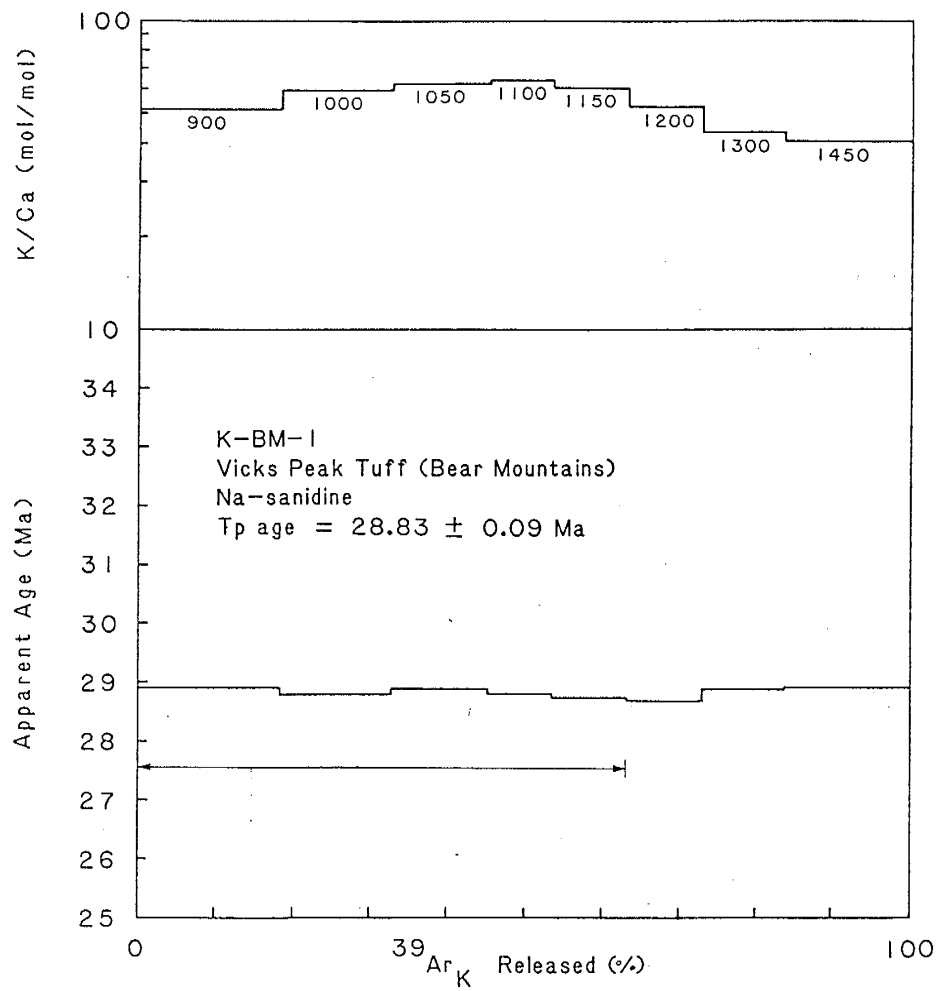


Figure 17. K-BM-1 Na-sanidine age spectrum

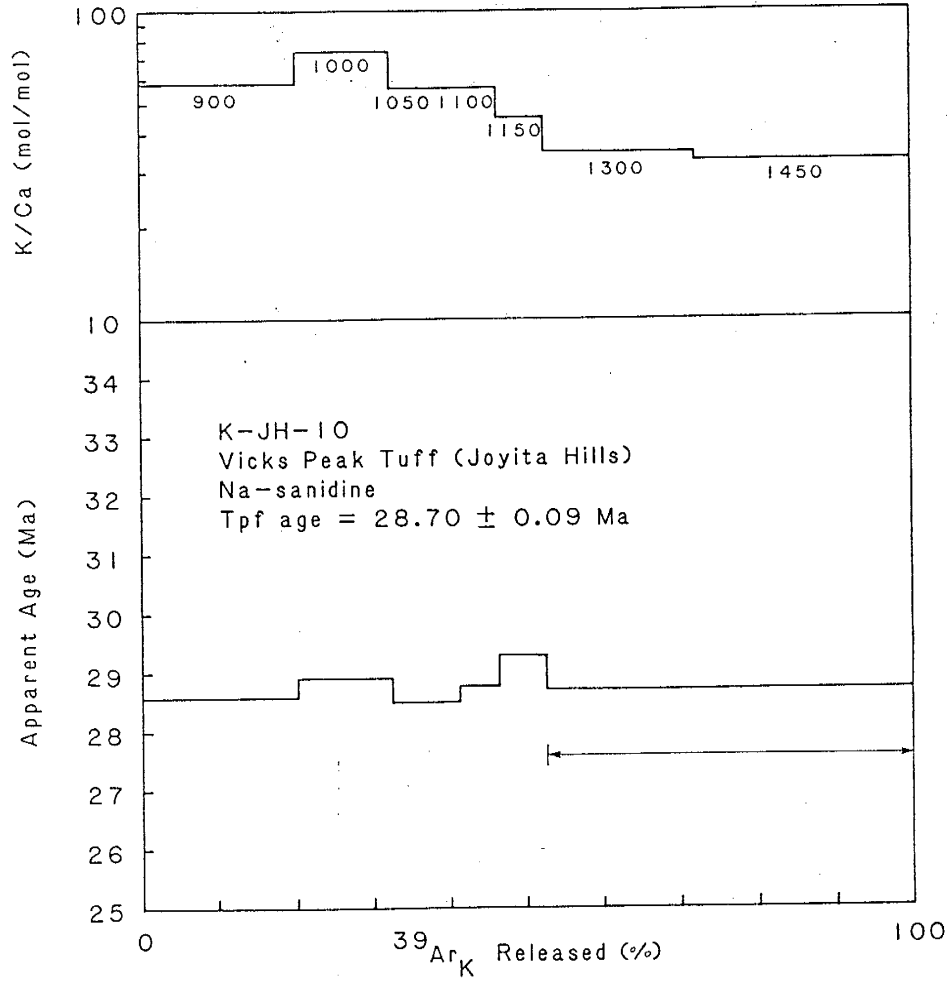


Figure 18. K-JH-10 Na-sanidine age spectrum

K-JH-10

This Na-sanidine sample was degassed in seven temperature steps from 900° to 1450°C. The age-spectrum pattern for this sample is unusual and did not form a plateau (fig. 18). Large proportions of the total $^{39}\text{Ar}_K$ were released at both the low temperature and high temperature steps. The intermediate steps contained small amounts of the $^{39}\text{Ar}_K$ released and are irregular in apparent age. The total gas age is 28.72 Ma. The unusual age spectrum pattern may indicate that the sample's potassium-argon system has been disturbed or it may be an artifact of the heating steps chosen. The last two highest temperature heating steps, 1300° and 1450°C, contain 47.4% of the total $^{39}\text{Ar}_K$ released. The preferred age from these two steps equals 28.70 ± 0.09 Ma, which is statistically the same as the total-gas age. The K/Ca ratio began at approximately 60, increased to a maximum value of 70, then decreased to approximately 35.

Lemitar Tuff

Two biotite separates and one Na-sanidine separate were obtained from two locations. Sample K-TS-1, collected near Torreon Springs, is white, crystal-rich tuff from the upper recrystallization zone of the

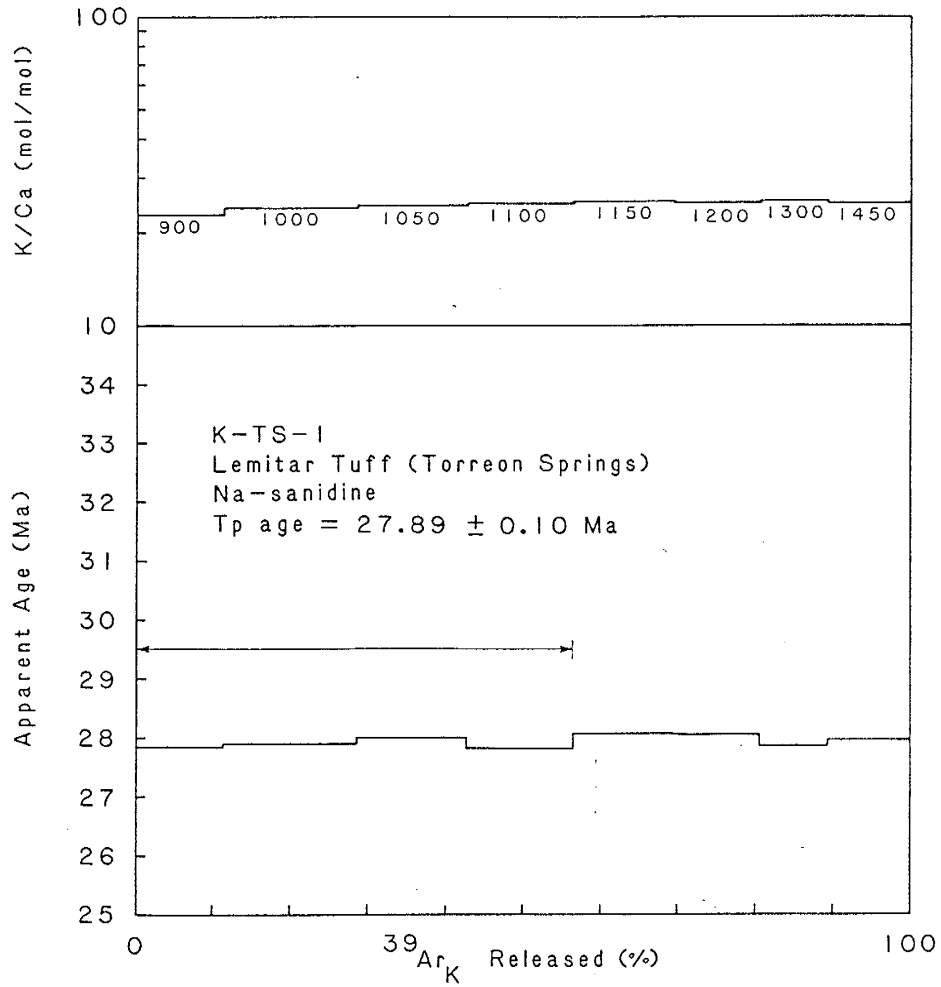


Figure 19. K-TS-1 Na-sanidine age spectrum

Lemitar Tuff. Sample K-JH-24, collected in the Joyita Hills, is black crystal-rich vitrophyre from the base of the unit.

NA-SANIDINE

K-TS-1

This sample was degassed in eight temperature steps from 900° to 1450°C. The sample yielded an age spectrum plateau from the 900° to the 1100°C gas fractions, containing 56.5% of the total $^{39}\text{Ar}_K$ released (fig. 19). The plateau age equals 27.89 ± 0.10 Ma, statistically equivalent to the total-gas age of 27.93 ± 0.09 Ma. The K/Ca ratio remained at a constant value of approximately 20 over all temperature steps.

BIOTITE

K-JH-24

This sample was degassed in six temperature steps from 950° to 1450°C. The age spectrum produced a plateau from the 950° to the 1150°C gas fractions, which contain 72.6% of the total $^{39}\text{Ar}_K$ released (fig. 20). The plateau age equals 28.37 ± 0.06 Ma, statistically the same as the total-gas age of 28.44 Ma. The K/Ca ratio began at a nearly constant

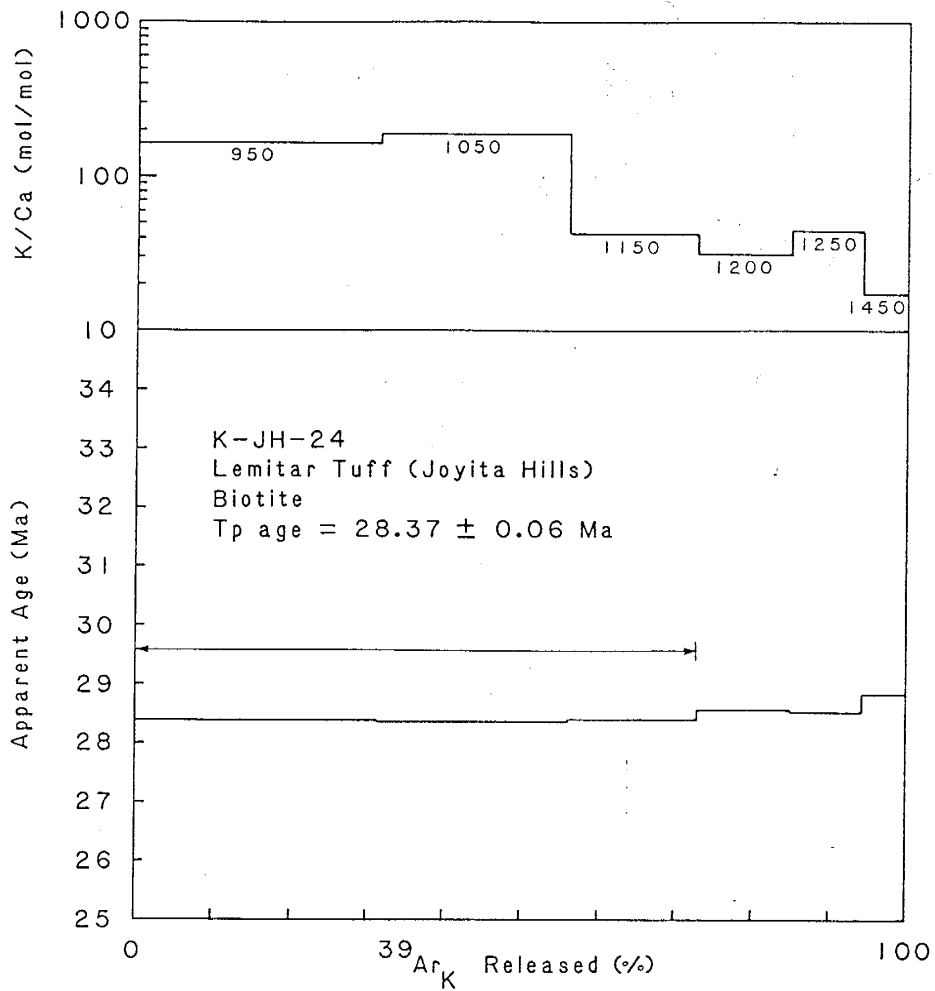


Figure 20. K-JH-24 biotite age spectrum

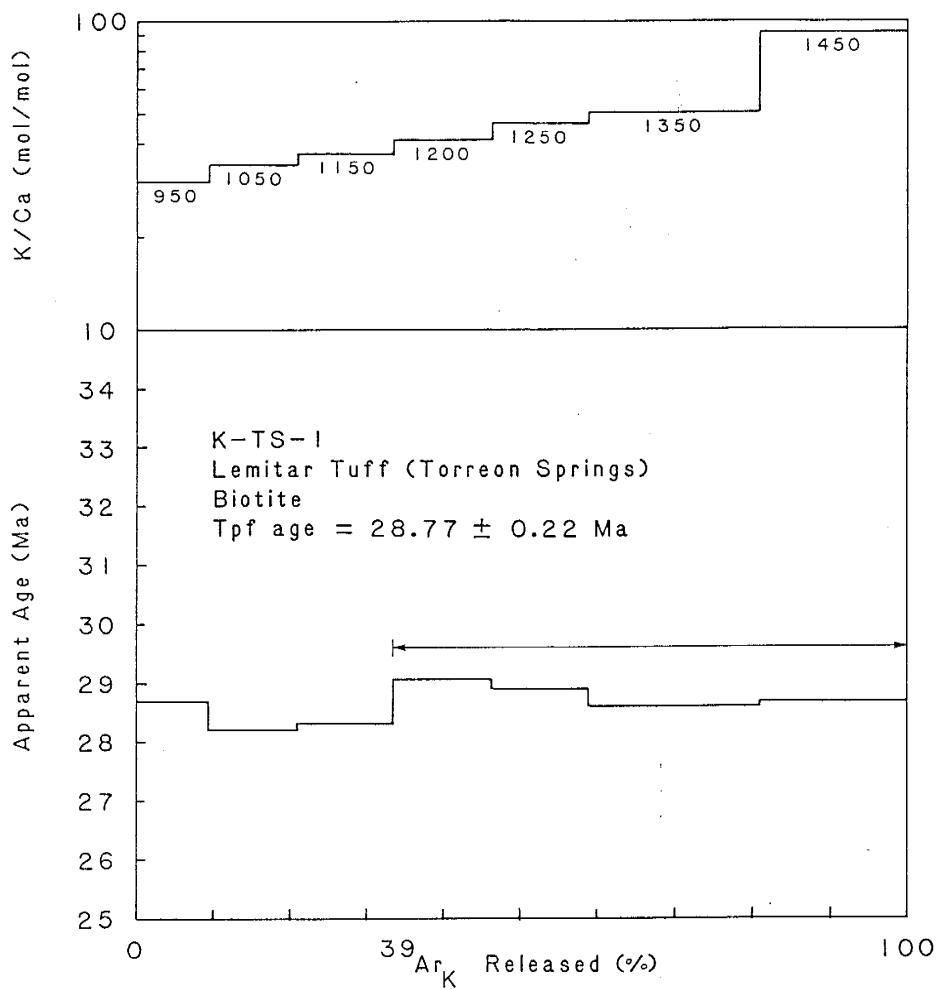


Figure 21. K-TS-1 biotite age spectrum

value of approximately 110, then decreased sharply at intermediate temperatures to a low value of approximately 10.

K-TS-1

This sample was degassed in seven temperature steps from 950° to 1450°C. The age spectrum did not generate a plateau (fig. 21), which suggests that the potassium-argon system of the sample was disturbed. The high-temperature steps should therefore yield the most reliable data. The preferred age for this sample is taken from the 1200° to the 1450°C gas fractions which contain 66.6% of the total $^{39}\text{Ar}_K$ released. The preferred age equals 28.77 ± 0.22 Ma, which is statistically the same as the total-gas age of 28.64 ± 0.28 Ma. The K/Ca ratio began at a value of 20 and steadily increased with increasing temperature to a high value of 90.

South Canyon Tuff

One sample of the South Canyon Tuff collected from the Joyita Hills produced a Na-sanidine separate. The sample, from the upper portion of the unit, is purple-grey, moderately welded tuff.

K-JH-22

This Na-sanidine was degassed in eight temperature steps from 900° to 1450°C. The age spectrum diagram did not yield a plateau (fig. 22). The total-gas age equals 27.60 ± 0.17 Ma. The high-temperature fractions should yield the most reliable data, so a preferred age was generated from the 1100° to the 1450°C gas fractions. The preferred age is 27.76 ± 0.09 Ma, which is statistically the same as the total-gas age. The K/Ca ratio remained at a nearly constant value of approximately 25 over all temperature steps.

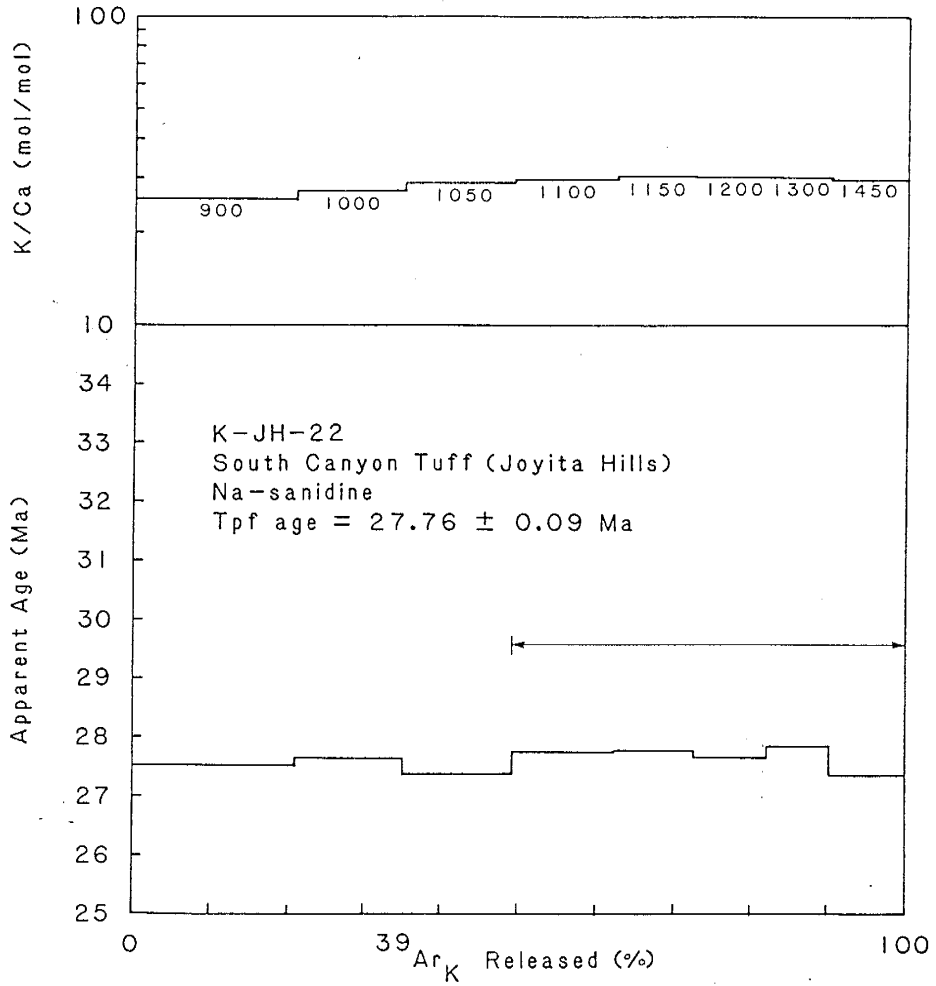


Figure 22. K-JH-22 Na-sanidine age spectrum

INTERPRETATION OF DATA

Interpretation of the $^{40}\text{Ar}/^{39}\text{Ar}$ results included data selection, age calculation, and age evaluation. A set of criteria was developed to choose the most representative data. From this data an age was calculated for each stratigraphic unit. The calculated ages were then evaluated for unit resolution and preservation of stratigraphic order.

Mineral Reliability

The data from each mineral was examined to determine if there was any variation between minerals. A Na-sanidine and biotite reliability comparison was made with the Hells Mesa and Lemitar tuffs. The aspects considered in the comparison were the presence or absence of age-spectrum plateaus, the uncertainty assigned to each sample age, the consistency of the K/Ca ratio within a unit, and the radiogenic yields of the plateau gas fractions (Table 4). An age-spectrum plateau indicates a homogeneous distribution of potassium and $^{40}\text{Ar}^*$ within the mineral grains for the sites being degassed during those temperature steps. The absence of a plateau may indicate a disturbed potassium-argon system. The uncertainty in the sample age is a measure

TABLE 4
Hells Mesa Tuff and Lemitar Tuff Mineral Data

Unit	Mineral	Sample Number	Age + 1 (Ma)	Plateau	K/Ca (mol/mol)	Radiogenic Yield (%)
Hells Mesa Tuff	Na-sanidine	K-JH-26	32.18 ± 0.08	yes	62.5	93.4
	Na-sanidine	K-D-1	32.05 ± 0.10	yes	62.1	97.2
	Na-sanidine	K-BM-3	32.25 ± 0.09	yes	55.1	92.2
	Na-sanidine	K-CM-2	31.77 ± 0.09	yes	59.3	90.8
	Na-sanidine	SU-4-77	31.87 ± 0.11	yes	53.77	77.6
	Biotite	K-JH-26	32.28 ± 0.10	yes	58.5	77.4
Lemitar Tuff	Biotite	K-BM-3	32.34 ± 0.31	no	38.9	83.6
	Biotite	K-CM-2	32.30 ± 0.17	no	118.4	86.6
	Biotite	SU-4-77	32.11 ± 0.19	no	15.0	68.6
	Biotite	SU-5-77	32.09 ± 0.10	yes	11.1	60.3
	Hornblende	K-JH-26	32.25 ± 0.14	NA	0.062	68.3
	Hornblende	K-D-1	31.86 ± 0.10	NA	0.063	61.5
Lemitar Tuff	Na-sanidine	K-TS-1	27.89 ± 0.10	yes	24.5	86.2
Lemitar Tuff	Biotite	K-TS-1	28.77 ± 0.22	no	45.2	74.9
	Biotite	K-JH-24	28.37 ± 0.06	yes	58.0	84.9

of the variance of the data with respect to the average age. The total K/Ca ratio of a mineral is characteristic of the chemical composition of the parent magma. A significant variation in the K/Ca ratio for a given mineral within a unit, may indicate the presence of xenocrystic material in the samples, a disturbed chemical system within the mineral, inhomogeneities, such as tiny inclusions of other minerals or fluids, correlation problems, or vertical zonation within the unit. The radiogenic yield of a gas fraction is a measure of the atmospheric argon contamination, which affects the error in a directly proportional manner.

In this study, biotites tend to yield more irregular data than cogenetic Na-sanidines. Each Hells Mesa and Lemitar tuff Na-sanidine separate formed an age-spectra plateau; while, only 3 out of 7 of the biotite separates formed plateaus. Most analytical uncertainties associated with the biotite ages were greater than those for Na-sanidine ages. The total K/Ca ratios of the Na-sanidines were reasonably consistent and characteristic for a given unit. The biotite total K/Ca ratios, however, vary greatly within each unit and cannot be considered as an identifying feature of the units. The radiogenic yields of the plateau portions of Na-sanidine spectra average about 90%, whereas the radiogenic yields of biotite spectra range from 60% to 77%, adding to the uncertainty of the biotite ages.

Several theories have been proposed to explain the irregular behavior of the biotite mineral separates during argon extraction in the laboratory. Biotite, a hydrous phyllosilicate, experiences dehydration and delamination during laboratory heating in a vacuum. These reactions alter the structure of the mineral, and affect the degassing pattern (Harrison, 1983). The biotite grains may also contain interlayered brittle micas, which might cause a disturbance of the age spectrum. However, due to the difficulty in obtaining detailed x-ray diffraction patterns on biotite separates, the presence of two interlayered mineral phases was not proven in this study.

In general, biotite separates produce less precise data than the cogenetic Na-sanidine and hornblende separates. As a result, the plateau ages of Na-sanidine and hornblende were considered more reliable than biotite ages for these tuffs (J.F. Sutter, 1984, oral commun.). The closed nature of the potassium-argon system in these Na-sanidines has an interesting implication for argon retention in potassium feldspars. Foland (1974) suggested that perthitization of potassium feldspar allows diffusive loss of ^{40}Ar at very low temperatures. The Na-sanidines analyzed in this study are cryptoperthitic (J.I. Lindley, 1984, written comm.) but show no indication of diffusive loss of ^{40}Ar . This suggests that the effective diffusion distance for argon in cryptoperthitic Na-sanidines must be less than or equal to the width of the perthite lamellae.

Assignment of ages

The Na-sanidine data for each unit was evaluated before the biotite and hornblende data. In each mineral group, the critical value test (Appendix I) was used to exclude individual sample ages from the population. The standard deviation on the mean was calculated from the remaining dates using:

$$SD = [\sum \sigma_i^2 / n^2]^{1/2}$$

σ_i is the standard deviation on each age and n is the number of ages averaged (A.L. Gutjahr, 1984, written commun.). The averages for the different minerals were then compared and tested with the critical-value test. If the mineral ages were statistically similar, a total average was calculated for the unit. However, if the mineral ages differed, the sample data was reexamined and the best data used for the average age. This data is presented in Table 4.

HELLS MESA TUFF

Five Na-sanidine separates were analyzed and displayed age-spectrum plateaus. The critical-value test applied to these plateau ages indicated that two samples had ages statistically different from the other samples. As a result, K-CM-2 and SU-4-77 were eliminated; the average of the remaining three sample ages was 32.17 ± 0.05 Ma.

Five biotite separates were analyzed; however, only two produced age-spectrum plateaus. The critical value test showed that the two plateau ages were statistically similar. Therefore, the two biotite plateau ages were averaged to produce an age of 32.18 ± 0.07 Ma.

Two hornblende samples were analyzed by the three-step fusion method. The critical value test indicated that the two hornblende ages were not the same at the 95% confidence level and therefore were not averaged but treated as two separate ages.

An evaluation of the average mineral ages indicated that no age difference could be detected between the Na-sanidine and biotite plateau ages and the age of hornblende sample K-JH-26. The critical-value test demonstrated that hornblende sample K-D-1 was statistically younger than the other ages; consequently, it was eliminated. The remaining Na-sanidine, hornblende, and biotite ages were averaged resulting in the unit age 32.18 ± 0.04 Ma. The large uncertainties associated with the biotite ages were balanced by the number of ages averaged.

There are several other ways in which the Hells Mesa Tuff data may be treated. Inclusion of the biotite preferred ages, which agree with the plateau ages at the 95% confidence level, results in an average age of 32.21 ± 0.05 Ma. Assuming that the variation in ages is not real but due to underestimation of the analytical error, the critical value test can be disregarded. The average of all plateau ages is 32.07 ± 0.03 Ma and the average of all plateau and preferred ages is 32.11 ± 0.04 Ma. These alternative methods for manipulating the data are not as strict as

the initial method and leave more room for doubt.

LA JENCIA TUFF

The two Na-sanidine separates from the La Jencia Tuff both displayed age-spectrum plateaus. The critical value test indicated that the plateau ages were statistically identical. The average of these plateau ages produced the unit age of 28.76 ± 0.06 Ma.

VICKS PEAK TUFF

Two Na-sanidine separates were analyzed, but only one produced a plateau. Na-sanidine sample K-BM-1 yielded a plateau age of 28.83 ± 0.09 Ma. The critical value test demonstrated that the preferred age for sample K-JH-10 was statistically equivalent to the K-BM-1 plateau age. The two ages were averaged to give a unit age of 28.76 ± 0.06 Ma.

LEMITAR

The Na-sanidine sample, K-TS-1, was analyzed and produced a plateau age of 27.89 ± 0.10 Ma. Two biotites were analyzed and sample K-JH-24 yielded a plateau age of 28.37 ± 0.06 Ma. Sample K-TS-1 biotite did not produce an age spectrum plateau, so a preferred age of 28.77 ± 0.22 was assigned.

An evaluation of the Na-sanidine and biotite ages indicated that they differ significantly. The two Lemitar Tuff samples were collected from the extremes of the outflow sheet. K-JH-24 was taken from the thick, basal vitrophyre in the Joyita Hills, whereas K-TS-1 was collected from the vapor-phase recrystallization zone (Smith, 1960) at the top of the unit near Torreon Springs.

The vitrophyre is the zone of most intense welding in the unit. The vapor phase was squeezed out of this zone shortly after emplacement, which allowed the glass shards and pumice to be preserved in a glassy state. No devitrification has occurred and all phenocrysts are fresh and unaltered.

The vapor-phase recrystallization zone has undergone complete devitrification and recrystallization of the glass shards and pumice in the presence of vapors rising from the main body of the cooling tuff. Void spaces between shards have been filled with alkali feldspars and silica minerals deposited from the vapor phase and the rock is hard and dense, even though it is only slightly welded. The biotite phenocrysts are oxidized to a coppery color, but the Na-sanidine phenocrysts appear unaltered.

The basal vitrophyre and upper vapor-phase recrystallization zones represent two extremes in the cooling history of the tuff. The disparate nature of these two zones in the tuff unit suggest that the unit was not sampled properly for geochronology. The question remains; which of these sample ages is the best for the Lemitar Tuff?

There are several possible interpretations of the Lemitar Tuff $^{40}\text{Ar}/^{39}\text{Ar}$ data: 1) the biotite age from the Joyita Hills vitrophyre is anomalously old; 2) the Na-sanidine age from the Torreón Springs recrystallization zone is anomalously young; and, 3) both ages are correct for the Lemitar Tuff. The biotite from the Torreón Springs sample did not form an age-spectrum plateau and was disregarded.

There are two explanations for why the biotite separate from the Joyita Hills vitrophyre sample may yield an anomalously old age. The biotite may contain excess ^{40}Ar which was not evident in the age spectrum. The age spectrum did not exhibit the saddle shape characteristic of a biotite containing excess ^{40}Ar (Lanphere and Dalrymple, 1976), but other studies (Foland, 1983) have shown that biotites with excess argon may still exhibit age spectrum plateaus. Alternatively, the biotite may have lost a portion of its potassium content through leaching or weathering. However, the whole-rock major-element chemical analysis and thin section examination showed no evidence for alteration or weathering of the vitrophyre sample.

The possible data interpretation that the Torreón Springs sample Na-sanidine age is anomalously young gives rise to three explanations. The Torreón Springs sample may have gained potassium during a hydrothermal alteration event, much younger than the tuff. However, the whole-rock major-element chemical analysis and thin section examination

show no evidence of potassium alteration. In addition, a detailed analytical study of potassium metasomatized tuffs in the Socorro area (J.I. Lindley, 1984, written commun.) has shown that Na-sanidine phenocrysts are not affected by slight to moderate levels of alteration.

A second explanation is that the Na-sanidine phenocrysts have lost a portion of their $^{40}\text{Ar}^*$ component by volume diffusion. This is unlikely, as the Na-sanidine phenocrysts in the other tuff units are chemically and structurally similar to those in the Lemitar Tuff (J.I. Lindley, 1984, written commun.) and do not show any evidence of $^{40}\text{Ar}^*$ loss.

The third explanation for the anomalously young Torreon Springs Na-sanidine age is that the potassium-argon system in the Lemitar Tuff was reset by emplacement of the overlying South Canyon Tuff. The Torreon Springs sample was collected from within 50 m of the top of the unit, which is directly overlain by more than 100 m of South Canyon Tuff. The Torreon Springs Na-sanidine age is indistinguishable from the age of the South Canyon Tuff. This explanation is unlikely due to the following argument. The argon blocking temperature of Na-sanidine is probably on the order of 300° to 350°C (J.F. Sutter, 1984, oral commun.). To reset the potassium-argon system in the Na-sanidine phenocrysts, this temperature must have penetrated 50 meters into the top of the Lemitar Tuff unit. Taking into account the poor heat conduction properties of rock, a circulating fluid phase would be necessary to conduct the heat into the tuff. However,

there is no evidence in the thin section or in the field for the presence of a hot circulating fluid phase. In addition, lower temperatures would have caused only partial loss of ^{40}Ar from the Na-sanidine phenocrysts which then would have exhibited a disturbed age spectrum.

The final interpretation of the data is that both ages are correct for the Lemitar Tuff. The younger age of the Torreon Springs sample may be due to a time break during the eruption of the tuff. However, the section of Lemitar Tuff exposed near Torreon Springs shows no breaks in the welding of the unit. The ages may represent the time span of the eruption of the Lemitar Tuff, since one was collected from the base of the unit and the other from near the top. This interpretation is unlikely with the present models for ash-flow tuff eruptions. The ages may actually be the same but appear different due to underestimation of analytical error. For the Torreon Springs Na-sanidine age to agree with the Joyita Hills biotite age, at the 95% confidence level, the analytical error must be approximately doubled. This is too great a change in the analytical uncertainty to be attributed to underestimation.

The difference in the $^{40}\text{Ar}/^{39}\text{Ar}$ ages for the Lemitar Tuff cannot be easily explained and care must be exercised in assigning an age to this unit. The presence of an extremely thick section of basaltic andesite, deposited between the Lemitar Tuff and the overlying South Canyon Tuff in the Joyita Hills, suggests that the ages of these two tuff units may

be different. At the moment, it is felt that the plateau age of 28.37 ± 0.06 Ma for the biotite from the vitrophyre in the Joyita Hills (K-JH-24) should be used as the unit age for the Lemitar Tuff, until Na-sanidine samples from the interior portions of this unit can be collected and analyzed.

SOUTH CANYON TUFF

One Na-sanidine sample was analyzed and failed to produce an age-spectrum plateau. The preferred age for sample K-JH-22, 27.76 ± 0.09 Ma, is the best estimate currently available for the age of this unit.

Evaluation of Unit Ages

The critical-value test was used to verify unit age discrimination (Table 5). The ages of Hells Mesa Tuff and La Jencia Tuff have a critical value of 0.09 Ma and vary by 3.45 Ma. As a result, the ages of these units are easily distinguished from one another. The ages of La Jencia Tuff and Vicks Peak Tuff have a critical value of 0.12 Ma and vary by 0.0 Ma. These unit ages vary less than the critical value, and cannot be distinguished. The ages of Vicks Peak Tuff and Lemitar Tuff have a critical value of 0.14 Ma and vary by 0.39 Ma. These unit ages are statistically different and can be differentiated, provided that the

TABLE 5
Ash-Flow Tuff $^{40}\text{Ar}/^{39}\text{Ar}$ Unit Ages

Unit	Sample Number	Mineral	Sample	Age + 1 (Ma)		C.V. (Ma)	Diff. (Ma)
				Mineral	Unit		
South Canyon Tuff	K-JH-22	Na-sanidine	27.76 ± 0.09	27.76 ± 0.09	27.76 ± 0.09	0.21	0.61
	K-TS-1	Na-sanidine	27.89 ± 0.10	27.89 ± 0.10			
Lemitar Tuff	K-TS-1	Biotite	28.77 ± 0.22				
	K-JH-24	Biotite	28.37 ± 0.06	28.37 ± 0.06	28.37 ± 0.06	0.14	0.39
Vicks Peak Tuff	K-JH-10	Na-sanidine	28.70 ± 0.09	28.76 ± 0.06	28.76 ± 0.6		
	K-BM-1	Na-sanidine	28.83 ± 0.09				
La Jencia Tuff	K-JH-4	Na-sanidine	28.77 ± 0.07	28.76 ± 0.06	28.76 ± 0.06	0.12	0.00
	K-JH-5	Na-sanidine	28.75 ± 0.09				
Hells Mesa Tuff	K-JH-26	Na-sanidine	32.18 ± 0.08			0.09	3.42
	K-D-1	Na-sanidine	32.05 ± 0.10				
	K-BM-3	Na-sanidine	32.25 ± 0.09	32.17 ± 0.05			
	K-CM-2	Na-sanidine	31.77 ± 0.09				
	SU-4-77	Na-sanidine	31.87 ± 0.11				
	K-JH-26	Biotite	32.28 ± 0.10				
	K-BM-3	Biotite	32.34 ± 0.31		32.18 ± 0.07		
SU-4-77	K-CM-2	Biotite	32.30 ± 0.17				
	SU-4-77	Biotite	32.11 ± 0.19				
	SU-5-77	Biotite	32.09 ± 0.10				
K-JH-26	K-JH-26	Hornblende	32.25 ± 0.14	32.25 ± 0.14			
	K-D-1	Hornblende	31.86 ± 0.10				

age for the Lemitar Tuff is confirmed by additional Na-sanidine analyses. The ages of Lemitar Tuff and South Canyon Tuff have a critical value of 0.21 Ma and vary by 0.61 Ma. Therefore, these units may be distinguished, provided that both of these unit ages can be confirmed by additional Na-sanidine analyses.

The ages were additionally examined for agreement with the stratigraphic order. The stratigraphic order of the units in ascending order is Hells Mesa Tuff, La Jencia Tuff, Vicks Peak Tuff, and Lemitar Tuff, South Canyon Tuff. This stratigraphic order is not violated by the $^{40}\text{Ar}/^{39}\text{Ar}$ ages obtained in this study.

DISCUSSION

In an attempt to evaluate the results of this study, three questions were considered: 1) How does the data solve the thesis problems?; 2) How does the data relate to the geologic context?; and, 3) Is the $^{40}\text{Ar}/^{39}\text{Ar}$ method appropriate for this type of study? Each of these topics will be discussed individually.

Thesis Problem

The objectives of the thesis were: 1) to obtain precise ages for the five ash-flow tuff units in the Socorro area; 2) to resolve the observed discrepancy in conventional potassium-argon ages between cogenetic biotite and Na-sanidine phenocrysts; and, 3) to correlate the outflow sheets with their source cauldrons by age relationships.

HIGH-PRECISION DATING

The Hells Mesa, La Jencia, and Vicks Peak tuffs were precisely dated by multiple analyses. The uncertainties assigned to the ages are sufficiently small so that differentiation and correlation with units in

other parts of the volcanic field are potentially possible.

The study failed to produce reliable age estimates for the Lemitar and South Canyon tuffs; these units did not have multiple Na-sanidine analyses performed. Therefore, the Lemitar Tuff age is currently based on the data from a single biotite analysis, and the South Canyon Tuff age is based on the data from one Na-sanidine analysis. Thus, at the current time, the ages of these units are not sufficiently reliable for comparison with units in other areas of the volcanic field and the first thesis objective is only partially fulfilled. However, subsequent analyses of multiple Na-sanidine samples from the Lemitar Tuff and South Canyon Tuff should provide precise age estimates for these units that can be used in regional correlation studies.

NA-SANIDINE-BIOTITE CONVENTIONAL K-AR AGE DISCREPANCY

Conventional potassium-argon ages of cogenetic Na-sanidine and biotite phenocrysts show a discrepancy, with Na-sanidine yielding consistently younger apparent ages than biotite (fig. 3). In this study, $^{40}\text{Ar}/^{39}\text{Ar}$ age-spectrum concordancy differed from one mineral to another. However, the lack of significant variation between plateau or preferred ages of biotite, Na-sanidine, and hornblende in the Hells Mesa Tuff implies that discordance in the conventional potassium-argon ages was due to analytical methodology, and not to argon retention differences in these minerals.

The following conclusions concerning discrepancies between biotite and Na-sanidine conventional potassium-argon ages, have been reached. Since these ash-flow tuffs have cooled instantaneously with respect to their ages, the potassium-argon age discrepancy is not likely due to argon blocking temperature differences between the two minerals. Since there is no discrepancy in the $^{40}\text{Ar}/^{39}\text{Ar}$ ages, it is unlikely that the conventional age discrepancy is due to differences in argon retention caused by the different crystal structures of biotite and Na-sanidine. It is also not likely that this apparent age discrepancy is due to alteration by low-temperature hydrothermal fluids or by surficial weathering. The samples of the tuffs which showed the apparent age discrepancy are not visibly altered or weathered. In addition, Clauer (1981) has shown that the potassium-argon age of biotite would be lowered relative to potassium feldspar in a weathering situation. The most likely cause of the conventional age discrepancy between Na-sanidine and biotite is incomplete extraction of argon from the Na-sanidine in the laboratory (McDowell, 1983). Feldspars yield a more viscous melt than biotites; as a result, higher temperatures and longer heatings are required for complete argon extraction. Heating techniques used for most minerals can leave as much as 15% of the $^{40}\text{Ar}^*$ trapped in a feldspar sample. Argon extraction with elevated temperatures and a fluxing agent may still leave 2% residual $^{40}\text{Ar}^*$ (McDowell, 1983), which is sufficient to cause the age discrepancies in the ash-flow tuff data. Also, small discrepancies may be caused by impurities in the mineral separates. Separates for conventional potassium-argon dating are not

often hand-picked for purity, due to the large quantities of minerals required, usually in excess of 0.5 grams. Thus, impurities such as xenocrysts, groundmass, and glass fragments may be included in the analysis. Glass or fine-grained groundmass, containing potassium and having lost argon by diffusion, may cause anomalously young ages. Xenocrysts of older material or that contain excess argon may cause anomalously old ages.

CAULDRON CORRELATION

The last thesis objective was to correlate the outflow sheets with their source cauldrons using age relationships. Due to extensive hydrothermal alteration in known source cauldrons and lack of known cauldrons for some units, the evaluation of this objective was limited to one $^{40}\text{Ar}/^{39}\text{Ar}$ cauldron-fill sample from the Hells Mesa Tuff. The plateau age for the Na-sanidine from the cauldron-fill facies is younger, using the critical value test, than the calculated unit age for the Hells Mesa Tuff outflow sheet.

At least six explanations are possible for the apparent discrepancy between the Na-sanidine cauldron-fill age and the the Hells Mesa Tuff unit age. First, the apparent age difference may not represent a real time lapse, but rather a slight potassium metasomatism of the cauldron-fill sample. Whole-rock major-element chemical analysis

indicated that the cauldron-fill sample has a K_2O content that is approximately 1.26% greater than the mean of the outflow-sheet samples. Most of the exposed cauldron-fill tuff has undergone potassium metasomatism and manganese mineralization (Eggleston, 1982). Although the dated sample was collected from outside the area of known alteration, it may have been slightly affected (C.E. Chapin, 1983, oral commun.). The Na-sanidine phenocrysts may have absorbed approximately 1% excess potassium into their structures, causing the age reduction. This explanation is unlikely, however, since a detailed analytical study of the potassium metasomatized ash-flow tuffs in the Socorro area (J.I. Lindley, 1984, written commun.) has shown that, except for severely altered samples, the Na-sanidine phenocrysts are totally unaffected by this type of alteration.

Second, the loss of a portion of the $^{40}Ar^*$ trapped in the mineral is another means of reducing the sample age. Two mechanisms, involving the cooling history of the cauldron, may have accomplished this for the cauldron-fill sample. The cauldron may have remained an area of high heat flow for a significant period of time following the cessation of ash-flow volcanism, because of the great thickness of the cauldron-fill tuff, the presence of an underlying pluton, and post-resurgence filling of the moat with local ash-flow tuffs and lava flows (Eggleston, 1982). Cauldron development, from the major ash-flow eruption through resurgence, may occur in less than 100,000 years (Smith and Bailey, 1968). The elevated temperatures would cause the thick accumulation of

cauldron-fill tuff to cool slowly compared with the outflow sheet. During cooling, the partially disordered monoclinic Na-sanidine phenocrysts may have undergone an increase in ordering of aluminum and silica ions. The more ordered potassium feldspars may retain less argon than Na-sanidine (Foland, 1974). A small amount of argon loss associated with increased ordering may be sufficient to explain the reduced age. In addition, slow cooling may cause the exsolution of potassium and sodium-bearing phases into a perthitic structure. Perthitic exsolution lamellae reduce the effective grain size for diffusive loss of argon (Foland, 1974) and diffusion may occur at lower temperatures. X-ray diffraction analysis of the cauldron-fill Na-sanidine is necessary to evaluate these possibilities.

Third, the high temperatures in the cauldron area may have allowed the cauldron-fill tuff to cool slowly and the minerals to pass through their argon blocking temperatures after the outflow sheet had cooled. The argon blocking temperature of Na-sanidine has not been measured but studies of other potassium feldspars indicate that the argon blocking temperature increases with decreasing order (J.F. Sutter, 1984, oral commun.). Therefore, Na-sanidine, the most disordered potassium feldspar, likely has the highest argon blocking temperature of potassium feldspars, probably in excess of 300°C; and thus, biotite and sanidine should yield a similar age for the cauldron-fill tuff.

Fourth, the apparent age difference between cauldron-fill and outflow-sheet Na-sanidines may represent a true time lapse in the development of the cauldron. The biotite cauldron-fill sample failed to produce a plateau; thus, an anomalous age may have been concealed by the large uncertainty associated with the preferred age. The cauldron-fill tuff may have been sampled from the upper part of the unit which represented the last material erupted. This material may have been erupted some time after the bulk of the ash-flow tuff, and its younger age may indicate the time span of the eruptive activity. However, this is unlikely according to the accepted models for ash-flow tuff eruptions and cauldron formation (Smith and Bailey, 1968).

Fifth, the relatively young cauldron-fill Na-sanidine age may involve underestimation of the analytical error. Assuming that there is no difference between the cauldron-fill and the outflow sheet ages, the analytical error would have to be on the order of 0.6% higher to satisfy the critical-value test. This is too great a difference to be attributed to underestimation of error.

Sixth, the area from which the cauldron-fill sample was collected may have been affected by a post-cauldron thermal anomaly which reset the mineral potassium-argon systems through diffusive loss of ^{40}Ar . The fact that both of the samples that gave anomalously young ages in this study (the Lemitar Tuff sample from Torreón Springs and the

cauldron-fill Hells Mesa Tuff sample) were collected within 10 km of each other (fig. 1) suggests this possibility.

Although the cauldron-fill Na-sanidine age is younger than the Hells Mesa Tuff outflow-sheet age, the ages are sufficiently close to correlate these two facies. In addition, the total K/Ca ratios of the Na-sanidines in the Hells Mesa Tuff are reasonably consistent and confirm the correlation. Therefore, this thesis objective was partially fulfilled.

Geologic Context

The data generated in this study relates to the geologic setting in three principle ways. On a local scale, the data represents the stratigraphic order of the tuff units. On a regional scale, the data relates to the development of the Mogollon-Datil volcanic field and the evolution of the Rio Grande rift.

STRATIGRAPHIC ORDER

Since the units were too closely spaced temporally to be distinguished by other radiometric dating techniques, the $^{40}\text{Ar}/^{39}\text{Ar}$ dating method revealed the ages and confirmed the stratigraphic order of the five ash-flow tuff units (Table 5).

The ages of the units were found to be slightly to moderately different than previously accepted (figs. 3, 23). The four upper units are more closely spaced and there is a significant time lapse between these units and the Hells Mesa Tuff. The Hells Mesa Tuff is slightly younger than the 33.1 Ma age estimated from conventional potassium-argon analyses (Osburn and Chapin, 1983a). The La Jencia Tuff is younger than the estimated age and older than the conventional potassium-argon ages, which average 24.8 Ma. The unit age was previously estimated to be 30.9 Ma from conventional potassium-argon ages of overlying basaltic andesites and cauldron-fill units (Osburn and Chapin, 1983a). The age of Vicks Peak Tuff cannot be distinguished from the age of La Jencia Tuff. The Vicks Peak Tuff was previously dated by the fission-track method which yielded a meaningless age. However, these two units can be differentiated on the basis of the K/Ca ratios of the Na-sanidine phenocrysts. The age of Lemitar Tuff, approximately

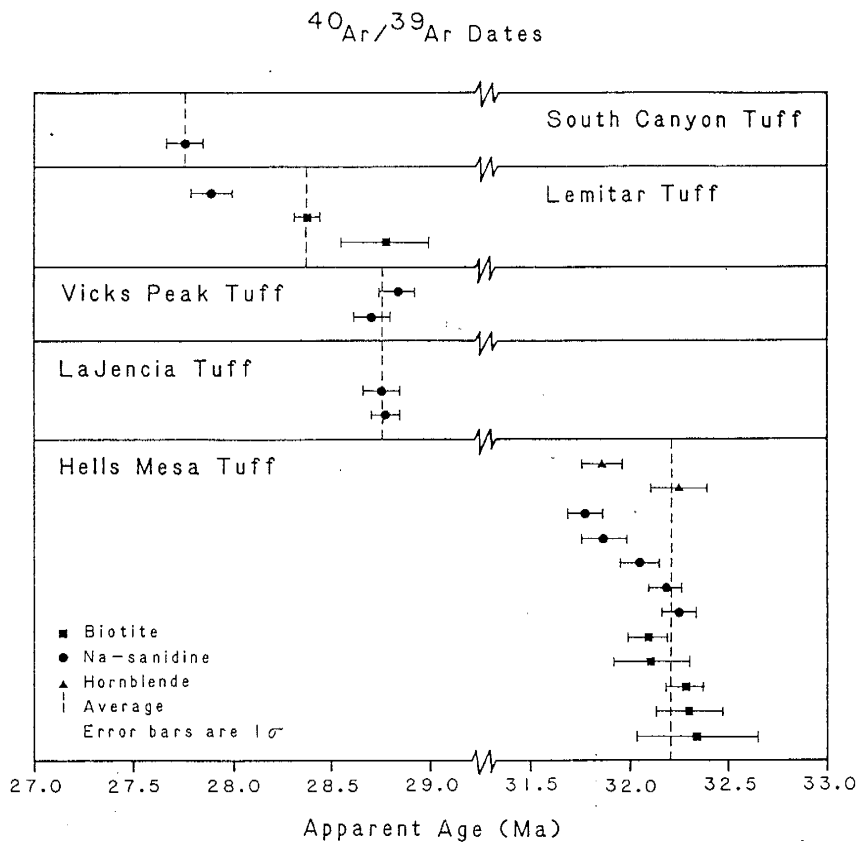


Figure 23. $^{40}\text{Ar}/^{39}\text{Ar}$ dates

the same as that determined with the conventional potassium-argon method, is now more precisely known. The South Canyon Tuff is older than the 26.5 Ma age indicated by conventional potassium-argon dating.

The $^{40}\text{Ar}/^{39}\text{Ar}$ ages for the samples collected in the Joyita Hills agree very well with the exposed stratigraphic sequence (Table 6). All five tuff units are present, they are unaltered, the emplacement sequence is easily discernable, and the area is accessible. Detailed geologic mapping and chemical analyses have been performed on the units in this area; thus, the ash-flow tuff units are well characterized (Appendix IV). For these reasons, the section of the five ash-flow tuffs exposed in the Joyita Hills should be regarded as the standard reference section of these units for geochronology. The section should be used for comparisons and correlations in future geochronologic studies in the Socorro area.

VOLCANIC FIELD

The precise $^{40}\text{Ar}/^{39}\text{Ar}$ ages of the ash-flow sheets have important implications in understanding the development of the Mogollon-Datil

TABLE 6
Joyita Hills Geochronologic Reference Section

Unit	Sample	Mineral	Age ± 1 (Ma)	K/Ca (mol/mol)
South Canyon Tuff	K-JH-22	Na-sanidine	27.76 \pm 0.09	30
Lemitar Tuff	K-JH-24	Biotite	28.37 \pm 0.06	58
Vicks Peak Tuff	K-JH-10	Na-sanidine	28.70 \pm 0.09	33
La Jencia Tuff	K-JH-5	Na-sanidine	28.75 \pm 0.09	28
	K-JH-4	Na-sanidine	28.77 \pm 0.07	29
Hells Mesa Tuff	K-JH-26	Na-sanidine	32.18 \pm 0.08	62
	K-JH-26	Biotite	32.28 \pm 0.10	58
	K-JH-26	Hornblende	32.25 \pm 0.14	0.062

volcanic field. The time lapse between the Hells Mesa Tuff and the overlying units indicates that two distinct periods of volcanism occurred in the northeastern portion of the field, and has important implications to petrogenesis.

The Hells Mesa Tuff, an important marker bed, is the first major unit of rhyolitic composition, which contains abundant quartz phenocrysts. Units of the Datil Group below the Hells Mesa Tuff are quartz-poor and generally more intermediate in composition (Osburn and Chapin, 1983b). The Hells Mesa Tuff is chemically and texturally zoned from quartz latite to rhyolite (Appendix IV). This ascending increase in silica content in the outflow sheet is the opposite of the zoning trend normally observed in tuffs. These observations may suggest that the Hells Mesa Tuff signals a change in the nature of volcanism in the northeastern Mogollon-Datil volcanic field.

The next major ash-flow unit, the La Jencia Tuff, was not emplaced for more than three million years in this area of the field. A recognizable unconformity exists between the Hells Mesa Tuff and the overlying units with evidence that a significant amount of erosion and channelling took place. Paleovalleys, cut in the Hells Mesa Tuff and filled with La Jencia Tuff, are known to occur in the Joyita Hills (Smith and others, 1983), on Grey Hill west of Magdalena (Wilkinson, 1976), in the Abbe Springs area (Mayerson, 1979), and in the Gallinas Mountains (Coffin, 1981; Laroche, 1981; Brouillard, 1984).

The four upper ash-flow tuffs were all erupted within a time period of approximately one million years. These closely spaced, major, ash-flow eruptions may reflect changes in regional tectonics.

RIO GRANDE RIFT

The time of initial rifting in the Socorro area has been estimated from detailed mapping and stratigraphic studies that have utilized the major regional ash-flow tuff sheets as time-stratigraphic markers (Chapin and Seager, 1975; Chapin, 1979; Chamberlin, 1978; 1983; Osburn and Chapin, 1983a; 1983b). Chapin and Seager postulated that the onset of extensional faulting, associated with the opening of the rift, broke the roof of an Oligocene batholith and permitted the intrusion of numerous stocks and dikes into a broad zone of normal faults. On the basis of the few conventional ages available at that time, they estimated regional extension to have begun after 30 to 31 Ma and before 28 Ma. The $^{40}\text{Ar}/^{39}\text{Ar}$ ages of this study and the new I.U.G.S. decay constants indicate, using the evidence of Chapin and Seager, that regional extension began in the Magdalena area before 29 Ma.

A more recent study (Chamberlin, 1978; 1983) focused on the Lemitar Mountains, north of Socorro, where the ash-flow tuff sheets dated in this study have been progressively offset by a series of extensional, domino-style, normal faults. Chamberlin reconstructed the area prior to each episode of faulting and showed that regional extensional faulting,

associated with rifting, began after emplacement of the Hells Mesa Tuff and prior to emplacement of the Lemitar Tuff. This indicates that the Socorro segment of the Rio Grande rift began to form between 32.18 Ma and 28.37 Ma.

The onset of regional extension coincides with changes in the eruption pattern of the northeastern Mogollon-Datil volcanic field. Four closely spaced, major ash-flow tuffs, La Jencia, Vicks Peak, Lemitar, and South Canyon, were erupted over a time interval of only one million years (28.76 Ma to 27.76 Ma) during the initial stage of rifting. This suggests that changes in the regional stress field may have served as a catalyst for the eruptions.

Suitability of Method

The successful outcome of this study suggests that the $^{40}\text{Ar}/^{39}\text{Ar}$ relative dating technique is a suitable method for resolution of certain stratigraphic problems in ash-flow tuffs. The level of precision attainable with this method extends the usefulness of radiometric dating. The Fish Canyon Tuff of southern Colorado and the timing of ore deposition in Portugal are two examples (J.F. Sutter, 1984, oral commun.) of successful high-precision studies, which have been performed by the U.S. Geological Survey. As $^{40}\text{Ar}/^{39}\text{Ar}$ laboratories are established, more high precision studies will be performed.

As shown in this study, the conventional potassium-argon method is clearly inadequate for high-precision studies. The conventional method is most effectively applied to studies of units which are not closely spaced or for which 2-3% precision is sufficient. In addition, the existing body of conventional data should be regarded as approximate ages, and the Na-sanidine conventional ages should be considered minimum ages, due to the analytical difficulties associated with complete argon extraction from feldspars.

CONCLUSIONS

Summary

Five regional ash-flow tuff units were dated with the $^{40}\text{Ar}/^{39}\text{Ar}$ method and produced more precise ages for the units than the conventional potassium-argon method. The $^{40}\text{Ar}/^{39}\text{Ar}$ results provided age differentiation and confirmation of correlations of these units in the northeastern Mogollon-Datil volcanic field.

The $^{40}\text{Ar}/^{39}\text{Ar}$ analyses of cogenetic Na-sanidine and biotite indicates that the cause of the conventional potassium-argon age discrepancy is laboratory methodology. The conventional Na-sanidine ages are anomalously young due to incomplete extraction of the trapped ^{40}Ar (McDowell, 1983). In addition, the $^{40}\text{Ar}/^{39}\text{Ar}$ analyses demonstrated that Na-sanidine yields more precise $^{40}\text{Ar}/^{39}\text{Ar}$ data than biotite.

An attempt to confirm the outflow sheet-cauldron correlation of the Hells Mesa Tuff was a partial failure. The cauldron-fill sample yielded a slightly younger apparent age than the outflow sheet, although it was distinguishable from the other tuff units. The experiment should be repeated with additional pairs of outflow-sheet-cauldron-fill samples to see if this apparent age difference is real or a result of insufficient analytical data.

The $^{40}\text{Ar}/^{39}\text{Ar}$ ages of the tuffs proved the existence of a 3.4 Ma hiatus in the evolution of the northeastern Mogollon-Datil volcanic field between the eruptions of the Hells Mesa Tuff and the La Jencia Tuff. This hiatus has major implications to petrogenesis of the volcanic rock suites and to initiation of the Rio Grande rift. The dates also more accurately bracket the onset of regional extension, which corresponds to the beginning of the Rio Grande rift. These results demonstrate the suitability of the $^{40}\text{Ar}/^{39}\text{Ar}$ dating method to high-precision studies of this nature.

Suggestions for Further Research

The objectives, which were not fulfilled in this study, could be accomplished by collection and analysis of additional samples. Both the South Canyon and Lemitar tuffs should be analyzed further to provide multiple Na-sanidine ages for these units. The cauldron-fill sample of the Hells Mesa Tuff should be re-analyzed to determine if the age discrepancy actually exists. If the cauldron-fill versus outflow-sheet age discrepancy does exist, x-ray diffraction and microprobe analyses of the Na-sanidine phenocrysts would be useful in determining the cause. In addition, more pairs of outflow-sheet and cauldron-fill samples from other units should be dated to evaluate possible correlations of ash-flow tuffs with source cauldrons. Samples of the tuffs from geographic locations not included in this study should be analyzed to further test the ash-flow tuff chronology.

Future studies of this type should include detailed characterization of the units, similar to tephrochronology studies. Phenocryst chemistry and x-ray diffraction analyses combined with paleomagnetism determinations would greatly aid in the correlation of the units.

The Hells Mesa Tuff, extensively dated in this study, should be utilized as a regional datum for future age comparisons. The Joyita Hills measured section through the tuff units (Appendix IV) should be employed as a regional reference section for the sequence of tuffs in the northeastern Mogollon-Datil volcanic field (Table 6).

APPENDIX I

The Critical Value Test

The critical value test (Dalrymple and Lanphere, 1969) is a non-statistician's two-sided confidence interval. It is a test to determine, at a 95% confidence level, if two dates are the same.

$$\text{C.V.} = 1.960 (\sigma_1^2/n_1 + \sigma_2^2/n_2)^{1/2}$$

The σ_1 and σ_2 are the standard deviations on each date and n_1 and n_2 are the number of measurements made on each date. For there to be a distinction between two dates, the apparent difference, $|x_1 - x_2|$, must exceed the critical value. If the apparent difference is less than the critical value, the samples are not necessarily the same age. The equation only shows that any difference in the ages is too small to be detected at the 95% confidence level, and could be explained totally by analytical uncertainty.

EXAMPLE 1

$$\text{sample 1} = 30.9 \pm 1.1 \text{ Ma}$$

$$\text{sample 2} = 32.1 \pm 0.7 \text{ Ma}$$

$$|x_1 - x_2| = |30.9 - 32.1| = 1.2 \text{ Ma}$$

$$\text{C.V.} = 1.960 [(1.1)^2/1 + (0.7)^2/1]^{1/2} = 2.56 \text{ Ma}$$

There is no difference detected at the 95% confidence level.

EXAMPLE 2

$$\text{sample 1} = 32.1 \pm 0.7 \text{ Ma}$$

$$\text{sample 2} = 28.6 \pm 1.0 \text{ Ma (average of 2 analyses)}$$

$$|x_1 - x_2| = |32.1 - 28.6| = 3.5 \text{ Ma}$$

$$\text{C.V.} = 1.960 [(0.7)^2/1 + (1.0)^2/2]^{1/2} = 1.95 \text{ Ma}$$

There is a difference between these two dates at the 95% confidence level.

APPENDIX II

Conventional Potassium-Argon Ages

(all ages in Ma)

All averages are weighted by the inverses of the variances of the sample ages. The variance, the square of the standard deviation, is a measure of the uncertainty in the age. By weighting the sample ages by the inverse of their variances, the sample ages with the lowest uncertainty are weighted the most. The references for the ages are listed in Table 2.

HELLS MESA TUFF

Biotite weighted average = 33.17 ± 0.63

a) 34.0 ± 1.3

b) 33.2 ± 1.1

c) 33.0 ± 1.1

d) 32.3 ± 1.5

Na-sanidine

a) 32.1 ± 0.7 C.V. a-c = 2.39

b) 30.9 ± 1.1 diff. = 3.5

c) 28.6 ± 1.0 date c excluded

weighted average = 31.75 ± 0.74

Plagioclase

a) 31.1 ± 1.9

Fission-track

a) 31.4 ± 1.4 weighted average = 30.49 ± 1.06

b) 29.3 ± 1.6

Weighted averages:

biotite 33.17 ± 0.63 C.V. = 1.20

Na-sanidine 31.75 ± 0.74 diff. = 1.42

There is a difference between these dates.

biotite 33.17 ± 0.63 C.V. = 1.59

fission-track 30.49 ± 1.06 diff. = 2.68

There is a difference between these dates.

Weighted average:

Na-sanidine + plagioclase + fission-track

31.43 ± 0.63

LA JENCIA TUFF

Na-sanidine

a) 28.1 ± 1.2 C.V. c-d = 2.51

b) 25.0 ± 0.6 diff. = 2.80

c) 24.8 ± 1.0 Date d is excluded.

d) 22.0 ± 0.8

Whole-rock

e) 24.7 ± 0.7 weighted average = 25.20 ± 0.45

VICKS PEAK TUFF

Fission-track

a) 31.3 ± 2.6

LEMITAR TUFF

Biotite

a) 28.8 ± 0.7 C.V. e-f = 2.29

b) 28.8 ± 1.2 diff. = 4.1

c) 28.3 ± 1.1 Date f is excluded.

d) 27.7 ± 1.1

e) 27.0 ± 1.0

Whole-rock

f) 22.9 ± 0.6 weighted average = 28.22 ± 0.46

SOUTH CANYON TUFF

Na-sanidine

a) 26.5 ± 1.0 weighted average = 25.54 ± 0.49

b) 24.5 ± 0.9

c) 24.5 ± 1.0

Biotite

d) 26.9 ± 1.0

STRATIGRAPHIC ORDER

By ages:

La Jencia Tuff	25.20 \pm 0.45		
	C.V. = 0.65	diff. = 0.34	
South Canyon Tuff	25.54 \pm 0.49		
	C.V. = 0.63	diff = 2.68	
Lemitar Tuff	28.22 \pm 0.46		
	C.V. = 5.11	diff = 3.08	
Vicks Peak Tuff	31.30 \pm 2.6		
	C.V. = 5.13	diff = 0.13	
Hells Mesa Tuff	31.43 \pm 0.63		

By stratigraphy:

South Canyon Tuff
 Lemitar Tuff
 Vicks Peak Tuff
 La Jencia Tuff
 Hells Mesa Tuff

The conventional ages do not preserve the stratigraphic order and most units cannot be differentiated. The Hells Mesa Tuff shows a discrepancy between the Na-sanidine and biotite dates.

APPENDIX III

Sample Locations

I. Samples K-JH-1 through K-JH-26

Joyita Hills

Mesa Del Yeso 7.5' quadrangle, Sevilleta Grant

(unsurveyed)

secs. 10, 11, T1S, R1E

34°14'- 34°14'15" N, 106°49'- 106°49'30" W

Geology from Spradlin, 1976

II. Samples K-BM-1 through K-BM-11

Bear Mountains

Mesa Cencerro 7.5' quadrangle

center of side common to sec. 36 T2N, R5W and

sec. 31 T2N, R4W

34°21'15" N, 107°18'20" W

Geology from Tonking, 1957, and Massingill, 1979

III. Sample K-D-1

Datil area

Sugarloaf Mountain 7.5' quadrangle

center SW 1/4, NW 1/4, NW 1/4, sec. 28 T2S, R10W

34°06'30" N, 107°53'20" W

Geology from Lopez and Bornhorst, 1979

IV. Sample K-CM-2

Chupadera Mountains

Luis Lopez 7.5' quadrangle

center SW 1/4, NW 1/4, sec. 29, T4S, R1W

33°56'05" N, 106°58'20" W

Geology from Eggleston, 1982

V. Sample K-TS-1

Torreon Springs

Molino Peak 7.5' quadrangle

center sec. 9, T5S, R2W

33°53'25" N, 107°03'15" W

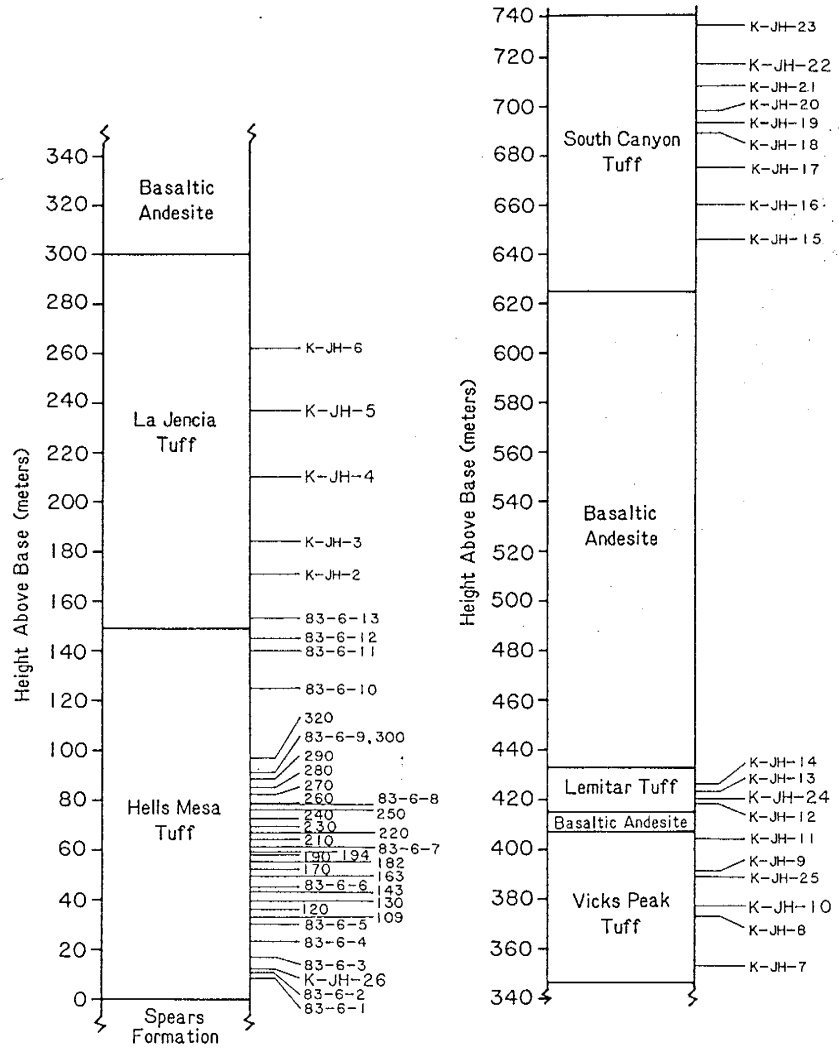
Geology from Osburn and others, 1981

APPENDIX IV

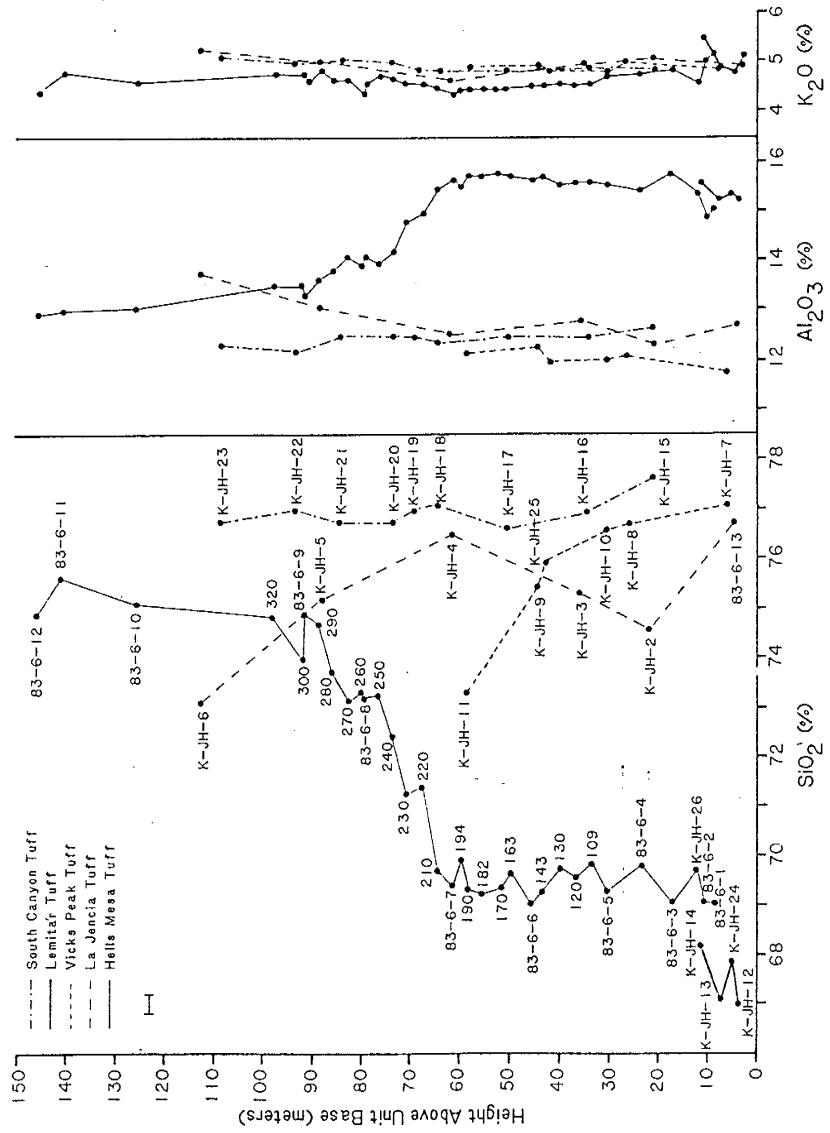
Measured Sections and Chemical Data

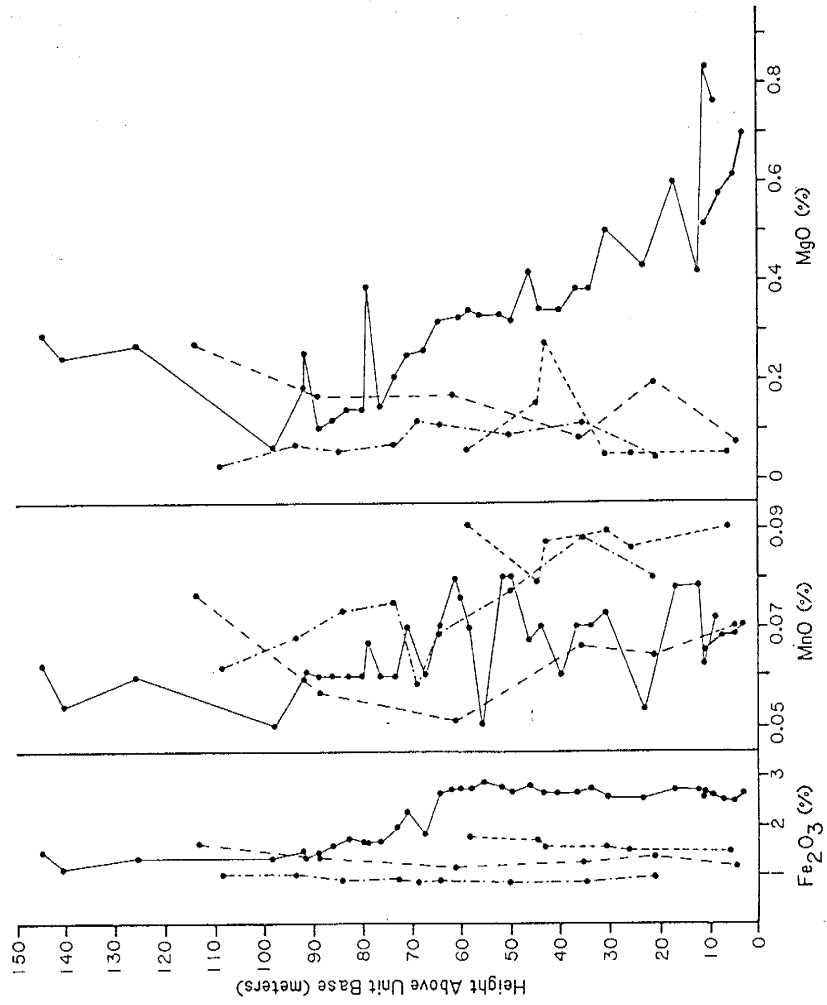
Three sections were measured through one or more of the ash-flow tuff units in the Joyita Hills, Bear Mountains, and near Torreon Springs. Samples were collected at intervals through the sections and analyzed for major-element chemical composition by x-ray fluorescence spectrometry (Norrish and Hutton, 1969). The analytical uncertainty of the Rigaku 3064 x-ray fluorescence spectrometer at the New Mexico Bureau of Mines and Mineral Resources is shown in the upper right-hand corner of each plot (Bobrow, 1984). The section near Torreon Springs was measured, sampled, and the chemical analyses performed by G.R. Osburn (1983, written commun.). The Hells Mesa Tuff section in the Bear Mountains was measured and sampled by C.E. Chapin and G.R. Osburn and the chemical analyses were performed by G.R. Osburn (1983, written commun.) The Hells Mesa Tuff section in the Joyita Hills was measured, sampled, and the chemical analyses performed by G.R. Osburn and L.L. Kedzie.

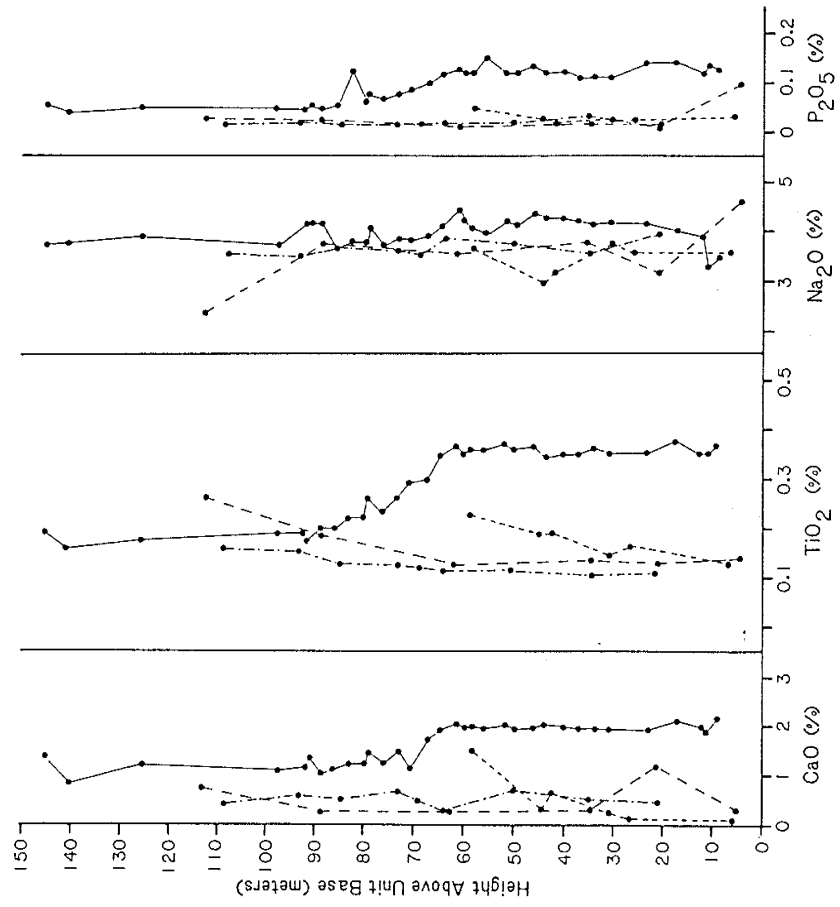
Joyita Hills Measured Section



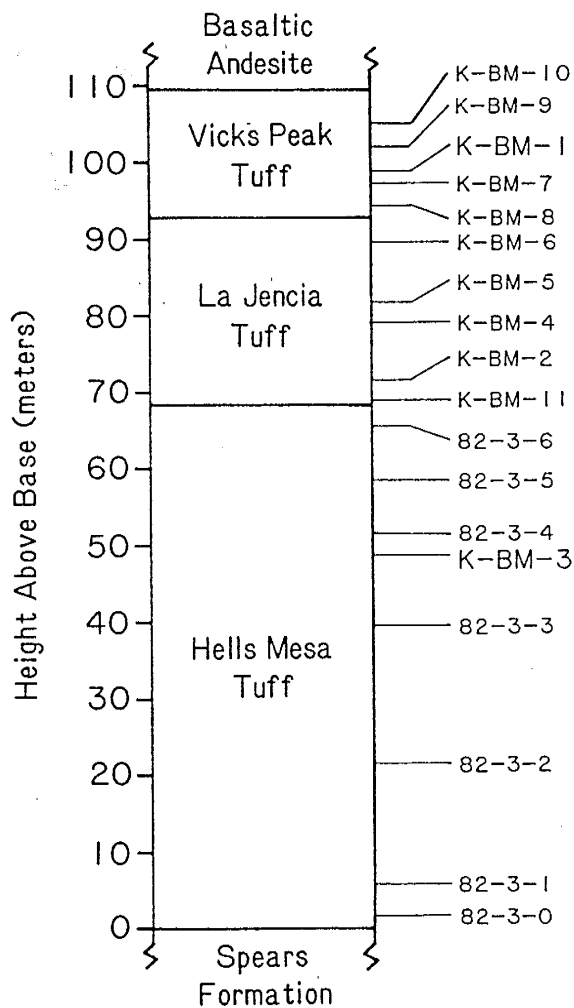
Chemical Data
Joyita Hills Measured Section

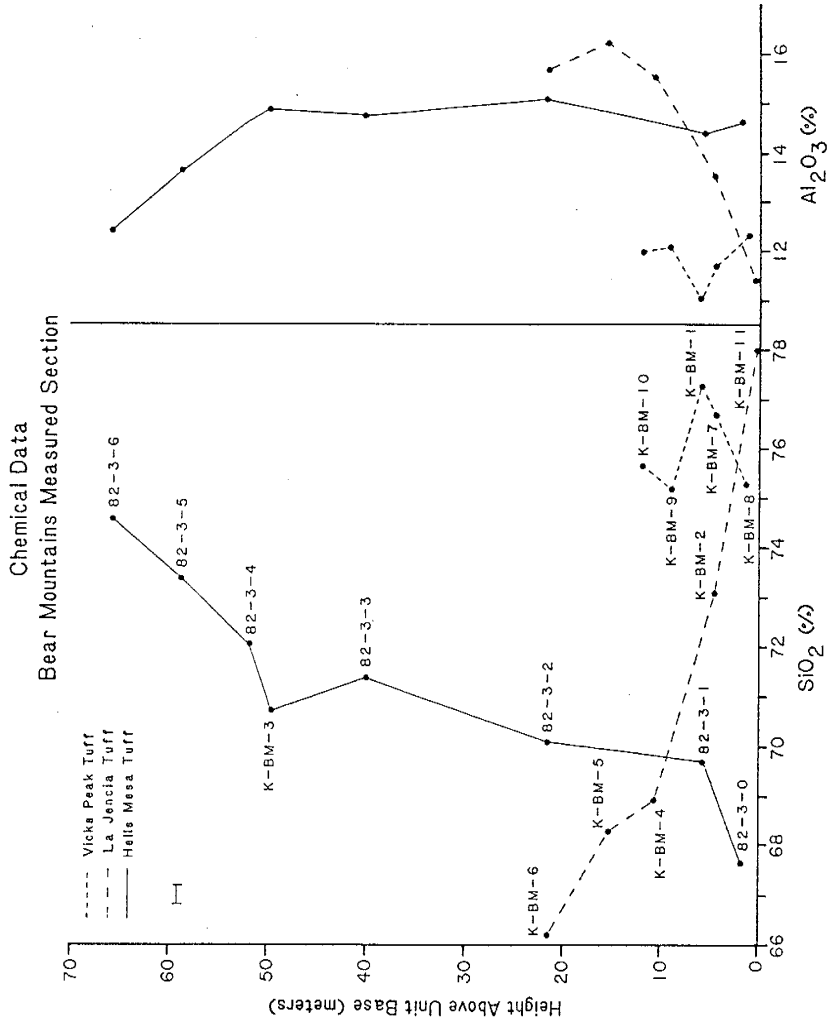


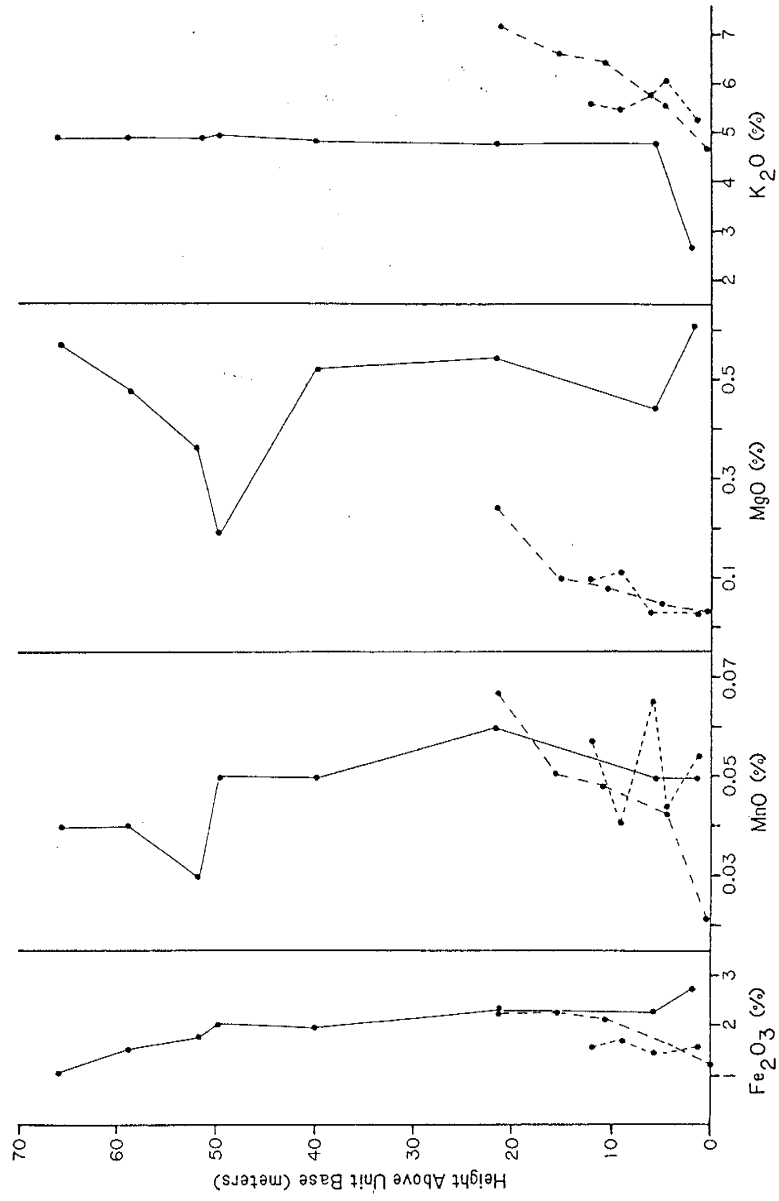


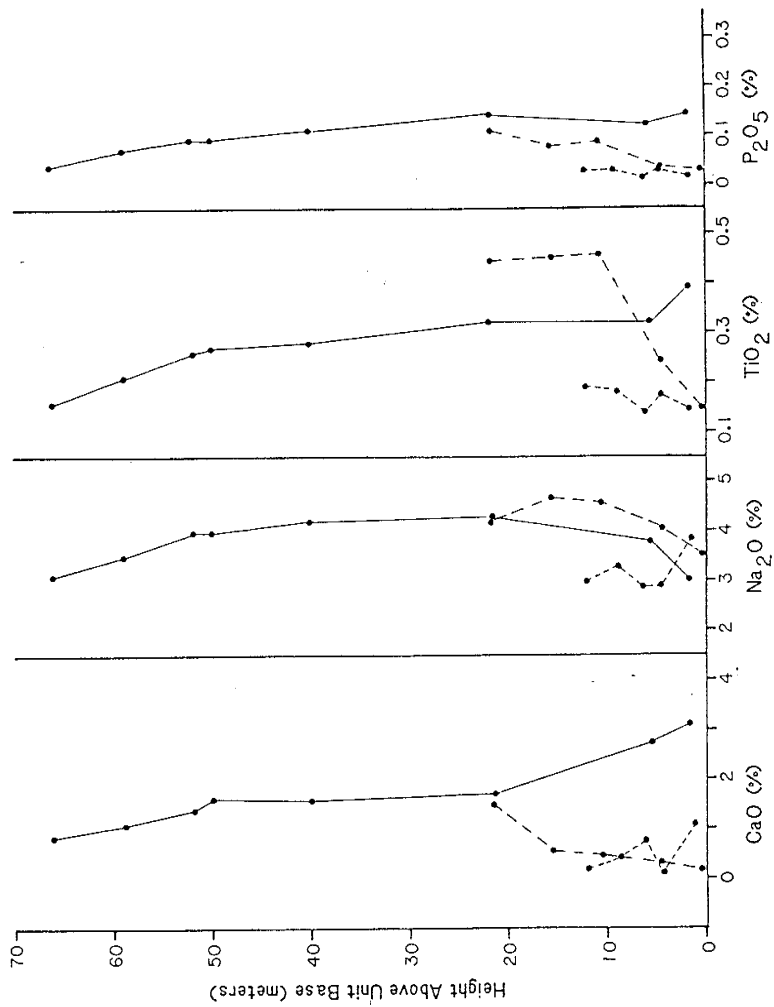


Bear Mountains Measured Section

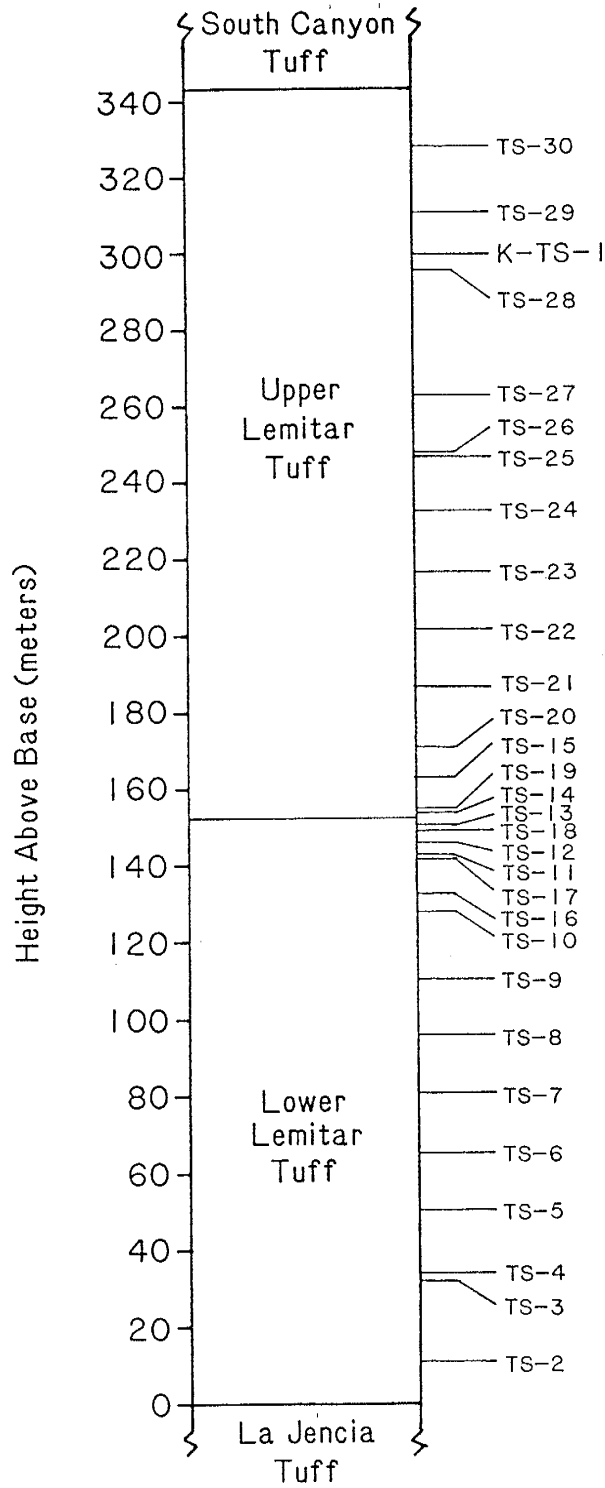


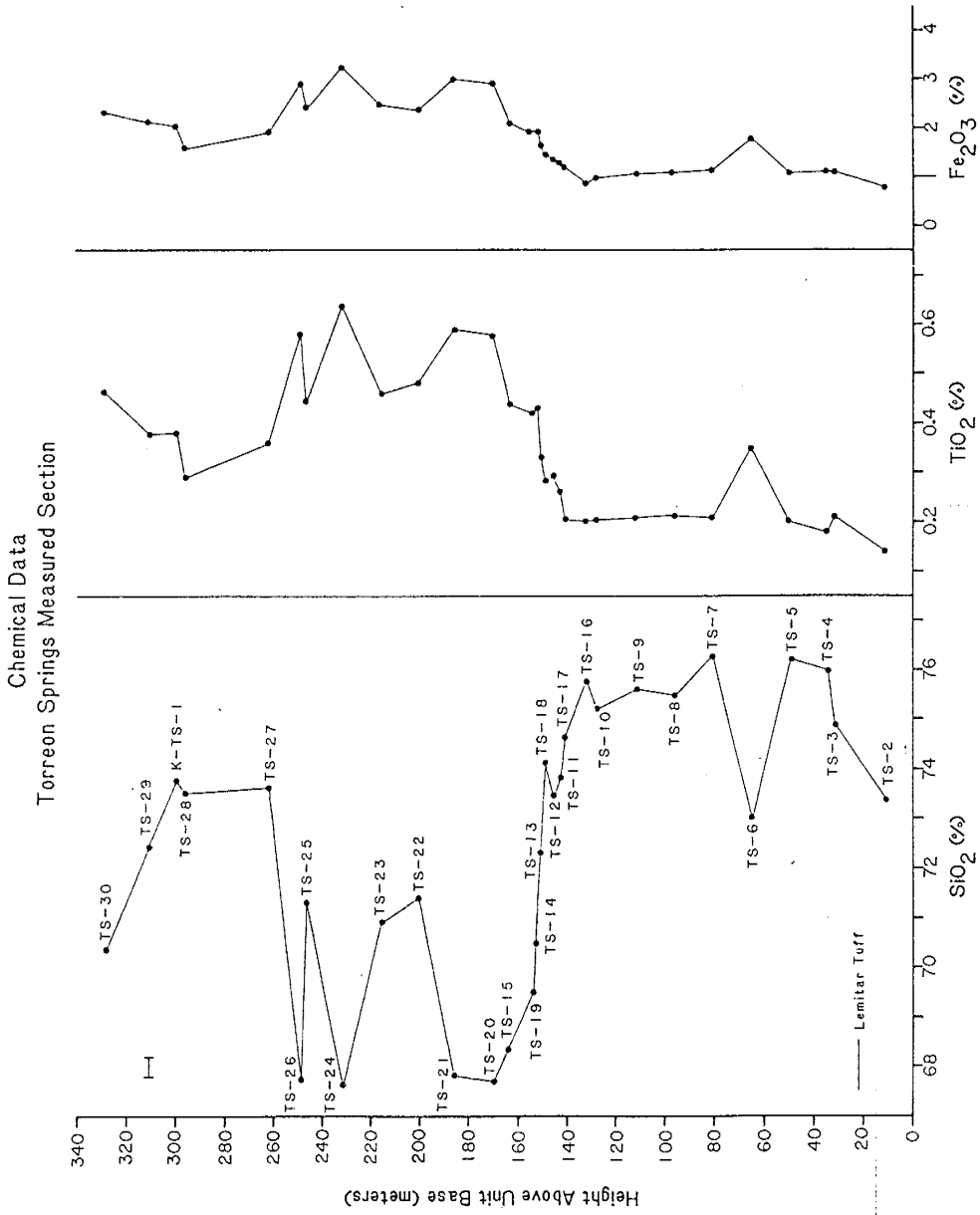


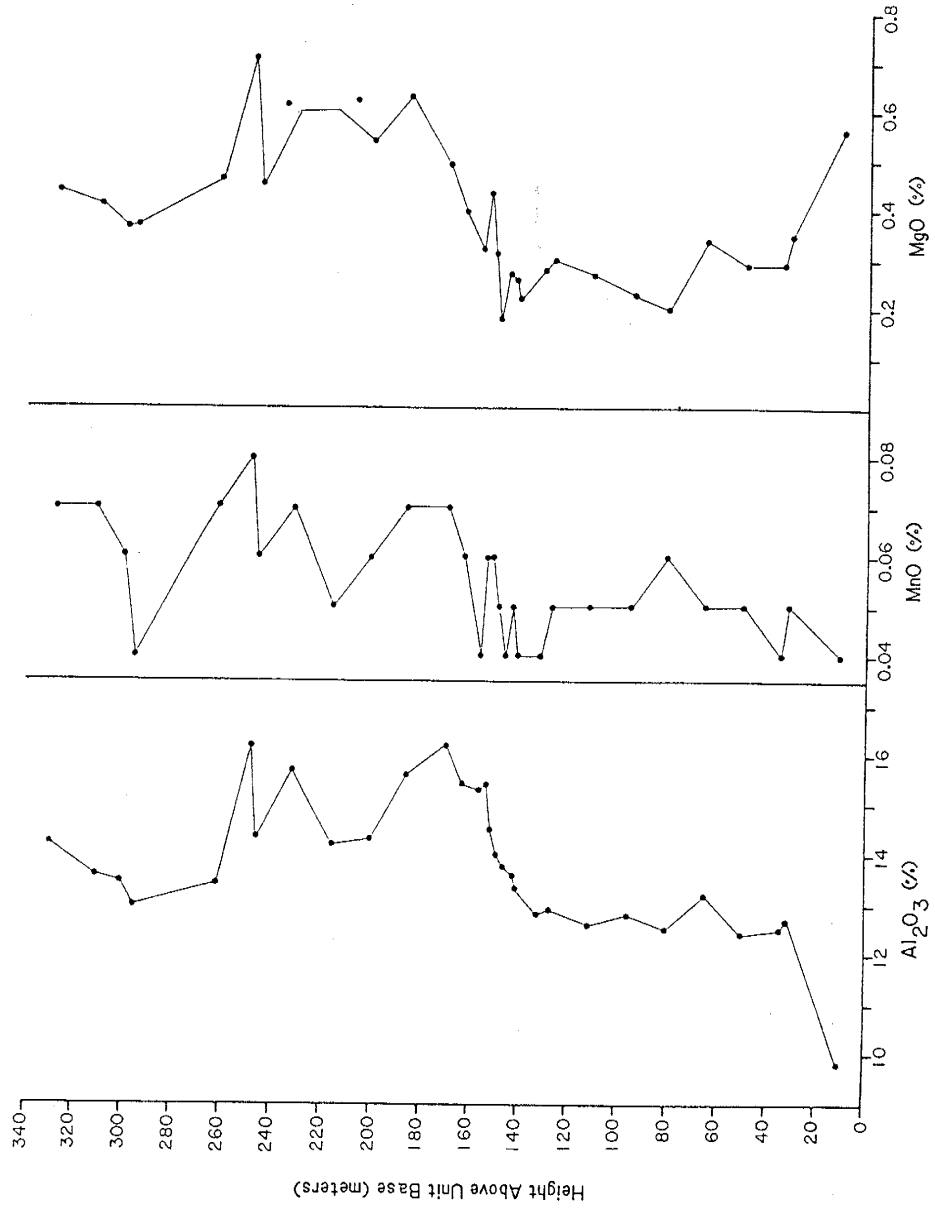


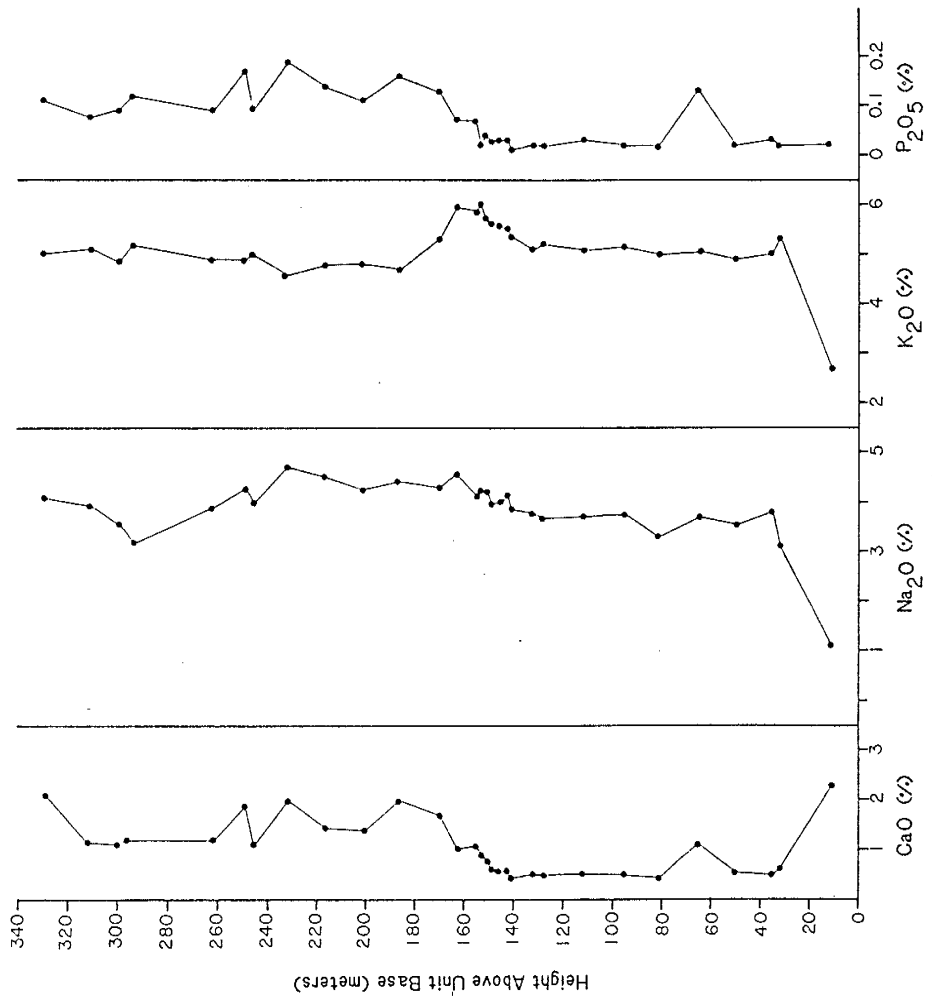


Torreón Springs Measured Section









Chemical Data

Hells Mesa Tuff

	83-6-1	83-6-2	K-JH-26	83-6-3	83-6-4	83-6-5
SiO ₂	69.04	69.05	69.45	69.06	69.78	69.27
TiO ₂	0.36	0.35	0.33	0.38	0.35	0.35
Al ₂ O ₃	15.02	14.91	15.38	15.72	15.44	15.55
Fe ₂ O ₃	2.54	2.53	2.68	2.70	2.54	2.57
MnO	0.07	0.06	0.08	0.08	0.05	0.07
MgO	0.76	0.83	0.32	0.60	0.43	0.50
CaO	2.14	1.90	1.97	2.05	1.92	1.94
Na ₂ O	3.43	3.25	3.79	3.96	4.09	4.16
K ₂ O	5.11	4.99	4.57	4.80	4.73	4.71
P ₂ O ₅	0.12	0.13	0.11	0.14	0.14	0.11
LOI	1.64	1.93	0.61	1.52	1.08	0.95
TOTAL	100.23	99.93	99.29	101.01	100.55	100.18

	109	120	130	143	83-6-6	163
SiO ₂	69.82	69.59	69.71	69.24	69.09	69.65
TiO ₂	0.36	0.35	0.35	0.34	0.37	0.36
Al ₂ O ₃	15.52	15.56	15.55	15.70	15.67	15.71
Fe ₂ O ₃	2.71	2.62	2.63	2.65	2.79	2.67
MnO	0.07	0.07	0.06	0.07	0.07	0.08
MgO	0.38	0.38	0.34	0.34	0.42	0.32
CaO	1.95	1.97	1.99	2.04	1.98	1.95
Na ₂ O	4.13	4.17	4.24	4.18	4.34	4.12
K ₂ O	4.56	4.51	4.54	4.50	4.51	4.47
P ₂ O ₅	0.11	0.11	0.12	0.13	0.14	0.12
LOI	0.50	0.47	0.33	0.39	0.93	0.42
TOTAL	100.10	99.80	99.86	99.57	100.31	99.86

	170	182	190	194	83-6-7	K-JH-1
SiO ₂	69.32	69.26	69.30	69.90	69.36	68.80
TiO ₂	0.37	0.36	0.36	0.35	0.37	0.35
Al ₂ O ₃	15.77	15.70	15.70	15.52	15.64	15.49
Fe ₂ O ₃	2.74	2.85	2.71	2.70	2.70	2.90
MnO	0.08	0.05	0.07	0.08	0.08	0.08
MgO	0.33	0.33	0.34	0.33	0.41	0.37
CaO	2.05	1.92	2.04	1.98	2.04	2.06
Na ₂ O	4.15	3.93	4.03	4.14	4.40	3.89
K ₂ O	4.45	4.45	4.44	4.46	4.39	4.42
P ₂ O ₅	0.12	0.15	0.12	0.12	0.13	0.12
LOI	0.39	0.55	0.44	0.37	0.90	0.56
TOTAL	99.78	99.56	99.56	99.96	100.42	99.05

	210	220	230	240	250	83-6-8
SiO ₂	69.69	71.37	71.20	72.33	73.24	73.26
TiO ₂	0.35	0.30	0.29	0.26	0.23	0.26
Al ₂ O ₃	15.47	14.93	14.76	14.18	13.95	14.11
Fe ₂ O ₃	2.66	2.32	2.25	1.93	1.68	1.81
MnO	0.07	0.06	0.07	0.06	0.06	0.07
MgO	0.32	0.26	0.25	0.21	0.14	0.40
CaO	1.97	1.72	1.72	1.50	1.29	1.46
Na ₂ O	4.13	3.90	3.82	3.83	3.69	4.07
K ₂ O	4.47	4.56	4.57	4.64	4.74	4.59
P ₂ O ₅	0.12	0.10	0.09	0.08	0.07	0.08
LOI	0.35	0.48	0.51	0.41	0.32	0.65
TOTAL	99.60	99.99	99.52	99.43	99.40	100.76

	260	270	280	290	83-6-9	300
SiO ₂	73.31	73.12	73.69	74.67	74.90	73.94
TiO ₂	0.22	0.22	0.20	0.20	0.18	0.19
Al ₂ O ₃	13.90	14.08	13.80	13.60	13.29	13.46
Fe ₂ O ₃	1.65	1.71	1.51	1.47	1.33	1.44
MnO	0.06	0.06	0.06	0.06	0.06	0.06
MgO	0.14	0.17	0.12	0.10	0.25	0.18
CaO	1.26	1.25	1.18	1.06	1.33	1.17
Na ₂ O	3.79	3.69	3.63	3.52	4.16	3.81
K ₂ O	4.66	4.71	4.65	4.74	4.64	4.64
P ₂ O ₅	0.07	0.06	0.06	0.05	0.05	0.05
LOI	0.30	0.33	0.36	0.40	0.71	0.35
TOTAL	99.36	99.40	99.27	99.87	100.90	99.29

	320	83-6-10	83-6-11	83-6-12	K-CM-2	K-D-1
SiO ₂	74.86	75.16	75.65	74.90	71.78	71.46
TiO ₂	0.18	0.17	0.16	0.20	0.27	0.31
Al ₂ O ₃	13.45	13.04	12.99	12.94	14.04	14.98
Fe ₂ O ₃	1.37	1.35	1.15	1.49	1.76	1.94
MnO	0.05	0.06	0.05	0.06	0.04	0.07
MgO	0.06	0.27	0.25	0.29	0.26	0.33
CaO	1.14	1.23	0.84	1.24	1.55	1.65
Na ₂ O	3.72	3.90	3.75	3.72	2.85	4.13
K ₂ O	4.78	4.63	4.81	4.55	6.06	4.68
P ₂ O ₅	0.05	0.05	0.05	0.05	0.08	0.10
LOI	0.34	0.67	0.45	0.66	1.36	0.38
TOTAL	100.00	100.53	100.15	100.10	100.05	100.02

	82-3-0	82-3-1	82-3-2	82-3-3	K-BM-3	82-3-4
SiO ₂	67.64	69.66	70.08	71.36	70.66	72.02
TiO ₂	0.39	0.32	0.32	0.28	0.26	0.26
Al ₂ O ₃	14.56	14.39	15.06	14.77	14.90	14.62
Fe ₂ O ₃	2.72	2.24	2.28	1.96	2.02	1.78
MnO	0.05	0.05	0.06	0.05	0.05	0.03
MgO	1.38	0.44	0.54	0.52	0.19	0.36
CaO	3.08	2.73	1.72	1.59	1.62	1.42
Na ₂ O	3.08	3.81	4.27	4.21	4.02	4.00
K ₂ O	2.63	4.76	4.74	4.85	4.92	4.89
P ₂ O ₅	0.14	0.12	0.14	0.11	0.09	0.09
LOI ⁵	1.10	1.59	0.60	0.72	0.55	0.76
TOTAL	96.77	100.11	99.81	100.42	99.28	100.23

	82-3-5	82-3-6
SiO ₂	73.38	74.57
TiO ₂	0.21	0.16
Al ₂ O ₃	13.65	12.50
Fe ₂ O ₃	1.51	1.09
MnO	0.04	0.04
MgO	0.48	0.57
CaO	1.12	0.86
Na ₂ O	3.52	3.14
K ₂ O	4.89	4.85
P ₂ O ₅	0.07	0.04
LOI ⁵	1.19	2.07
TOTAL	100.06	99.89

La Jencia Tuff

	K-JH-2	K-JH-3	K-JH-4	K-JH-5	K-JH-6
SiO ₂	74.55	75.21	76.46	75.16	73.10
TiO ₂	0.13	0.13	0.13	0.18	0.27
Al ₂ O ₃	12.31	12.78	12.52	13.02	13.71
Fe ₂ O ₃	1.31	1.22	1.18	1.35	1.62
MnO	0.06	0.07	0.05	0.06	0.08
MgO	0.19	0.08	0.17	0.16	0.27
CaO	1.14	0.28	0.28	0.30	0.76
Na ₂ O	3.13	3.70	3.53	3.72	2.36
K ₂ O	5.04	4.94	4.66	5.02	5.30
P ₂ O ₅	0.01	0.02	0.01	0.03	0.03
LOI ⁵	1.92	1.91	1.06	1.00	1.21
TOTAL	99.80	100.35	100.05	100.00	98.70

	K-BM-11	K-BM-2	K-BM-4	K-BM-5	K-BM-6
SiO ₂	77.96	73.16	68.89	68.29	66.27
TiO ₂	0.15	0.24	0.46	0.45	0.44
Al ₂ O ₃	11.32	13.45	15.47	15.67	15.71
Fe ₂ O ₃	1.23	1.60	2.13	2.23	2.21
MnO	0.02	0.04	0.05	0.05	0.07
MgO	<0.04	0.03	0.08	0.10	0.24
Ca	0.18	0.31	0.50	0.54	1.46
Na ₂	3.55	4.08	4.58	4.68	4.25
K ₂ O	4.69	5.52	6.41	6.54	7.15
P ₂ O ₅	0.02	0.04	0.08	0.07	0.11
LOI ⁵	0.50	0.44	0.36	0.45	1.24
TOTAL	99.49	98.91	99.00	99.08	99.14

Vicks Peak Tuff

	K-JH-7	K-JH-8	K-JH-10	K-JH-9	K-JH-11
SiO ₂	77.06	76.68	76.51	75.38	73.20
TiO ₂	0.13	0.16	0.14	0.19	0.22
Al ₂ O ₃	11.75	12.05	11.99	12.20	12.10
Fe ₂ O ₃	1.44	1.49	1.50	1.61	1.73
MnO	0.09	0.09	0.09	0.08	0.08
MgO	<0.04	<0.04	<0.04	0.16	0.03
CaO	0.10	0.13	0.20	0.30	1.49
Na ₂ O	3.54	3.52	3.73	2.96	3.53
K ₂ O	4.84	4.97	4.81	4.91	4.92
P ₂ O ₅	0.03	0.02	0.02	0.05	0.04
LOI ⁵	0.25	0.28	0.30	1.99	2.77
TOTAL	99.18	99.39	99.30	99.82	100.11

	K-BM-8	K-BM-7	K-BM-1	K-BM-9	K-BM-10
SiO ₂	75.24	76.68	77.28	75.21	75.64
TiO ₂	0.14	0.17	0.14	0.18	0.19
Al ₂ O ₃	12.28	11.68	11.04	12.02	11.98
Fe ₂ O ₃	1.56	1.47	1.44	1.65	1.53
MnO	0.06	0.04	0.06	0.04	0.06
MgO	0.03	0.03	0.03	0.11	0.09
CaO	0.10	0.14	0.07	0.43	0.20
Na ₂ O	3.82	2.90	2.86	3.29	3.00
K ₂ O	5.32	6.08	5.72	5.44	5.54
P ₂ O ₅	0.02	0.03	0.02	0.03	0.02
LOI ⁵	0.54	0.66	0.58	1.00	0.79
TOTAL	99.11	99.88	99.24	99.40	99.05

Lemitar Tuff

	K-JH-12	K-JH-24	K-JH-13	K-JH-14	K-TS-1
SiO ₂	66.66	67.69	67.01	68.12	73.77
TiO ₂	0.46	0.45	0.49	0.50	0.38
Al ₂ O ₃	15.22	15.28	15.21	15.53	13.41
Fe ₂ O ₃	2.58	2.46	2.47	2.56	2.02
MnO	0.07	0.07	0.07	0.06	0.06
MgO	0.64	0.58	0.58	0.51	0.36
CaO	1.87	1.75	1.78	2.04	1.10
Na ₂ O	3.69	3.86	4.05	4.10	3.55
K ₂ O	5.12	4.83	4.89	5.47	4.84
P ₂ O ₅	0.14	0.13	0.13	0.16	0.09
LOI	3.10	2.64	2.82	0.65	0.20
TOTAL	99.55	99.74	99.50	99.69	99.78

	TS-1	TS-2	TS-3	TS-4	TS-5	TS-6
SiO ₂	69.63	73.25	74.99	75.90	76.07	73.06
TiO ₂	0.48	0.14	0.19	0.18	0.19	0.35
Al ₂ O ₃	14.99	9.99	12.77	12.51	12.45	13.19
Fe ₂ O ₃	2.13	0.81	1.06	1.07	1.07	1.82
MnO	0.08	0.04	0.05	0.04	0.05	0.05
MgO	0.31	0.57	0.36	0.29	0.28	0.35
CaO	1.04	2.33	0.59	0.47	0.53	1.13
Na ₂ O	4.93	1.14	3.12	3.76	3.55	3.70
K ₂ O	6.05	2.76	5.31	5.00	4.91	5.06
P ₂ O ₅	0.10	0.02	0.02	0.03	0.02	0.13
LOI	0.64	0.69	1.18	0.56	0.72	1.21
TOTAL	100.38	99.50	99.64	99.81	99.84	100.05

	TS-7	TS-8	TS-9	TS-10	TS-11	TS-12
SiO ₂	76.20	75.56	75.47	75.17	73.86	73.52
TiO ₂	0.19	0.19	0.19	0.19	0.25	0.29
Al ₂ O ₃	12.57	12.84	12.66	12.98	13.62	13.70
Fe ₂ O ₃	1.14	1.13	1.09	1.02	1.28	1.34
MnO	0.06	0.05	0.05	0.05	0.05	0.04
MgO	0.20	0.24	0.28	0.30	0.26	0.27
CaO	0.46	0.48	0.48	0.44	0.57	0.62
Na ₂ O	3.38	3.77	3.68	3.70	4.10	3.99
K ₂ O	5.03	5.13	5.07	5.20	5.46	5.50
P ₂ O ₅	0.02	0.02	0.03	0.02	0.03	0.03
LOI	0.91	0.51	0.68	0.68	0.75	0.56
TOTAL	100.16	99.92	99.68	99.76	100.23	99.86

	TS-13	TS-14	TS-15	TS-16	TS-17	TS-18
SiO ₂	72.24	69.55	68.87	75.84	74.53	73.74
TiO ₂	0.33	0.43	0.43	0.19	0.21	0.28
Al ₂ O ₃	14.49	15.40	15.49	12.80	13.41	13.97
Fe ₂ O ₃	1.59	1.98	2.06	0.99	1.22	1.45
MnO	0.06	0.06	0.06	0.04	0.04	0.05
MgO	0.36	0.44	0.40	0.29	0.22	0.18
CaO	0.79	0.96	1.09	0.48	0.48	0.64
Na ₂ O	4.49	4.18	4.56	3.78	3.83	3.96
K ₂ O	5.70	5.99	5.93	5.10	5.37	5.58
P ₂ O ₅	0.04	0.02	0.07	0.02	0.01	0.03
LOI	0.60	0.84	0.63	0.52	0.84	0.36
TOTAL	100.39	99.90	99.59	100.05	100.20	99.88

	TS-19	TS-20	TS-21	TS-22	TS-23	TS-24
SiO ₂	70.50	67.42	67.77	71.21	71.08	67.81
TiO ₂	0.42	0.58	0.60	0.47	0.47	0.64
Al ₂ O ₃	15.37	16.34	15.62	14.35	14.23	15.66
Fe ₂ O ₃	1.97	2.87	3.01	2.36	2.51	3.27
MnO	0.04	0.07	0.07	0.06	0.05	0.07
MgO	0.31	0.48	0.64	0.53	0.60	0.70
Ca	1.02	1.71	2.01	1.40	1.42	1.99
Na ₂ O	4.16	4.33	4.39	4.25	4.49	4.66
K ₂ O	5.94	5.35	4.73	4.82	4.78	4.74
P ₂ O ₅	0.07	0.13	0.16	0.11	0.14	0.19
LOI	0.52	0.35	0.34	0.34	0.45	0.39
TOTAL	100.35	99.68	99.34	99.90	100.22	100.12

	TS-25	TS-26	TS-27	TS-28	TS-29	TS-30
SiO ₂	71.37	67.44	73.69	73.58	72.25	70.20
TiO ₂	0.45	0.57	0.36	0.29	0.38	0.45
Al ₂ O ₃	14.29	16.16	13.42	13.04	13.62	14.25
Fe ₂ O ₃	2.42	2.93	1.98	1.62	2.14	2.36
MnO	0.06	0.08	0.06	0.04	0.07	0.07
MgO	0.45	0.71	0.46	0.37	0.41	0.45
CaO	1.14	1.97	1.20	1.19	1.08	2.15
Na ₂ O	4.02	4.27	3.87	3.20	3.91	4.06
K ₂ O	0.36	0.77	0.51	1.69	0.79	1.10
P ₂ O ₅	0.09	0.17	0.09	0.12	0.08	0.11
LOI	0.36	0.77	0.51	1.69	0.79	1.10
TOTAL	99.73	99.98	100.57	100.34	99.84	100.26

South Canyon Tuff

	K-JH-15	K-JH-16	K-JH-17	K-JH-18	K-JH-19	K-JH-20
SiO ₂	77.42	76.88	76.57	77.05	76.98	76.72
TiO ₂	0.10	0.11	0.11	0.11	0.12	0.12
Al ₂ O ₃	12.62	12.42	12.42	12.36	12.44	12.48
Fe ₂ O ₃	0.96	0.85	0.84	0.88	0.90	0.92
MnO	0.08	0.09	0.08	0.07	0.06	0.08
MgO	0.03	0.11	0.09	0.11	0.12	0.07
CaO	0.42	0.50	0.69	0.37	0.46	0.67
Na ₂ O	3.89	3.55	3.72	3.84	3.54	3.61
K ₂ O	4.88	4.84	4.82	4.84	4.88	5.00
P ₂ O ₅	0.02	0.03	0.02	0.01	0.02	0.02
LOI ⁵	0.32	0.67	0.76	0.35	0.57	0.63
TOTAL	100.74	100.04	100.12	100.00	100.09	100.27

	K-JH-21	K-JH-22	K-JH-23
SiO ₂	76.72	76.96	76.73
TiO ₂	0.13	0.15	0.16
Al ₂ O ₃	12.48	12.14	12.27
Fe ₂ O ₃	0.91	1.01	1.04
MnO	0.07	0.07	0.06
MgO	0.06	0.06	0.03
CaO	0.56	0.60	0.44
Na ₂ O	3.71	3.49	3.56
K ₂ O	5.08	5.00	5.12
P ₂ O ₅	0.02	0.02	0.02
LOI ⁵	0.59	0.56	0.51
TOTAL	100.33	100.06	99.93

APPENDIX V

Mineral Separation

The separation of phenocrysts from the welded ash-flow tuffs was a multistage process that varied for each sample. It was composed of three main procedures: 1) reducing the size of the sample; 2) separating the minerals; and, 3) purifying and cleaning the separate.

SAMPLE REDUCTION

The amount of sample needed for processing was estimated from the phenocryst content of each sample and the amount of mineral required for analysis. Approximately 25% of the available phenocrysts were isolated during separation. The appropriate quantity of each sample was then crushed, ground, sieved, and examined. The crushing was done by several different models of jaw crushers, such as the Sturtevant Jaw Crusher 2x6 (fig. 24). The small chips from the jaw crushers were ground to a fine sand in a roller mill, the Denver Crushing Rolls 10x6, type D (fig. 25). At this point, a split of each sample was taken and pulverized for chemical analysis.

The sand of each sample was sieved to separate the different size fractions. Four sieves, 60, 80, 100, and 120 mesh, were used in a RoTap automatic sieve shaker. A small sample from each size fraction was

washed in deionized water, dried, and examined under a microscope. The fraction containing the most crystals and the fewest crystal-glass aggregates was chosen for mineral separation. For most samples, the fraction chosen was the 100-120 mesh (149-125 μ) size.

MINERAL SEPARATION

Two methods of separation, based upon different physical characteristics of minerals, were used to isolate the mineral phases. The Frantz isodynamic magnetic separator divided minerals by their magnetic susceptibilities. Heavy liquids were used to separate minerals of differing densities. These techniques were used together and repeatedly to perform the separations.

Magnetic Separation

The Frantz isodynamic magnetic separator (fig. 26) consists of an electromagnetic field applied to one side of a tilted, inclined, bifurcated chute. A sample traveling down the chute concentrates magnetic mineral grains on one side. The forward and side tilts and the strength of the magnetic field are adjustable to allow separation of minerals with varying magnetic susceptibilities. Muller (1967) presents a table of Frantz magnetic separator settings and the minerals separable at each.

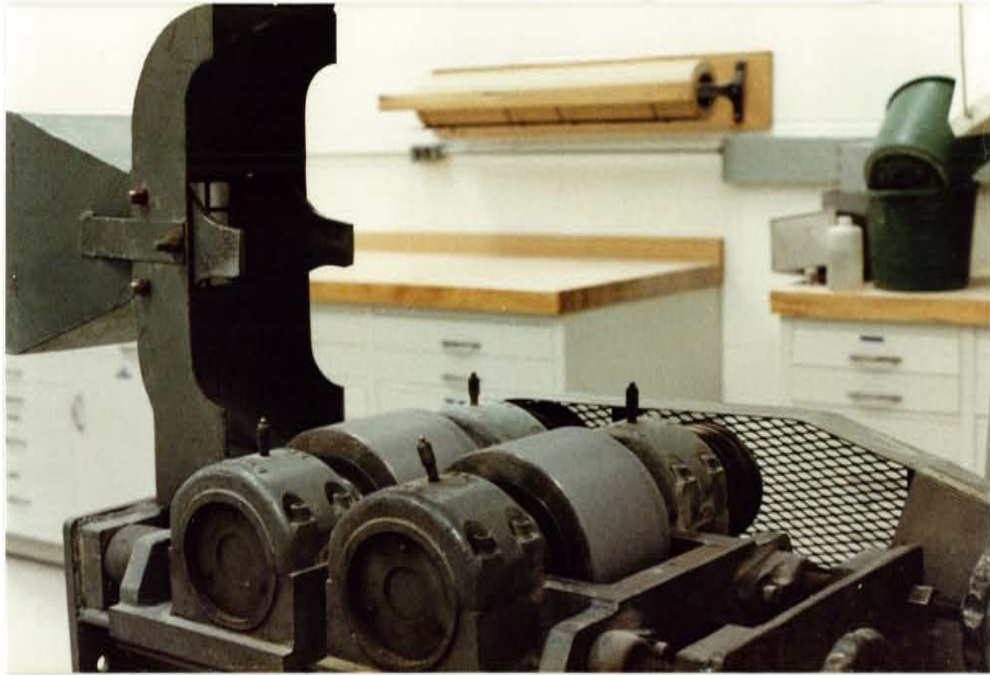


Figure 25. Denver crushing rolls, shown in the open position for cleaning, located at the U. S. Geological Survey, Reston, Virginia.

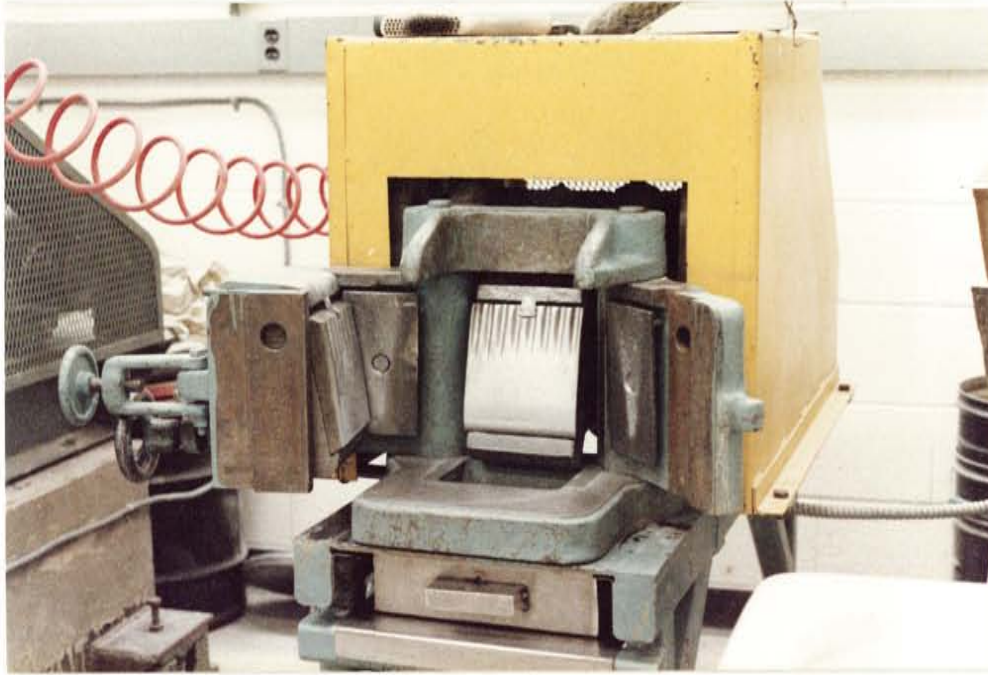


Figure 24. Sturtevant jaw crusher, shown in the open position to facilitate cleaning, located at the U. S. Geological Survey, Reston, Virginia.



Figure 26. Frantz isodynamic magnetic separator, featuring a modified sample feed system, located in the U. S. Geological Survey, Reston, Virginia.

The Frantz separator was utilized to separate biotite and iron-stained glass in the crystal-rich tuffs. It was also employed to separate feldspar and quartz crystals from non-iron-stained glass.

Gravity Separation

Separation of minerals by gravity involves the use of heavy liquids (high-density halogenated hydrocarbons). These liquids are toxic and should only be handled under a fume hood (Sax, 1979). The heavy liquids utilized were: bromoform (tribromoethane), CHBr_3 ; methylene iodide (diiodomethane), CH_2I_2 ; dimethylformamide, $(\text{CH}_3)_2\text{NCHO}$; and, acetone (dimethyl ketone), CH_3COCH_3 . Two of these liquids have high densities, bromoform (density 2.89 g/cc) and methylene iodide (density 3.325 g/cc). The liquids were diluted to the desired densities by dimethylformamide (density 0.945 g/cc). Acetone was used to wash the heavy liquids from the mineral separates.

Heavy liquids were utilized mainly to separate quartz from Na-sanidine, hornblende from biotite, and biotite from other magnetic minerals (fig. 27). Hurlbut and Klein (1977) present a table of minerals ordered by their specific gravities.



Figure 27. Heavy liquid mineral separation, showing the separation of a sample due to density differences between the minerals.

FINAL PURIFICATION

The mineral separates for $^{40}\text{Ar}/^{39}\text{Ar}$ dating must be >99% pure. To reach this level of purity, the biotites were paper-shaken, and all separates were hand-picked.

Paper-shaking is a quick method to isolate platy minerals, such as biotite, from more rounded mineral grains. The sample is shaken lightly on a sheet of filter paper. The rounded mineral grains rolled off of the paper and were discarded.

All separates were hand-picked beneath a binocular microscope, and the biotite and hornblende separates were visually checked for purity. The Na-sanidine separates were examined for purity by optical properties in immersion oils under a petrographic microscope.

Before packaging for irradiation, the samples were cleaned in a series of liquids in an ultrasonic cleaner. The Na-sanidine samples were first subjected to a 7% hydrofluoric acid wash for three minutes to remove any glassy coatings on the grains. Then all separates were cleaned for three minutes each in acetone, ethyl alcohol, water, and deionized water. The acetone removed any residual heavy liquids from the separates and the other solvents removed the acetone. The separates were dried and packaged for irradiation.

APPENDIX VI

The $^{40}\text{Ar}/^{39}\text{Ar}$ Dating Method

The $^{40}\text{Ar}/^{39}\text{Ar}$ method for dating geologic materials is a recent modification of the conventional potassium-argon dating method. The use of the $^{40}\text{Ar}/^{39}\text{Ar}$ ratio as a dating tool was first suggested by Wanke and König (1956). Their method, which proposed a counting technique for measurement of ^{39}Ar , did not gain acceptance. The first proposal of the $^{40}\text{Ar}/^{39}\text{Ar}$ method as it is recognized today came from Sigureirsson (1962). However, because this report was published in Icelandic, the origination of the method is commonly credited to Merrihue (1965) and Merrihue and Turner (1966).

Both the potassium-argon and the $^{40}\text{Ar}/^{39}\text{Ar}$ dating methods are based upon the radioactive decay of ^{40}K to ^{40}Ar . ^{40}K is the only naturally occurring radioactive isotope of potassium and undergoes branching decay to produce both ^{40}Ar and ^{40}Ca (fig. 28). Upon crystallization and cooling of a rock the ^{40}Ar is trapped within the mineral crystal lattices.

For the ^{40}Ar to begin to accumulate, the temperature must decrease to the point where the vibrational energy of the lattice no longer allows ^{40}Ar to escape by diffusion. This temperature, called the

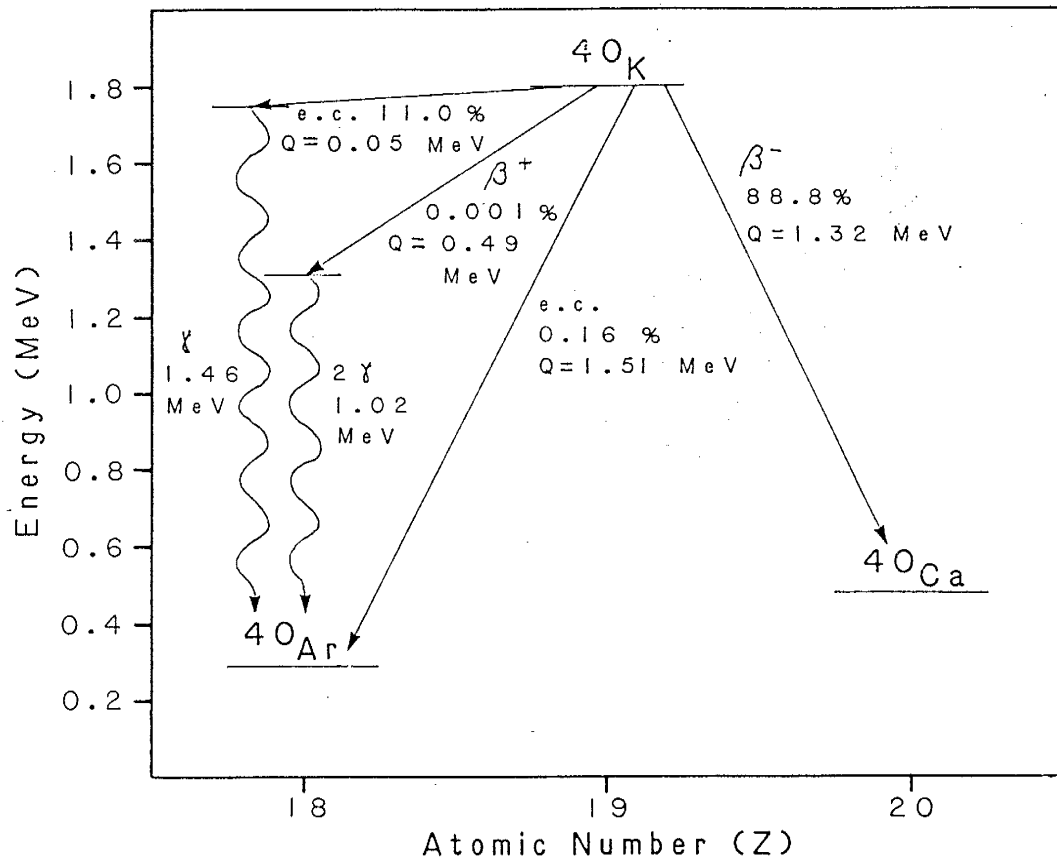


Figure 28. Branching decay of ^{40}K (Faure, 1977)

blocking temperature, is that point where ^{40}Ar loss becomes negligible compared to the rate of ^{40}Ar accumulation. Thus, the potassium-argon and $^{40}\text{Ar}/^{39}\text{Ar}$ ages represent the time since the sample cooled through its blocking temperature.

For volcanic rocks, this cooling is very rapid and all cogenetic minerals should give the same age. Plutonic and metamorphic rocks cool much more slowly. Each mineral has its own characteristic blocking temperature for a given rate of cooling, so, when slow cooling occurs, cogenetic minerals will not yield the same ages. This discordancy gives valuable information about the cooling rate of the formations involved. Relative blocking temperatures are hornblendes > muscovite > biotite > potassium feldspars (Dallmeyer and Van Breeman, 1981; Harrison and McDougall, 1982).

Four basic assumptions are made in the potassium-argon and $^{40}\text{Ar}/^{39}\text{Ar}$ dating methods: 1) the decay rate of ^{40}K is constant and has not changed through geologic time, and the decay constant for ^{40}K is accurately known; 2) no fractionation of potassium occurs so the isotopic composition of potassium is only changed by radioactive decay; 3) no Ar is present in the rock at the time of formation; and 4) the rock or mineral has remained a closed system for potassium and argon since formation.

When a discrepancy occurs in a K-Ar or $^{40}\text{Ar}/^{39}\text{Ar}$ age, one or more of these assumptions has broken down. The first two assumptions are rarely questioned, so most problems arise from the last two. The third assumption is almost never valid, but is accounted for by an atmospheric argon correction. Problems may still be present if the original argon component trapped in the rock does not have the same isotopic composition as the modern atmosphere. The fourth assumption is not always true and is the cause of many discordant ages. If the system has not remained closed, argon and potassium may have been added to or removed from the system in varying proportions, possibly in several separate incidents. The consequences of the last two assumptions are discussed later.

In the potassium-argon dating method, a sample is divided into aliquots for separate potassium and ^{40}Ar analyses. The potassium content is commonly determined by flame photometry. The ^{40}Ar is extracted from the sample by heating, and then purified, spiked, and measured with a mass spectrometer using the isotope dilution technique. The age of the sample is calculated using the basic age equation (1):

$$t = 1/\lambda \ln [^{40}\text{Ar}^*/^{40}\text{K} (\lambda/\lambda_e) + 1] \quad (1)$$

In this equation, λ is the total decay constant for ^{40}K , λ_e is the ^{40}K decay constant for electron capture to ^{40}Ar , $^{40}\text{Ar}^*$ is the amount of radiogenic ^{40}Ar in the sample, and ^{40}K is the amount of ^{40}K in the sample.

In the $^{40}\text{Ar}/^{39}\text{Ar}$ method, both the potassium and ^{40}Ar analyses are performed on the same aliquot of the sample. The sample is irradiated with fast neutrons in a nuclear reactor to convert a proportion of the ^{39}K present to ^{39}Ar by the nuclear reaction $^{39}\text{K} (n,p) ^{39}\text{Ar}$. The sample is then heated to release the argon which is measured as the ratio of $^{40}\text{Ar}/^{39}\text{Ar}$ by a mass spectrometer. The calculation of the sample age is complicated by interfering nuclear reactions which occur during irradiation. These will be discussed later.

The advantages of the $^{40}\text{Ar}/^{39}\text{Ar}$ method over the potassium-argon method are readily apparent. The $^{40}\text{Ar}/^{39}\text{Ar}$ method overcomes the problem of sample inhomogeneity by measuring ^{40}Ar and K on the same aliquot. This also reduces the amount of sample required for an analysis. The $^{40}\text{Ar}/^{39}\text{Ar}$ method overcomes problems caused by incomplete extraction of argon from a sample. The age is calculated from the ratio of argon isotopes, not the absolute amount of ^{40}Ar in the sample. This ratio measurement is more precise than measuring the ^{40}Ar by isotope dilution and does not require that all the argon be extracted from the sample.

SAMPLE PREPARATION

The choice of sample and subsequent preparation are among the most important steps in the analytical procedure. The choice of sample material obviously depends upon the geologic problem to be solved and the materials available in the field. The material must have a

sufficient potassium content or contain potassium-bearing minerals to be dated by this method. The basic choice of sample materials is between whole-rock and single-mineral analyses. Whole-rock $^{40}\text{Ar}/^{39}\text{Ar}$ analyses have many problems, especially with interfering isotopes created during irradiation. While successful whole-rock $^{40}\text{Ar}/^{39}\text{Ar}$ studies have been made on basalts (Bottomley and York, 1976; Fleck and others, 1977; Ozima and Saito, 1973), the method gives best results when mineral separates are analyzed. The presence of only one mineral phase eliminates much ambiguity in data interpretation and permits more precise comparisons between samples. A procedure for the preparation of mineral separates is discussed in Muller (1977) and Appendix V. To insure only one mineral phase is present, the mineral separates must be extremely pure, preferably hand picked under a microscope.

The amount of sample to be irradiated is determined by the K_2O content of the material and the neutron flux available (Turner, 1971a). The limiting factor is the production of sufficient ^{39}Ar to be detected by the mass spectrometer, without generation of large amounts of interfering isotopes by a long irradiation time. Once the optimum sample sizes are calculated, the samples are weighed into small cylindrical aluminum foil capsules, crimped closed, numbered, and leak tested (fig. 29). Monitor standards are packaged in the same manner.



Figure 29. Packaging a mineral separate.

- a. A mineral separate is poured into an aluminum capsule before weighing.



Figure 29. Packaging a mineral separate.

b. The aluminum capsule is trimmed and crimped closed.



Figure 29. Packaging a mineral separate.

c. Encapsulated samples are arranged in quartz glass vials.

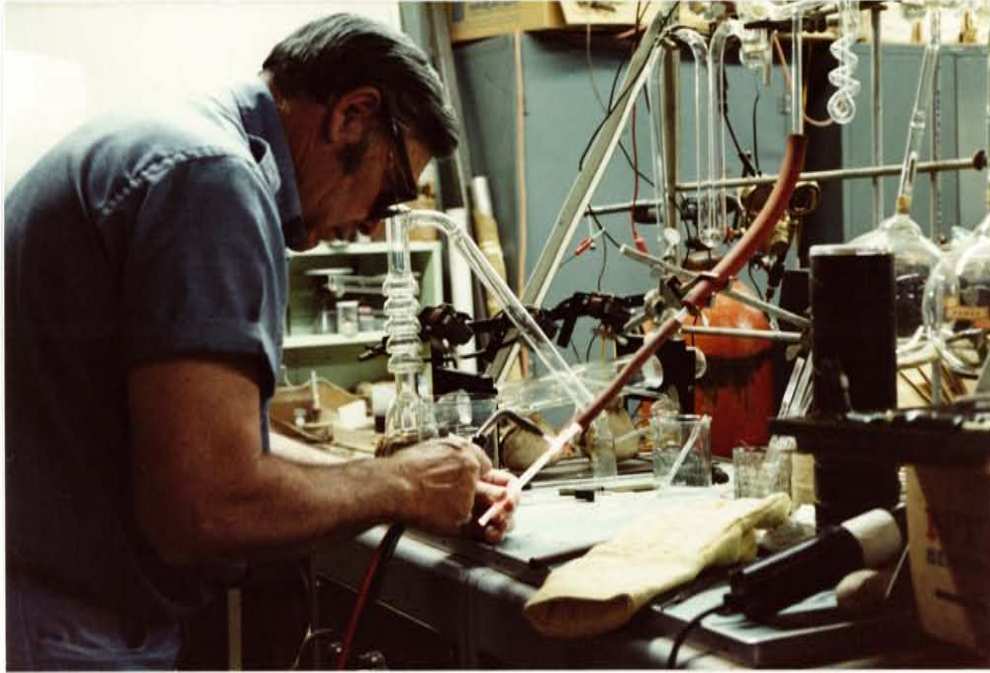


Figure 30. Closure of an irradiation vial. The quartz glass vials are heat sealed under a low vacuum. Pictured is scientific glassblower Alfred Heine of Virginia.

IRRADIATION

The packets containing samples and monitors are placed in quartz glass vials with the monitors evenly spaced throughout the package. The vials are heat sealed under a moderate vacuum (fig. 30). The position of each packet is measured from the base of the vial and recorded. The vials are then placed in a cylindrical aluminum rack and wired into place. The rack is enclosed in an aluminum cylinder cold welded closed at both ends (fig. 31). This complicated packaging is needed for safety, waterproofing, and to insure exact placement of the samples within the reactor core. Aluminum is used to reduce shielding of the samples and minimize the activity of the irradiated package.

The ^{39}K (n,p) ^{39}Ar reaction requires a flux of fast neutrons. The reactor utilized in this study is the U.S. Geological Survey TRIGA reactor, although any reactor supplying a flux of fast neutrons can be used. The U.S.G.S. TRIGA reactor has a flux over the entire energy spectrum of $1.1 \times 10^{17} \text{ n/cm}^2\text{-MWH}$ and a fast/thermal ratio in the central thimble of 1.17 (for fast neutrons $> 0.6 \text{ MeV}$; Dalrymple and others, 1981). The reactor is operated for eight hours a day, five days a week, so irradiation is performed incrementally.

The ^{39}Ar produced is calculated from the following equation (2),

$$^{39}\text{Ar} = ^{39}\text{K} \Delta T \int \phi(\epsilon) \sigma(\epsilon) d\epsilon \quad (2)$$

where ^{39}K is the number of atoms of ^{39}K in the sample, ΔT is the length of the irradiation, $\phi(\epsilon)$ is the neutron flux density at energy ϵ , $\sigma(\epsilon)$



Figure 31. Components of an irradiation package. The quartz glass vials were wired into place in the aluminum rack which will be placed inside the aluminum cylinder. The lens cap is 5 cm in diameter.

is the capture cross section of ^{39}K for neutrons of energy ϵ , and the expression is integrated over the energy spectrum of the neutrons (Mitchell, 1968). Equation 2 is difficult to evaluate as the neutron flux density and the capture cross-section values are nearly impossible to determine. The need to solve equation 2 is eliminated by irradiating monitor standards of known age with the unknowns. By comparing the ^{39}Ar produced in the monitors with the unknowns, the variables in equation 2 cancel.

ARGON EXTRACTION

The apparatus and procedures used for argon extraction and analysis are very similar to those used in conventional potassium-argon dating (Dalrymple and Lanphere, 1969). The procedures described below are those used in the $^{40}\text{Ar}/^{39}\text{Ar}$ laboratory at the U.S. Geological Survey National Center in Reston, Virginia. On the whole, interlab variation of equipment and procedures is minor. The samples are degassed by heating with a radiofrequency heater, the reactive gases are removed, and the remaining gas is analyzed.

The entire extraction line, either pyrex glass or metal tubing, is operated at ultra-high vacuum pressures of 10^{-8} torr or below. The vacuum is maintained by several pumps of different design. The first type is a turbo-molecular pump. This device contains turbine blades which spin at very high revolutions per minute and physically push the

molecules of gas out of the system. The turbo-molecular pump is backed by a roughing pump which is used to evacuate the system after it has been opened to the atmosphere. This procedure keeps the turbo-molecular pump operating at maximum rpm at all times and saves mechanical wear. Another type of pump, an ion pump, consists of a series of parallel metal plates with a high potential difference applied between them. Ions of gas are attracted to the plates because of the difference in charge and become physically embedded on the surface of the plates.

After exposure to the atmosphere, the high vacuum in the line is achieved by baking the system. A large oven covers the entire section of the extraction line which has been open to the air. The line is baked at 150°-200°C for six hours or more while open to the turbo-molecular pump. The heat frees gas molecules which had adhered to the walls of the pyrex or the valves, permitting the pump to remove them from the line.

HEATING SYSTEM

Sample heating takes place in a detachable Pyrex glass bottle which facilitates changing crucibles and samples. The bottle is double-walled pyrex-glass cooled by a water jacket, and lined with a quartz glass sleeve for easy cleaning and low blank values (fig. 32a). The bottle neck is cooled by forced air to help prevent breakage due to thermal stress. The bottle is attached to the extraction line by a copper

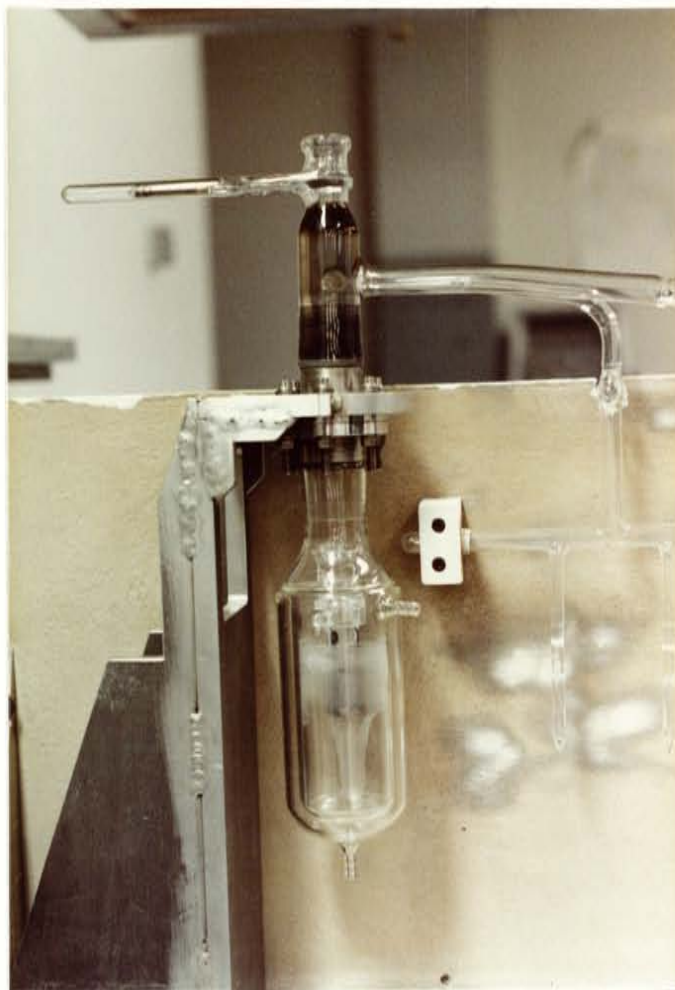


Figure 32. Argon extraction sample bottle.

- a. The sample bottle in place in the argon extraction line. Sidearm for sample storage is in the upper right.

gasket between two knife-edge seals. Within the bottle, the molybdenum crucible is suspended by molybdenum straps from a pyrex funnel. The funnel aids in dropping samples into the crucible from a storage sidearm above.

A radio-frequency induction system is used for heating. The radio-frequency waves generated are transmitted to a coil surrounding the sample bottle and there induce a current flow in the molybdenum crucible, which heats due to the resistance of the metal (fig. 32b). Temperatures are determined with an optical pyrometer.

GAS PURIFICATION

As the sample is heated, the gases given off are trapped on an activated charcoal finger cooled with liquid nitrogen. This serves to keep the pressure in the sample bottle low during heating, thus preventing ionization of the evolving gases. The first cleaning stage for the gases is a Cu-CuO getter at 450°-550°C which oxidizes or ignites any hydrocarbons present and oxidizes hydrogen into water (fig. 33). The gases then pass through a synthetic molecular sieve dessicant to remove the water and remnant hydrocarbons. Next, the gases are reacted with a Ti getter at two different activation temperatures. At 650°C the Ti will combine with any nitrogen present, and at 350°C with any excess hydrogen. These compounds plate out on the interior of the getter leaving only a mixture of inert gases to be analyzed.

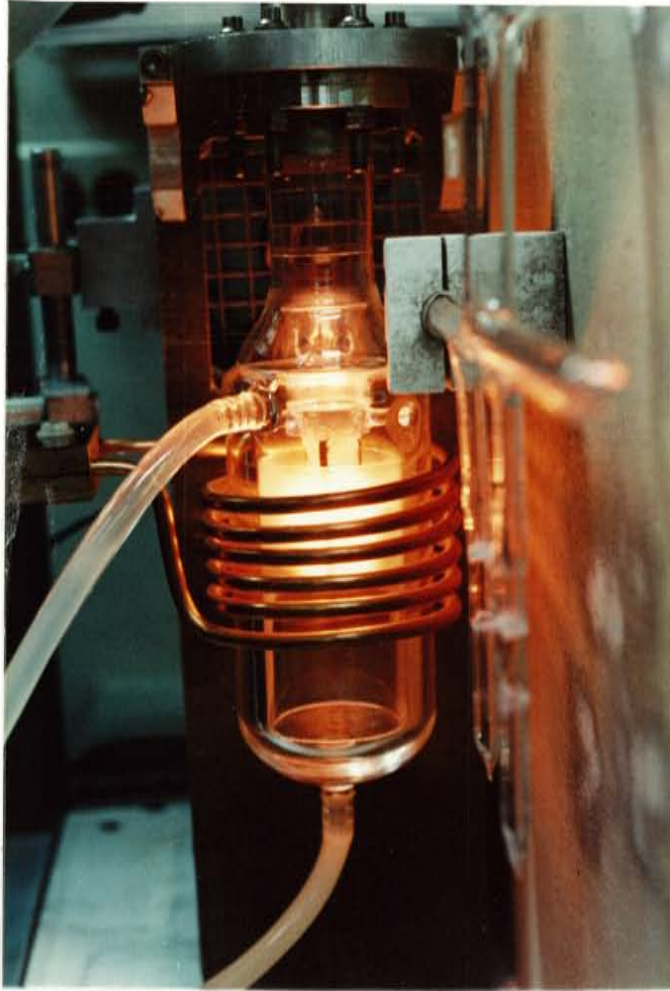


Figure 32. Argon extraction sample bottle.

- b. A sample being heated by the RF induction coil. The molybdenum crucible can be seen glowing a bright yellow. Tubes connected to the bottle are for a circulating water cooling system.

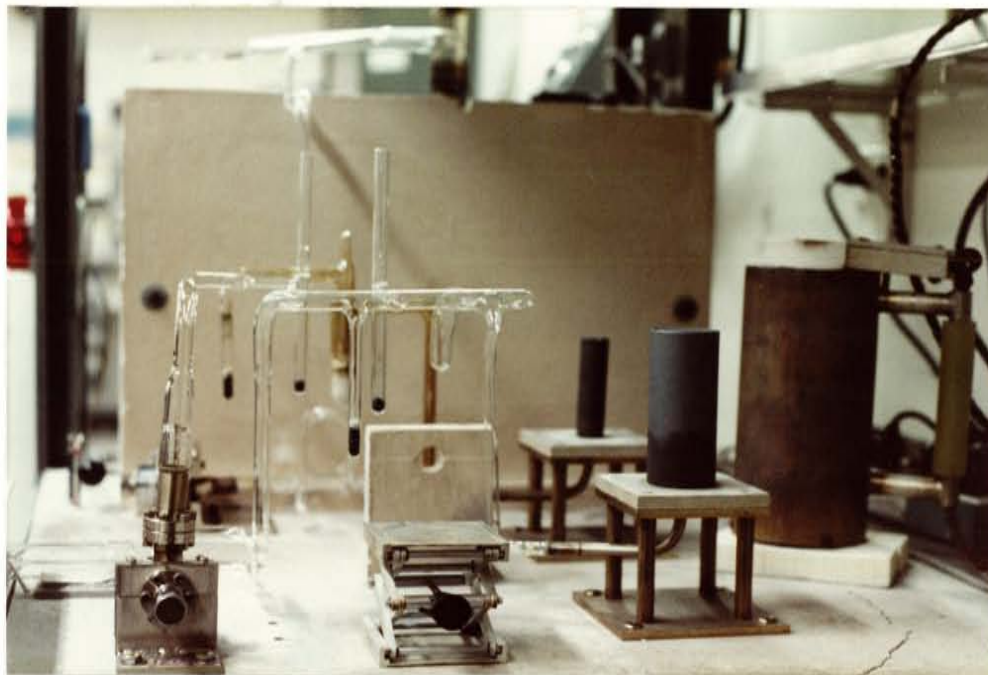


Figure 33. Argon gas purification line. Pictured are the Ti getter (foreground) and the Cu-CuO getter (background), which eliminate any reactive gases from the sample.

ARGON ANALYSIS

The argon-isotopic content of the sample gas is determined by mass spectrometry. Simply stated, mass spectrometry divides and detects ions on the basis of their masses. Incoming gas is ionized by a stream of electrons. The ions are accelerated and focused into a beam which then passes through the field of an electromagnet. A moving charged particle in a magnetic field will be deflected from a straight path proportionally to its mass. Past the magnetic field, the ions impact a stationary detector. By varying the strength of the magnetic field, the ions of different mass can be detected.

For the argon analyses, the mass spectrometer is operated in the static mode. The gas sample is admitted to the flight tube of the instrument in one aliquot. The spectrometer is then run through several cycles of magnet settings to detect and record the different isotopes. During the course of the analysis the gas sample is fractionated, so the individual isotopic values must be recalculated to time zero, the instant the sample was admitted to the instrument. The final isotopic values must be corrected for mass spectrometer discrimination, the difference between the accepted values for atmospheric argon ratios and those same ratios as measured by the instrument. For the Micromass 1200B mass spectrometer used in this study (fig. 34), the measured atmospheric $^{40}\text{Ar}/^{36}\text{Ar}$ ratio is 296.5, as compared to the accepted value of 295.5 (Steiger and Jager, 1977).

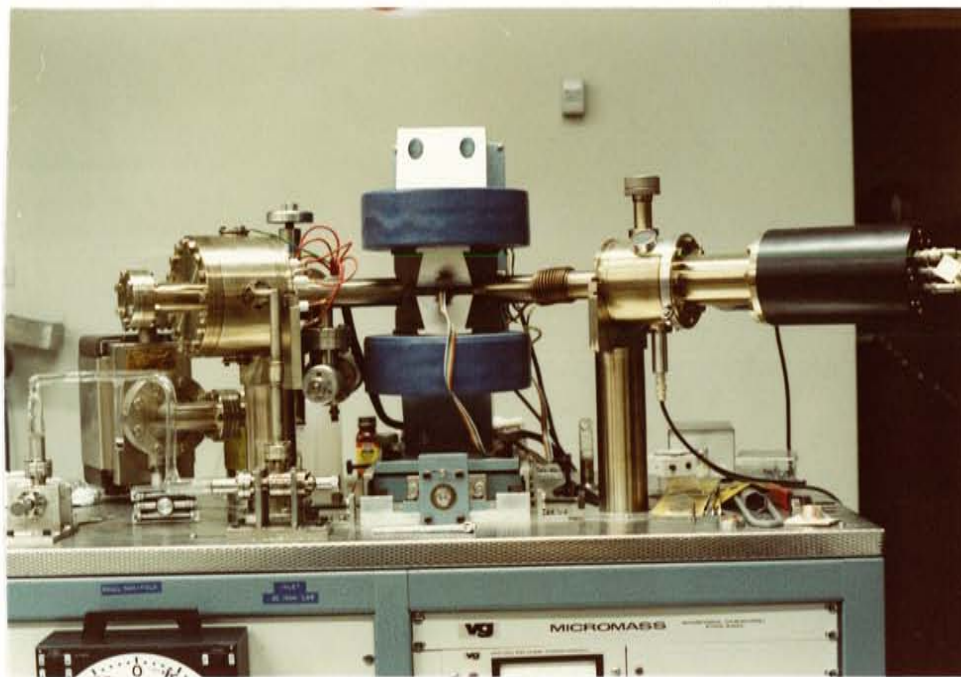


Figure 34. The VG-Micromass 1200B Mass Spectrometer.

INTERFERING NUCLEAR REACTIONS

Four elements can produce argon isotopes from nuclear reactions. These elements and the reactions are summarized in Table 7. Of all the possible reactions, only four occur with sufficient frequency to warrant corrections (Turner, 1971a). These reactions are $^{40}\text{Ca}(n,\alpha)^{36}\text{Ar}$, $^{42}\text{Ca}(n,\alpha)^{39}\text{Ar}$, $^{40}\text{K}(n,p)^{40}\text{Ar}$, and $^{41}\text{K}(n,d)^{40}\text{Ar}$. According to Roddick (1983), for high chlorine samples irradiated with a high thermal-flux component, the Cl-derived interferences become large and necessitate correction.

Correction factors for these interferences are determined for each reactor, as they depend upon the neutron flux characteristics. Reagent-grade K_2SO_4 crystals and optical-grade CaF_2 crystals are irradiated and analyzed. To calculate the correction factors it is assumed that all ^{36}Ar in the K_2SO_4 is atmospheric, all ^{40}Ar in the CaF_2 is atmospheric, and all ^{37}Ar is derived from calcium. This last assumption is valid due to the extremely small amounts of ^{37}Ar generated from ^{39}K and ^{36}Ar (Brereton, 1970). From repeated irradiations and analyses, the reactor constants, or correction factors, $(^{36}\text{Ar}/^{37}\text{Ar})_{\text{Ca}}$, $(^{39}\text{Ar}/^{37}\text{Ar})_{\text{Ca}}$, and $(^{40}\text{Ar}/^{39}\text{Ar})_{\text{K}}$ (the subscripts denote the source of the isotopes) can be calculated. For the U.S.G.S. TRIGA reactor, the calcium-derived constants are very reproducible but the potassium-derived constant varies by as much as a factor of 50 (Dalrymple and others, 1981). The effect of these interference

TABLE 7
Interfering Nuclear Reactions

Target Element	Argon Isotopes Produced				
	^{36}Ar	^{37}Ar	^{38}Ar	^{39}Ar	^{40}Ar
Ca	$^{40}\text{Ca} (n, n\alpha)$	$^{40}\text{Ca} (n, \alpha)$	$^{42}\text{Ca} (n, n\alpha)$	$^{42}\text{Ca} (n, \alpha)$ $^{43}\text{Ca} (n, n\alpha)$	$^{43}\text{Ca} (n, \alpha)$ $^{44}\text{Ca} (n, n\alpha)$
K		$^{39}\text{K} (n, nd)$	$^{40}\text{K} (n, d)$ $^{41}\text{K} (n, \alpha)$ $^{38}\text{Cl} \xrightarrow{\beta}$	$^{39}\text{K} (n, p)$ $^{40}\text{K} (n, d)$	$^{40}\text{K} (n, p)$ $^{41}\text{K} (n, d)$
Ar		$^{36}\text{Ar} (n, \gamma)$	$^{40}\text{Ar} (n, nd) \xrightarrow{-}$ $^{38}\text{Cl} \xrightarrow{\beta}$	$^{38}\text{Ar} (n, \gamma)$ $^{40}\text{Ar} (n, d) \xrightarrow{+}$ $^{39}\text{Cl} \xrightarrow{\beta}$	
Cl	$^{35}\text{Cl} (n, \alpha) \xrightarrow{+}$ $^{36}\text{Cl} \xrightarrow{\beta}$		$^{37}\text{Cl} (n, \gamma) \xrightarrow{+}$ $^{38}\text{Cl} \xrightarrow{\beta}$		

corrections can be minimized by careful choice of sample size and irradiation time (Turner, 1971).

One other correction must be applied to the data. This correction is not for an isotope produced during irradiation but for atmospheric argon incorporated into the sample. It is assumed that this atmospheric component has the same composition as the modern atmosphere, an $^{40}\text{Ar}/^{36}\text{Ar}$ ratio of 295.5 (Steiger and Jager, 1977). The correction is applied by multiplying the corrected ^{36}Ar measurement by 295.5 and subtracting this product from the ^{40}Ar measurement.

MONITORS

To calculate an age from $^{40}\text{Ar}/^{39}\text{Ar}$ data, the amount of ^{39}K converted into ^{39}Ar must be known. As shown in equation 2, this quantity is difficult if not impossible to determine. Therefore, monitor standards are used to simplify the calculations.

A monitor mineral must meet several criteria before being useful. The age of the monitor must be very well constrained by conventional potassium-argon dating. The mineral must have a uniform ratio of $^{40}\text{Ar}^*$ to ^{40}K , as well as a homogeneous distribution of both $^{40}\text{Ar}^*$ and K. The monitor should also be fairly coarse-grained, available in reasonable quantities, and similar in both age and K/Ca ratio to the unknowns.

Many monitors have been used in the past with varying amounts of success. Dalrymple and others (1981) and Roddick (1983) have compared many of these materials and shown that several are not completely homogeneous and therefore not acceptable as standards. The monitor used in this study, MMhb-1, is one which Roddick (1983) reported as homogeneous at the 0.1% level. This hornblende is from the McClure Mountain Complex in Fremont County, Colorado and has been dated at 519.4 Ma (Alexander and others, 1978).

Monitor samples are distributed throughout each reactor package and irradiated with unknown samples. By comparing the $^{40}\text{Ar}^*/^{39}\text{Ar}$ ratio of the unknown sample to that of the monitor of known age, the parameters of the irradiation from equation 2 are eliminated. Sample ages so determined are actually ages relative to the particular monitor that was employed.

AGE CALCULATION

One of the first steps in calculating an age from argon isotopic data is correction of the ^{37}Ar data for radioactive decay. ^{37}Ar is a radioactive isotope produced in the reactor which has a half-life of 35.1 days. Decay of this isotope occurs both during and after irradiation and the correction formula used depends upon the irradiation schedule. If the irradiation occurred continuously, then equation 3 is used,

$${}^{37}\text{Ar}_o/{}^{39}\text{Ar} = {}^{37}\text{Ar}/{}^{39}\text{Ar} \lambda t e^{\lambda t'} / (1 - e^{-\lambda t}) \quad (3)$$

where ${}^{37}\text{Ar}_o$ is the amount of ${}^{37}\text{Ar}$ produced, ${}^{37}\text{Ar}$ is the amount measured, t is the irradiation time, t' is the time elapsed between irradiation and measurement, and λ is the ${}^{37}\text{Ar}$ decay constant. If irradiation was incremental, then equations 4 and 5 are used.

$${}^{37}\text{Ar}_o/{}^{39}\text{Ar} = {}^{37}\text{Ar}/{}^{39}\text{Ar} \sum [P_i t_i / I t_i \lambda e^{-\lambda t'} / (1 - e^{-\lambda t'})] \quad (4)$$

$$I = \sum P_i t_i \text{ in MWH} \quad (5)$$

P is the reactor power level, t is the increment length, t' is the corresponding time for that increment from irradiation to measurement, and MWH stands for megawatt hours.

After irradiation, the ${}^{40}\text{Ar}^*/{}^{39}\text{Ar}$ ratio of a sample is given by equation 6.

$${}^{40}\text{Ar}^*/{}^{39}\text{Ar} = \lambda_e / \lambda \quad {}^{40}\text{K}/{}^{39}\text{K} \quad 1/\Delta T e^{\lambda t - 1} / \int \phi(\epsilon) \sigma(\epsilon) d\epsilon \quad (6)$$

By defining a term J as:

$$J = \lambda / \lambda_e \quad {}^{39}\text{K}/{}^{40}\text{K} \quad \Delta T \int \phi(\epsilon) \sigma(\epsilon) d\epsilon \quad (7)$$

and substituting J into equation 6, the expression is much simplified (Faure, 1977):

$${}^{40}\text{Ar}^*/{}^{39}\text{Ar} = e^{\lambda t - 1} / J \quad (8)$$

By utilizing the monitor samples to solve equation 8 for J , an accurate assessment of the irradiation parameters is made for each position in the irradiation package. The appropriate J value is then substituted into the basic age equation (1) to yield the age of the sample.

$$t = 1/\lambda \ln [1 + J ({}^{40}\text{Ar}^*/{}^{39}\text{Ar}_K)] \quad (9)$$

Equation 9 does not take into account the corrections needed for atmospheric contamination and interfering isotopes. Incorporating all

of these corrections into one expression gives equation 10,

$$\frac{{}^{40}\text{Ar}^*/{}^{39}\text{Ar}_K}{(40\text{Ar}/39\text{Ar}) - 295.5[(36\text{Ar}/39\text{Ar}) - (36\text{Ar}/37\text{Ar})_{\text{Ca}}(37\text{Ar}/39\text{Ar})] - (40\text{Ar}/39\text{Ar})_K} = \frac{1 - (39\text{Ar}/37\text{Ar})_{\text{Ca}}(37\text{Ar}/39\text{Ar})}{(10)}$$

where $(36\text{Ar}/37\text{Ar})_{\text{Ca}}$, $(39\text{Ar}/37\text{Ar})_{\text{Ca}}$, and $(40\text{Ar}/39\text{Ar})_K$ are the reactor constants for interfering isotopes (Dalrymple and others, 1981).

ANALYTICAL PRECISION

The uncertainty in ${}^{40}\text{Ar}/{}^{39}\text{Ar}$ age determinations is estimated from the analytical precision of the method. This estimate has been derived by Dalrymple and Lanphere (1971), from which the following discussion is taken.

The quantity F is defined as ${}^{40}\text{Ar}^*/{}^{39}\text{Ar}_K$. The error in F is estimated from the random errors in the measured isotopic ratios of the sample. The variance in F , σ_F^2 , is calculated in equation 11.

$$\sigma_F^2 = A^2 \sigma_A^2 + C_1^2 B^2 \sigma_B^2 + [C_4 A - C_1 C_4 B + C_1 C_2]^2 D^2 \sigma_D^2 / F^2 \quad (11)$$

The letters are as defined below:

$$A = {}^{40}\text{Ar}/{}^{39}\text{Ar} \text{ measured}$$

$$B = {}^{36}\text{Ar}/{}^{39}\text{Ar} \text{ measured}$$

$$C = 295.5$$

$$D = {}^{37}\text{Ar}/{}^{39}\text{Ar}, \text{ measured and corrected for decay}$$

$$C = ({}^{36}\text{Ar}/{}^{37}\text{Ar})_{\text{Ca}}$$

$$C = ({}^{40}\text{Ar}/{}^{39}\text{Ar})_{\text{K}}$$

$$C = ({}^{39}\text{Ar}/{}^{37}\text{Ar})_{\text{Ca}}$$

$$\sigma_A^2 = \text{estimated variance in A (in \%)}$$

$$\sigma_B^2 = \text{estimated variance in B (in \%)}$$

$$\sigma_D^2 = \text{estimated variance in D (in \%)}$$

The estimated analytical error in the calculated age is:

$$\sigma_t = [J^2 F^2 (\sigma_F^2 + \sigma_J^2) / t^2 \lambda^2 (1 + FJ)^2]^{1/2} \quad (12)$$

where the variances of $F(\sigma_F^2)$ and $J(\sigma_J^2)$ are in percent.

DATA PRESENTATION

Several accepted forms may be used for presentation of data generated by the ${}^{40}\text{Ar}/{}^{39}\text{Ar}$ dating method. The simplest, a total fusion age, is roughly equivalent to a conventional potassium-argon age. The sample is degassed in one heating step and an age is calculated from the data. It is usually restricted to samples which are too small to be degassed incrementally, since the data is too limited to detect geologic error in the sample. More complicated forms of presentation are derived from incremental heating of samples. The samples are degassed in a

series of heating steps with the gas released in each step analyzed separately. The data set for each sample can then be plotted as an age-spectrum diagram or an argon-isotope correlation diagram.

An age-spectrum diagram plots the apparent age of each increment of gas versus the percentage of the total ^{39}Ar that was released in each step. The gas in each increment is corrected for interfering isotopes and atmospheric contamination and an age for that step is calculated. If the sample being analyzed has been undisturbed since the closure of the potassium-argon system, the apparent age for each increment should be the same and plot as a straight line or plateau. If there is no plateau, the potassium-argon system in the sample has been disturbed.

The problems with this diagram stem from the atmospheric correction applied to each increment. It is assumed that the atmospheric component has the same $^{40}\text{Ar}/^{36}\text{Ar}$ ratio as the modern atmosphere. If this assumption is incorrect, the apparent ages are miscalculated and the interpretation of the spectrum is in error. Also, there is little agreement as to what constitutes a plateau, and overall spectrum interpretation is somewhat subjective.

The argon isotope correlation diagrams overcome many of the problems associated with the age-spectrum diagrams. The correlation diagrams plot a ratio of argon isotopes on each axis; two different sets of parameters have been mentioned in the literature.

The first argon isotope correlation diagram, proposed by Merrihue and Turner (1966), plots $^{40}\text{Ar}/^{36}\text{Ar}$ versus $^{39}\text{Ar}/^{36}\text{Ar}$. This is also referred to as an Ar isochron plot. The basic premise of this plot is that there are two types of argon present in the system, potassium-derived argon and contamination. This contamination includes both excess argon and atmospheric argon (Faure, 1977). Thus the measured ratio of $^{40}\text{Ar}/^{36}\text{Ar}$ is equal to:

$$(^{40}\text{Ar}/^{36}\text{Ar})_m = (^{40}\text{Ar}/^{36}\text{Ar})_c + (^{40}\text{Ar}^*/^{39}\text{Ar})_K \times (^{39}\text{Ar}/^{36}\text{Ar})_m$$

(13)

where m denotes a measured value, c the contamination value, and K the potassium-derived value. This is the equation of a straight line with the slope proportional to the age of the sample and the y-intercept equal to the $^{40}\text{Ar}/^{36}\text{Ar}$ contamination present in the sample. This plot eliminates the need to correct the incremental data for an atmospheric component, so no value need be assumed (Dalrymple and Lanphere, 1974).

The problem with this correlation diagram derives from the choice of ^{36}Ar as the reference isotope. ^{36}Ar is the smallest quantity involved and the errors in the ratios are dominantly due to ^{36}Ar . Thus, the errors in the two ratios are highly correlated and the diagram may appear to be linear because of this correlation. In the treatment of the data, the line is regressed by the method of York (1969) which takes into consideration the correlated errors.

An alternative choice of isotopic ratios is $^{36}\text{Ar}/^{40}\text{Ar}$ versus $^{39}\text{Ar}/^{40}\text{Ar}$ (McDougall, 1981). The equation of the line plotted is derived from equation 13, with an x-intercept proportional to the age and the y-intercept equal to the $^{36}\text{Ar}/^{40}\text{Ar}$ contamination. The linear array of data represents a binary mixing line between trapped argon and potassium-derived argon. The correlated error problem for this choice of axes is much less than with ^{36}Ar as the reference isotope because ^{40}Ar is the largest value involved, and can therefore be measured with higher precision. The linear regression is still done by York's (1969) method. Though reduced, the errors involved are still correlated.

DATA INTERPRETATION

The interpretation of data and the assignment of an age is a straight-forward procedure if the sample has remained a closed system. Many complications arise when the sample deviates from this ideal case.

The perfect sample for dating has remained a closed system since crystallization and cooling; it did not inherit any $^{40}\text{Ar}^*$ from older rocks during formation and has not lost any components since formation. Thus, all $^{40}\text{Ar}^*$ present is derived from in-situ decay of ^{40}K and all the $^{40}\text{Ar}^*$ formed is still trapped within the sample. Such a sample will yield a perfectly concordant age spectrum (Dalrymple and Lanphere, 1974). Each increment of gas will have the same apparent age and the diagram will be a straight horizontal line. This line, called a

plateau, will contain 100% of the ^{39}Ar released by the sample. The age assigned to the sample is the weight average of all the incremental ages in the plateau. The plateau age will be identical to the total fusion age on such a sample. The corresponding isotope-correlation diagrams will plot as straight lines which yield ages equivalent to the plateau age.

One of the complications to interpretation is the loss of argon from the sample since formation. Since argon is an inert gas, it is trapped by the crystal lattice but not bound to it. Thus, the argon may escape the lattice by volume diffusion if the lattice spacings are large enough. One way to increase the lattice spacings is by heating. Turner (1968,1969) studied the effect of such diffusive argon loss on a theoretical population of spheres. He assumed that following partial argon loss, the concentration of argon at the edge of the spheres is zero and approaches the previous concentration some distance into the sphere. When such a partially disturbed sample is analyzed, the age-spectrum diagram follows a regular pattern. The low-temperature steps yield the youngest ages, with the apparent age of the fractions increasing with temperature until a plateau is reached. The high-temperature steps represent the gas held in the undisturbed centers of the mineral grains. The age-spectrum diagram is a slightly blurred representation of the internal $^{40}\text{Ar}^*$ distribution (Harrison, 1983). Depending upon the extent of argon loss, the high-temperature steps yield either the age of the sample or a minimum value for the age. The total-gas age or total-fusion age of such a sample is a meaningless date

between the time of formation and the time of argon loss. The isotope-correlation diagrams for samples with argon loss do not add much information to the age spectra. The correlation diagrams yield straight lines with ages equal to the total-gas and total-fusion ages. The $^{40}\text{Ar}/^{36}\text{Ar}$ value may be slightly different from the atmospheric value, indicating only that the system has been disturbed. The measure of the goodness of fit of the line to the data points will be a large value reflecting the presence of geologic error (Fleck and others, 1977).

A second complication to data interpretation is the incorporation of excess argon into rocks and minerals prior to closure of the system. Excess argon is incorporated into rocks and minerals by processes other than in-situ decay of ^{40}K (Lanphere and Dalrymple, 1976). The total-gas and total-fusion ages of such samples are anomalously old and have no geologic significance except as a maximum limit on the age. The age spectra of excess-argon samples differ for igneous and metamorphic rocks and minerals. Lanphere and Dalrymple (1976) demonstrated that various igneous minerals yield saddle-shaped spectra. The apparent age of increments decreased to a broad minimum at intermediate amounts of ^{39}Ar released and then increased until all argon was released. The minimum in the spectra approaches the age of formation of the sample but is, at best, a maximum age. The corresponding correlation diagrams produced a meaningless scatter of points. Metamorphic rocks exhibit a much different form in the age spectra. The apparent ages of the increments rises sharply to a relatively flat plateau, at ages much greater than the metamorphic age (Roddick and others, 1980). The corresponding

correlation diagrams exhibit two linear trends, for low-temperature and high-temperature increments, and are not considered isochrons.

The last complication in interpretation is the effect of ^{39}Ar recoil during irradiation. The nuclear reaction producing ^{39}Ar releases a proton from the target atom. This release imparts a recoil energy to the ^{39}Ar atom sufficient to remove the ^{39}Ar atom from the near surface of a mineral grain. If the recoiled ^{39}Ar atoms are absorbed onto the surface of other mineral grains, anomalous age-spectrum patterns can result (Huneke and Smith, 1976). If the recoiled ^{39}Ar atoms are not absorbed, but lost into the irradiation vessel, the resulting age can be anomalously old (Villa and others, 1983). The limited number of studies on recoil effects leaves many unanswered questions. At present, recoil seems to affect only very fine-grained ($<100\mu$) samples in which both a potassium-rich and a potassium-poor phase are present (Huneke and Smith, 1976). The effect of ^{39}Ar recoil on coarse-grained ($>100\mu$) single-phase mineral separates is negligible (Harrison, 1983).

The complications to data interpretation discussed above are not the only ones possible. Harrison (1983) discusses several additional sources of ambiguity. Also, the complications above can occur in varying intensities and combinations. Much of $^{40}\text{Ar}/^{39}\text{Ar}$ data interpretation is still subjective when incremental heating data do not show a well-defined age-spectrum plateau.

APPENDIX VII

TABULAR $^{40}\text{Ar}/^{39}\text{Ar}$ DATA

K-JH-26 Hornblende

J = 0.005488
 Sample Weight = 0.4024 g
 $^{40}\text{Ar}/^{36}\text{Ar}$ atm. = 296.5

Temp C	$^{40}\text{Ar}/^{39}\text{Ar}$	$^{37}\text{Ar}/^{39}\text{Ar}$	$^{36}\text{Ar}/^{39}\text{Ar}$ ($\times 10^{-3}$)	$^{40}\text{Ar}/^{39}\text{Ar}$ Corrected (F)	^{39}Ar (mole) ($\times 10^{-13}$)	^{39}Ar (% of) (Total)	% Radiogenic ^{40}Ar	Apparent K/Ca (mol/mol)	Apparent Age ± 1 (Ma)
1000	8.153	8.134	18.18	3.4033	0.690	18.8	41.8	0.0636	33.37 ± 0.12
1450	4.824	8.359	7.363	3.2883	2.79	76.1	68.3	0.0619	32.25 ± 0.12
1500	18.710	8.378	53.73	3.4739	0.187	5.1	18.6	0.0617	34.06 ± 0.28
Total Gas									32.56
Preferred Age									32.25 ± 0.12

K-D-1 Hornblende

J = 0.005488
 Sample Weight = 0.4410 g
 $^{40}\text{Ar}/^{36}\text{Ar}$ atm. = 296.5

Temp C	$^{40}\text{Ar}/^{39}\text{Ar}$	$^{37}\text{Ar}/^{39}\text{Ar}$	$^{36}\text{Ar}/^{39}\text{Ar}$ ($\times 10^{-3}$)	$^{40}\text{Ar}/^{39}\text{Ar}$ Corrected (F)	^{39}Ar (mole) ($\times 10^{-13}$)	^{39}Ar (% of) (Total)	% Radiogenic ^{40}Ar	Apparent K/Ca (mol/mol)	Apparent Age ± 1 (Ma)
1000	13.125	7.662	34.81	3.4254	0.338	8.5	26.1	0.0675	33.60 ± 0.24
1350	4.659	8.294	6.938	3.2440	2.28	57.6	69.8	0.0623	31.83 ± 0.08
1500	6.873	8.355	14.42	3.2524	1.34	33.9	47.4	0.0619	31.92 ± 0.07
Total Gas									32.01
Preferred Age									31.86 ± 0.07

K-JH-26 Na-sanidine

J = 0.005488

Sample Weight = 0.0967g

 $^{40}\text{Ar}/^{36}\text{Ar}$ atm. = 296.5

Temp C	$^{40}\text{Ar}/^{39}\text{Ar}$	$^{37}\text{Ar}/^{39}\text{Ar}$ ($\times 10^{-3}$)	$^{36}\text{Ar}/^{39}\text{Ar}$ ($\times 10^{-4}$)	$^{40}\text{Ar}/^{39}\text{Ar}$ Corrected (F)	^{39}Ar (mole) ($\times 10^{-13}$)	^{39}Ar (% of) (Total)	% Radiogenic Ar	Apparent K/Ca (mol/mol)	Apparent Age ± 1 (Ma)
900	3.720	9.052	14.74	3.2788	2.24	13.3	86.1	57.4	32.17 \pm 0.10
1000	3.384	8.629	3.432	3.2770	2.18	13.0	96.8	60.3	32.16 \pm 0.09
1050	3.418	8.274	4.310	3.2855	2.57	15.3	96.1	62.8	32.24 \pm 0.07
1100	3.389	8.099	3.722	3.2740	2.12	12.6	96.6	64.2	32.13 \pm 0.08
1150	3.429	8.136	5.044	3.2746	1.96	11.6	95.5	63.9	32.13 \pm 0.08
1200	3.469	8.029	5.861	3.2902	1.99	11.8	94.9	64.8	32.28 \pm 0.07
1250	3.577	8.117	9.865	3.2805	1.46	8.7	91.7	64.1	32.19 \pm 0.08
1450	3.725	8.066	14.92	3.2785	2.32	13.8	88.0	64.5	32.17 \pm 0.10
Total Gas									32.18
Plateau Age									32.18 \pm 0.05

K-BM-3 Na-sanidine

Sample Weight = 0.0922 g

J = 0.005488

 $^{40}\text{Ar}/^{36}\text{Ar}$ atm. = 296.5

Temp C	$^{40}\text{Ar}/^{39}\text{Ar}$ ($\times 10^{-3}$)	$^{36}\text{Ar}/^{39}\text{Ar}$ ($\times 10^{-4}$)	$^{40}\text{Ar}/^{39}\text{Ar}$ Corrected (F)	^{39}Ar (mole ($\times 10^{-13}$))	^{39}Ar (% of (Total))	% Radiogenic ^{40}Ar	Apparent K/Ca (mol/mol)	Apparent Age ± 1 (Ma)
900	4.129	11.10	29.45	1.39	9.4	78.8	46.9	31.93 \pm 0.07
1000	3.622	9.774	11.26	1.70	11.6	90.7	53.2	32.22 \pm 0.08
1050	3.411	9.283	4.290	1.71	11.6	96.1	56.0	32.18 \pm 0.07
1100	3.423	8.975	4.538	1.94	13.2	95.9	57.9	32.22 \pm 0.08
1150	3.412	8.954	5.084	2.68	18.2	95.4	58.1	31.96 \pm 0.10
1200	3.529	9.069	7.945	2.22	15.1	93.2	57.3	32.27 \pm 0.09
1250	3.709	9.132	13.71	1.16	7.9	88.9	56.9	32.36 \pm 0.09
1450	3.765	9.815	15.96	1.91	13.0	87.3	53.0	32.26 \pm 0.08
Total Gas								32.16
Plateau Age								32.25 \pm 0.06

K-D-1 Na-sanidine

J = 0.005488

Sample Weight = 0.0576 g

 $^{40}\text{Ar}/^{36}\text{Ar}$ atm. = 296.5

Temp C	$^{40}\text{Ar}/^{39}\text{Ar}$ ($\times 10^{-3}$)	$^{37}\text{Ar}/^{39}\text{Ar}$ ($\times 10^{-3}$)	$^{36}\text{Ar}/^{39}\text{Ar}$ ($\times 10^{-4}$)	$^{40}\text{Ar}/^{39}\text{Ar}$ Corrected (F)	^{39}Ar (mole) ($\times 10^{-13}$)	^{39}Ar (% of) (Total)	% Radiogenic ^{40}Ar	Apparent K/Ca (mol/mol)	Apparent Age ± 1 (Ma)
900	3.843	9.032	18.53	3.2903	1.51	14.9	85.6	57.6	32.28 \pm 0.08
1050	3.372	8.441	3.608	3.2598	2.75	27.1	96.7	61.6	31.99 \pm 0.06
1150	3.347	8.022	2.324	3.2729	2.75	27.1	97.8	64.8	32.11 \pm 0.08
1250	3.460	7.943	5.724	3.2855	1.99	19.6	95.0	65.5	32.24 \pm 0.09
1350	3.810	8.183	18.37	3.2618	0.866	8.5	85.6	63.5	32.01 \pm 0.08
1450	5.516	11.14	74.69	3.3041	0.277	2.7	59.9	46.7	32.42 \pm 0.09
							Total Gas		32.13
							Plateau Age		32.05 \pm 0.07

K-CM-2 Na-sanidine

J = 0.005488

Sample Weight = 0.0829 g

 $^{40}\text{Ar}/^{36}\text{Ar}$ atm. = 296.5

Temp C	$^{40}\text{Ar}/^{39}\text{Ar}$ ($\times 10^{-3}$)	$^{37}\text{Ar}/^{39}\text{Ar}$ ($\times 10^{-3}$)	$^{36}\text{Ar}/^{39}\text{Ar}$ ($\times 10^{-4}$)	$^{40}\text{Ar}/^{39}\text{Ar}$ Corrected (F)	^{39}Ar (mole) ($\times 10^{-13}$)	^{39}Ar (% of) (Total)	% Radiogenic ^{40}Ar	Apparent K/Ca (mol/mol)	Apparent Age ± 1 (Ma)
900	4.558	10.95	44.15	3.2484	0.859	9.5	71.3	47.5	31.88 \pm 0.14
1000	3.575	9.240	10.82	3.2503	1.06	11.8	90.9	56.3	31.90 \pm 0.08
1050	3.505	8.722	8.729	3.2414	0.769	8.5	92.5	59.6	31.81 \pm 0.09
1100	3.527	8.412	10.09	3.2234	0.820	9.1	91.4	61.8	31.63 \pm 0.07
1150	3.507	8.575	8.788	3.2422	0.871	9.6	92.4	60.6	31.82 \pm 0.09
1200	3.539	8.717	10.11	3.2345	0.974	10.8	91.4	59.7	31.74 \pm 0.10
1250	3.618	8.662	12.35	3.2477	0.905	10.0	89.8	60.0	31.87 \pm 0.07
1350	3.577	8.819	11.41	3.2343	2.78	30.7	90.4	59.0	31.74 \pm 0.11
Total Gas									31.79
Plateau Age									31.77 \pm 0.06

SU-4-77 Na-sanidine

J = 0.004467

Sample Weight = 0.1329 g

 $^{40}\text{Ar}/^{36}\text{Ar}$ atm. = 296.5

Temp C	$^{40}\text{Ar}/^{39}\text{Ar}$	$^{37}\text{Ar}/^{39}\text{Ar}$ ($\times 10^{-3}$)	$^{36}\text{Ar}/^{39}\text{Ar}$ ($\times 10^{-4}$)	$^{40}\text{Ar}/^{39}\text{Ar}$ Corrected (F)	^{39}Ar (mole) ($\times 10^{-13}$)	^{39}Ar (% of) (Total)	% Radiogenic ^{40}Ar	Apparent K/Ca (mol/mol)	Apparent Age ± 1 (Ma)
750	7.228	49.85	103.0	0.207	1.1	57.8	10.4	33.38 \pm 0.20	
900	4.449	22.85	13.41	0.957	5.3	91.0	22.8	32.34 \pm 0.09	
1000	4.329	14.90	11.16	3.29	18.1	92.3	34.9	31.91 \pm 0.10	
1050	4.512	11.12	17.26	3.48	19.2	88.6	46.8	31.92 \pm 0.09	
1100	4.897	10.25	30.65	2.53	14.0	81.4	50.7	31.83 \pm 0.09	
1150	4.987	9.851	33.45	4.94	27.2	80.1	52.8	31.90 \pm 0.09	
1200	8.495	10.24	152.8	2.72	15.0	46.8	50.8	31.75 \pm 0.11	
Total Gas									31.91
Plateau Age									31.87 \pm 0.07

K-JH-26 Biotite

J = 0.005488

Sample Weight = 0.1001 g

 $^{40}\text{Ar}/^{36}\text{Ar}$ atm. = 296.5

Temp C	$^{40}\text{Ar}/^{39}\text{Ar}$ ($\times 10^{-3}$)	$^{37}\text{Ar}/^{39}\text{Ar}$ ($\times 10^{-3}$)	$^{36}\text{Ar}/^{39}\text{Ar}$ ($\times 10^{-3}$)	$^{40}\text{Ar}/^{39}\text{Ar}$ Corrected (F)	^{39}Ar (mole) ($\times 10^{-13}$)	^{39}Ar (% of) (Total)	% Radiogenic ^{40}Ar	Apparent K/Ca (mol/mol)	Apparent Age ± 1 (Ma)
850	7.830	42.18	14.82	3.4466	0.645	5.1	44.0	12.3	33.80 \pm 0.11
950	5.305	12.89	6.559	3.3615	0.688	5.4	63.4	40.3	32.98 \pm 0.12
1050	4.151	5.147	2.837	3.3075	1.22	9.6	79.7	101.0	32.45 \pm 0.07
1100	4.364	5.324	3.601	3.2941	1.55	12.2	75.5	97.7	32.32 \pm 0.07
1150	4.141	6.117	2.837	3.2973	1.68	13.3	79.6	85.0	32.35 \pm 0.10
1200	4.205	6.351	3.087	3.2870	1.81	14.3	78.2	81.9	32.25 \pm 0.10
1250	4.315	6.773	3.477	3.2825	1.65	13.0	76.1	76.8	32.21 \pm 0.07
1500	4.388	8.451	3.543	3.3361	3.42	27.0	76.0	61.5	32.73 \pm 0.11
							Total Gas		32.54
							Plateau Age		32.28 \pm 0.07

K-CM-2 Biotite

J = 0.005488

Sample Weight = 0.1023 g

 $^{40}\text{Ar}/^{36}\text{Ar}$ atm. = 296.5

Temp C	$^{40}\text{Ar}/^{39}\text{Ar}$	$^{37}\text{Ar}/^{39}\text{Ar}$ ($\times 10^{-3}$)	$^{36}\text{Ar}/^{39}\text{Ar}$ ($\times 10^{-3}$)	$^{40}\text{Ar}/^{39}\text{Ar}$ Corrected (F)	^{39}Ar (mole) ($\times 10^{-13}$)	^{39}Ar (% of) (Total)	% Radiogenic ^{40}Ar	Apparent K/Ca (mol/mol)	Apparent Age ± 1 (Ma)
950	3.816	3.255	1.927	3.2412	4.73	34.7	84.7	160.0	31.81 \pm 0.12
1050	3.731	3.495	1.481	3.2875	2.76	20.3	88.1	149.0	32.26 \pm 0.10
1150	3.752	4.180	1.521	3.2964	1.50	11.0	87.9	124.0	32.24 \pm 0.08
1250	3.839	4.816	1.792	3.3038	1.20	8.8	86.1	108.0	32.42 \pm 0.07
1350	3.880	6.316	1.895	3.3146	1.34	9.8	85.4	82.3	32.52 \pm 0.09
1450	3.865	6.832	1.991	3.2717	2.08	15.3	84.6	76.1	32.10 \pm 0.07
Total Gas									32.13
Preferred Age									32.30 \pm 0.16

K-BM-3 Biotite

J = 0.005488

Sample Weight = 0.1048

$^{40}\text{Ar}/^{36}\text{Ar}$ atm. = 296.5

Temp C	$^{40}\text{Ar}/^{39}\text{Ar}$ ($\times 10^{-2}$)	$^{36}\text{Ar}/^{39}\text{Ar}$ ($\times 10^{-3}$)	$^{40}\text{Ar}/^{39}\text{Ar}$ Corrected (F)	^{39}Ar (mole) ($\times 10^{-13}$)	^{39}Ar (% of) (Total)	% Radiogenic ^{40}Ar	Apparent K/Ca (mol/mol)	Apparent Age ± 1 (Ma)
850	9.612	3.642	3.4767	0.566	4.4	36.2	14.3	33.84 \pm 0.14
950	4.680	1.966	3.5026	1.05	8.1	74.8	26.5	34.09 \pm 0.10
1050	4.263	1.360	3.3665	1.51	11.7	79.0	38.2	32.78 \pm 0.12
1100	3.977	1.218	3.3618	1.23	9.5	84.5	42.7	32.73 \pm 0.09
1150	3.987	1.184	3.3383	1.26	9.8	83.7	43.9	32.50 \pm 0.09
1200	4.022	1.260	3.3524	1.25	9.6	83.4	41.3	32.64 \pm 0.11
1250	4.043	1.206	3.3255	1.33	10.3	82.2	43.1	32.38 \pm 0.08
1500	3.842	1.041	3.2817	4.73	36.6	85.4	50.0	31.96 \pm 0.20
Total Gas								32.54
Preferred Age								32.24 \pm 0.30

SU-4-77 Biotite

J = 0.004457

Sample Weight = 0.1031 g

 $^{40}\text{Ar}/^{36}\text{Ar}$ atm. = 296.5

Temp C	$^{40}\text{Ar}/^{39}\text{Ar}$ ($\times 10^{-2}$)	$^{37}\text{Ar}/^{39}\text{Ar}$ ($\times 10^{-2}$)	$^{36}\text{Ar}/^{39}\text{Ar}$ ($\times 10^{-3}$)	$^{40}\text{Ar}/^{39}\text{Ar}$ Corrected (F)	^{39}Ar (mole) ($\times 10^{-13}$)	^{39}Ar (% of) (Total)	% Radiogenic ^{40}Ar	Apparent K/Ca (mol/mol)	Apparent Age ± 1 (Ma)
550	24.976	11.15	74.25	0.0367	0.3	0.3	12.2	4.66	24.26 \pm 0.92
650	23.166	8.860	61.85	0.0206	0.2	0.2	21.1	5.87	38.90 \pm 1.81
750	13.988	8.926	34.59	0.0195	0.2	0.2	26.9	5.83	30.04 \pm 0.70
850	10.138	5.816	18.98	0.0467	0.4	0.4	44.7	8.94	36.05 \pm 0.40
950	6.482	2.537	7.684	0.278	2.4	2.4	64.9	20.5	33.52 \pm 0.11
1050	5.085	1.543	3.391	1.07	9.3	9.3	80.2	33.7	32.50 \pm 0.16
1100	6.428	1.527	8.163	0.787	6.8	6.8	62.4	34.0	31.97 \pm 0.10
1150	6.905	1.819	9.971	1.24	10.8	10.8	57.3	28.6	31.52 \pm 0.27
1200	6.289	2.676	7.709	2.53	21.9	21.9	63.7	19.4	31.93 \pm 0.20
1250	5.650	4.028	5.427	4.17	36.2	36.2	71.6	12.9	32.22 \pm 0.13
1300	15.047	7.184	37.58	1.33	11.5	11.5	26.2	7.24	31.42 \pm 0.18
Total Gas									32.03
Preferred Age									32.11 \pm 0.19

SU-5-77 Biotite

J = 0.004416

Sample Weight = 0.1115 g

 $^{40}\text{Ar}/^{36}\text{Ar}$ atm. = 296.5

Temp C	$^{40}\text{Ar}/^{39}\text{Ar}$ ($\times 10^{-2}$)	$^{37}\text{Ar}/^{39}\text{Ar}$ ($\times 10^{-2}$)	$^{36}\text{Ar}/^{39}\text{Ar}$ ($\times 10^{-3}$)	$^{40}\text{Ar}/^{39}\text{Ar}$ Corrected (F)	^{39}Ar (mole) ($\times 10^{-13}$)	^{39}Ar (% of) (Total)	% Radiogenic ^{40}Ar	Apparent K/Ca (mol/mol)	Apparent Age ± 1 (Ma)
550	24.608	19.75	70.05	0.0909	0.9	0.9	15.9	2.63	30.94 \pm 0.34
650	47.099	16.43	147.8	0.0227	0.2	0.2	7.3	3.16	27.12 \pm 1.31
750	22.134	11.13	61.02	0.0648	0.6	0.6	18.5	4.67	32.41 \pm 0.54
850	16.072	8.051	40.02	0.0884	0.08	0.08	26.4	6.46	33.51 \pm 0.33
950	6.166	3.936	6.543	0.556	5.3	5.3	68.6	13.2	33.38 \pm 0.14
1050	5.675	2.269	5.407	1.48	14.1	14.1	71.8	22.9	32.16 \pm 0.10
1100	5.801	2.126	5.857	2.03	19.4	19.4	70.1	24.5	32.11 \pm 0.14
1150	8.489	3.261	14.99	2.47	23.6	23.6	47.8	15.9	32.03 \pm 0.25
1200	7.039	4.846	9.898	3.02	28.9	28.9	58.4	10.7	32.47 \pm 0.16
1250	19.040	10.05	50.05	0.641	6.1	6.1	22.3	5.17	33.57 \pm 0.21
Total Gas									32.35
Plateau Age									32.09 \pm 0.10

K-JH-4 Na-sanidine

J = 0.005488

Sample Weight = 0.1001 g

 $^{40}\text{Ar}/^{36}\text{Ar}$ atm. = 296.5

Temp C	$^{40}\text{Ar}/^{39}\text{Ar}$ ($\times 10^{-2}$)	$^{37}\text{Ar}/^{39}\text{Ar}$ ($\times 10^{-2}$)	$^{36}\text{Ar}/^{39}\text{Ar}$ ($\times 10^{-4}$)	$^{40}\text{Ar}/^{39}\text{Ar}$ Corrected (F)	^{39}Ar (mole) ($\times 10^{-13}$)	^{39}Ar (% of) (Total)	% Radiogenic ^{40}Ar	Apparent K/Ca (mol/mol)	Apparent Age ± 1 (Ma)
900	3.601	1.862	21.60	2.9579	1.93	16.7	82.2	27.9	29.05 \pm 0.08
1000	3.078	1.830	4.860	2.9302	2.22	19.2	95.2	28.4	28.78 \pm 0.06
1050	3.073	1.810	4.706	2.9296	1.87	16.1	95.3	28.7	28.77 \pm 0.07
1100	3.143	1.791	7.003	2.9320	1.63	14.1	93.3	29.0	28.80 \pm 0.07
1150	3.240	1.766	10.52	2.9249	1.40	12.1	90.3	29.4	28.73 \pm 0.09
1200	3.323	1.767	13.20	2.9287	1.10	9.5	88.1	29.4	28.76 \pm 0.07
1300	3.524	1.743	18.23	2.9804	0.817	7.1	84.6	29.8	29.27 \pm 0.09
1450	4.104	1.788	39.95	2.9187	0.613	5.3	71.1	29.1	28.67 \pm 0.08
Total Gas									28.85
Plateau Age									28.77 \pm 0.03

K-JH-5 Na-sanidine

J = 0.005488

Sample Weight = 0.0931 g

 $^{40}\text{Ar}/^{36}\text{Ar}$ atm. = 296.5

Temp C	$^{40}\text{Ar}/^{39}\text{Ar}$ ($\times 10^{-2}$)	$^{37}\text{Ar}/^{39}\text{Ar}$ ($\times 10^{-2}$)	$^{36}\text{Ar}/^{39}\text{Ar}$ ($\times 10^{-4}$)	$^{40}\text{Ar}/^{39}\text{Ar}$ Corrected (F)	^{39}Ar (mole) ($\times 10^{-13}$)	^{39}Ar (% of) (Total)	% Radiogenic ^{40}Ar	Apparent K/Ca (mol/mol)	Apparent Age ± 1 (Ma)
900	3.769	1.956	26.93	2.9690	1.17	11.2	78.8	26.6	29.16 \pm 0.07
1000	3.150	1.917	8.814	2.8853	1.34	12.8	91.6	27.1	28.34 \pm 0.06
1050	3.088	1.894	5.431	2.9234	1.99	19.0	94.7	27.5	28.71 \pm 0.08
1100	3.119	1.859	6.262	2.9298	1.65	15.8	93.9	28.0	28.78 \pm 0.07
1150	3.374	1.823	15.16	2.9213	1.40	13.4	86.6	28.5	28.69 \pm 0.07
1200	3.244	1.837	10.22	2.9374	1.22	11.6	90.6	28.3	28.85 \pm 0.08
1300	3.391	1.826	16.49	2.8993	0.957	9.1	85.5	28.5	28.48 \pm 0.06
1450	4.034	1.864	37.09	2.9335	0.727	6.9	72.7	27.9	28.81 \pm 0.09
Total Gas									28.72
Plateau Age									28.75 \pm 0.07

K-BM-1 Na-sanidine

J = 0.005488

Sample Weight = 0.1028 g

 $^{40}\text{Ar}/^{36}\text{Ar}$ atm. = 296.5

Temp C	$^{40}\text{Ar}/^{39}\text{Ar}$ ($\times 10^{-3}$)	$^{37}\text{Ar}/^{39}\text{Ar}$ ($\times 10^{-3}$)	$^{36}\text{Ar}/^{39}\text{Ar}$ ($\times 10^{-3}$)	$^{40}\text{Ar}/^{39}\text{Ar}$ Corrected (F)	^{39}Ar (mole) ($\times 10^{-13}$)	^{39}Ar (% of) (Total)	% Radiogenic ^{40}Ar	Apparent K/Ca (mol/mol)	Apparent Age ± 1 (Ma)
900	3.993	10.10	3.540	2.9421	1.89	18.3	73.7	51.5	28.90 \pm 0.09
1000	3.259	8.782	1.093	2.9309	1.49	14.4	89.9	59.2	28.79 \pm 0.06
1050	3.352	8.372	1.375	2.9405	1.30	12.5	87.7	62.1	28.88 \pm 0.07
1100	3.449	8.163	1.733	2.9312	0.857	8.3	85.0	63.7	28.79 \pm 0.08
1150	3.278	8.608	1.175	2.9257	1.00	9.7	89.2	60.4	28.74 \pm 0.08
1200	3.296	9.906	1.255	2.9197	1.02	9.8	88.6	52.5	28.68 \pm 0.07
1300	3.326	11.99	1.288	2.9403	1.12	10.8	88.4	43.4	28.88 \pm 0.06
1450	3.414	12.80	1.577	2.9434	1.69	16.3	86.2	40.6	28.91 \pm 0.07
Total Gas									28.83
Plateau Age									28.83 \pm 0.07

K-JH-10 Na-sanidine

J = 0.005488

Sample Weight = 0.0959 g

 $^{40}\text{Ar}/^{36}\text{Ar}$ atm. = 296.5

Temp C	$^{40}\text{Ar}/^{39}\text{Ar}$ ($\times 10^{-3}$)	$^{37}\text{Ar}/^{39}\text{Ar}$ ($\times 10^{-3}$)	$^{36}\text{Ar}/^{39}\text{Ar}$ ($\times 10^{-3}$)	$^{40}\text{Ar}/^{39}\text{Ar}$ Corrected (F)	^{39}Ar (mole) ($\times 10^{-13}$)	^{39}Ar (% of) (Total)	% Radiogenic ^{40}Ar	Apparent K/Ca (mol/mol)	Apparent Age ± 1 (Ma)
900	3.549	8.949	2.147	2.9090	2.16	20.2	82.0	58.1	28.57 \pm 0.07
1000	3.355	7.037	1.375	2.9431	1.31	12.3	87.7	73.9	28.91 \pm 0.06
1050	3.338	9.236	1.462	2.9010	0.930	8.7	86.9	56.3	28.49 \pm 0.06
1100	3.448	9.217	1.741	2.9280	0.562	5.3	84.9	56.4	28.76 \pm 0.10
1150	3.376	11.45	1.319	2.9809	0.655	6.1	88.3	45.4	29.27 \pm 0.07
1300	3.123	14.98	0.6648	2.9221	2.07	19.5	93.5	34.7	28.70 \pm 0.07
1450	3.159	16.00	0.7855	2.9221	2.97	27.9	92.5	32.5	28.70 \pm 0.06
Total Gas									28.72
Preferred Age									28.70 \pm 0.07

K-TS-1 Na-sanidine

J = 0.005488

Sample Weight = 0.1016 g

 $^{40}\text{Ar}/^{36}\text{Ar}$ atm. = 296.5

Temp C	$^{40}\text{Ar}/^{39}\text{Ar}$ ($\times 10^{-2}$)	$^{37}\text{Ar}/^{39}\text{Ar}$ ($\times 10^{-2}$)	$^{36}\text{Ar}/^{39}\text{Ar}$ ($\times 10^{-3}$)	$^{40}\text{Ar}/^{39}\text{Ar}$ Corrected (F)	^{39}Ar (mole) ($\times 10^{-13}$)	^{39}Ar (% of) (Total)	% Radiogenic ^{40}Ar	Apparent K/Ca (mol/mol)	Apparent Age ± 1 (Ma)
900	3.896	2.283	3.582	2.8334	1.58	11.4	72.7	22.8	27.84 \pm 0.08
1000	3.178	2.168	1.133	2.8390	2.39	17.2	89.3	24.0	27.89 \pm 0.09
1050	3.190	2.125	1.137	2.8493	1.96	14.2	89.3	24.5	27.99 \pm 0.07
1100	3.138	2.100	1.025	2.8312	1.90	13.7	90.2	24.8	27.81 \pm 0.06
1150	3.190	2.068	1.111	2.8572	1.82	13.1	89.6	25.1	28.07 \pm 0.08
1200	3.295	2.079	1.473	2.8557	1.53	11.0	86.7	25.0	28.05 \pm 0.10
1300	3.519	2.055	2.296	2.8358	1.20	8.7	80.6	25.3	27.86 \pm 0.06
1450	3.688	2.088	2.830	2.8470	1.48	10.7	77.2	24.9	27.97 \pm 0.06
Total Gas									27.93
Plateau Age									27.89 \pm 0.08

K-JH-24 Biotite

J = 0.005488

Sample Weight = 0.1013 g

 $^{40}\text{Ar}/^{36}\text{Ar}$ atm. = 296.5

Temp C	$^{40}\text{Ar}/^{39}\text{Ar}$	$^{37}\text{Ar}/^{39}\text{Ar}$ ($\times 10^{-3}$)	$^{36}\text{Ar}/^{39}\text{Ar}$ ($\times 10^{-3}$)	$^{40}\text{Ar}/^{39}\text{Ar}$ Corrected (F)	^{39}Ar (mole) ($\times 10^{-13}$)	^{39}Ar (% of) (Total)	% Radiogenic ^{40}Ar	Apparent K/Ca (mol/mol)	Apparent Age ± 1 (Ma)
950	3.358	3.174	1.570	2.8890	4.09	31.5	86.0	164.0	28.38 \pm 0.08
1050	3.322	2.778	1.453	2.8870	3.19	24.5	86.9	187.0	28.36 \pm 0.08
1150	3.606	12.27	2.404	2.8904	2.19	16.9	80.2	42.4	28.39 \pm 0.08
1200	3.719	16.80	2.730	2.9074	1.56	12.0	78.2	30.9	28.56 \pm 0.10
1250	3.770	11.71	2.914	2.9042	1.23	9.4	77.0	44.4	28.53 \pm 0.07
1450	4.195	30.09	4.247	2.9358	0.739	5.7	70.0	17.3	28.83 \pm 0.08
							Total Gas		28.44
							Plateau Age		28.37 \pm 0.02

K-TS-1 Biotite

J = 0.005406

Sample Weight = 0.0914 g

 $^{40}\text{Ar}/^{36}\text{Ar}$ atm. = 296.5

Temp C	$^{40}\text{Ar}/^{39}\text{Ar}$ ($\times 10^{-2}$)	$^{37}\text{Ar}/^{39}\text{Ar}$ ($\times 10^{-2}$)	$^{36}\text{Ar}/^{39}\text{Ar}$ ($\times 10^{-3}$)	$^{40}\text{Ar}/^{39}\text{Ar}$ Corrected (F)	^{39}Ar (mole) ($\times 10^{-13}$)	^{39}Ar (% of) (Total)	% Radiogenic ^{40}Ar	Apparent K/Ca (mol/mol)	Apparent Age ± 1 (Ma)
950	6.382	1.726	11.55	2.9647	1.08	9.4	46.5	30.1	28.68 \pm 0.04
1050	4.499	1.522	5.347	2.9143	1.32	11.5	64.8	34.2	28.20 \pm 0.04
1150	4.062	1.403	3.829	2.9255	1.43	12.5	72.0	37.1	28.31 \pm 0.03
1200	3.960	1.257	3.217	3.0041	1.49	13.0	75.9	41.4	29.06 \pm 0.04
1250	3.982	1.117	3.350	2.9868	1.44	12.5	75.0	46.5	28.90 \pm 0.03
1350	3.895	1.031	3.160	2.9562	2.54	22.1	75.9	50.4	28.60 \pm 0.09
1450	4.058	0.5654	3.683	2.9647	2.18	19.0	73.0	92.0	28.68 \pm 0.05
Total Gas									28.64
Preferred Age									28.77 \pm 0.21

K-JH-22 Na-sanidine

J = 0.005488

Sample Weight = 0.0956 g

 $^{40}\text{Ar}/^{36}\text{Ar}_{\text{atm.}} = 296.5$

Temp C	$^{40}\text{Ar}/^{39}\text{Ar}$ ($\times 10^{-2}$)	$^{37}\text{Ar}/^{39}\text{Ar}$ ($\times 10^{-2}$)	$^{36}\text{Ar}/^{39}\text{Ar}$ ($\times 10^{-3}$)	$^{40}\text{Ar}/^{39}\text{Ar}$ Corrected (F)	^{39}Ar (mole) ($\times 10^{-13}$)	^{39}Ar (% of) (Total)	% Radiogenic ^{40}Ar	Apparent K/Ca (mol/mol)	Apparent Age ± 1 (Ma)
900	3.428	2.027	2.107	2.8009	2.77	20.8	81.7	25.7	27.52 \pm 0.10
1000	3.173	1.905	1.201	2.8136	1.91	14.3	88.7	27.3	27.64 \pm 0.06
1050	2.990	1.802	0.6715	2.7869	1.89	14.2	93.2	28.9	27.38 \pm 0.06
1100	3.223	1.757	1.329	2.8254	1.75	13.1	87.7	29.6	27.76 \pm 0.06
1150	3.152	1.709	1.084	2.8273	1.36	10.2	89.7	30.4	27.78 \pm 0.06
1200	3.228	1.718	1.381	2.8150	1.27	9.5	87.2	30.3	27.66 \pm 0.06
1300	3.355	1.726	1.742	2.7853	1.29	9.7	77.3	29.5	27.37 \pm 0.08
Total Gas									27.60
Preferred Age									27.76 \pm 0.08

REFERENCES CITED

- Alexander, E.C., Mickelson, G.M., and Lanphere, M.A.,
1978, MMHb-1: a new $^{40}\text{Ar}/^{39}\text{Ar}$ dating standard: U. S. Geological
Survey Open-File Report 78-701, p. 6-8.
- Bachman, G.O., and Mehnert, H.H., 1978, New K-Ar dates
and the late Pliocene to Holocene geomorphic history of the central
Rio Grande region, New Mexico: Geological Society of America
Bulletin, v. 89, p. 283-292.
- Bobrow, D.J., 1984, Geochemistry and petrology of
Miocene silicic lavas in the Socorro-Magdalena area of New Mexico
[M.S. Thesis]: Socorro, New Mexico Institute of Mining and
Technology, 145 p.
- Bornhorst, T.J., Jones, D.P., Elston, W.E., and others,
1982, New radiometric ages on volcanic rocks from the
Mogollon-Datil volcanic field, southwestern New Mexico:
Isochron/West, v. 35, p. 13-14.
- Bottomley, R.J., and York, D., 1976, ^{40}Ar - ^{39}Ar age
determinations on the Owyhee Basalt of the Columbia Plateau: Earth
and Planetary Science Letters, v. 31, p. 75-84.

- Brereton, N.R., 1970, Corrections for interfering isotopes in the $^{40}\text{Ar}/^{39}\text{Ar}$ dating method: Earth and Planetary Science Letters, v. 8, p. 427-433.
- Brouillard, L., 1984, Geology of the northeastern Gallinas Mountains [M.S. Thesis]: Socorro, New Mexico Institute of Mining and Technology, 161 p.
- Brown, D.M., 1972, Geology of the southern Bear Mountains, Socorro County, New Mexico [M.S. Thesis]: Socorro, New Mexico Institute of Mining and Technology, 110 p.
- Burke, W.H., Kenny, G.S., Otto, J.B., and others, 1963, Potassium-argon dates, Socorro and Sierra counties, New Mexico: New Mexico Geological Society 14th Annual Field Conference, Guidebook, p. 224.
- Chamberlin, R.M., 1978, Structural development of the Lemitar Mountains, an intrarift tilted fault-block uplift, central New Mexico: 1978 International Symposium on the Rio Grande Rift: Program and Abstracts, p. 22-24.
- , 1980, Cenozoic stratigraphy and structure of the Socorro Peak volcanic center, central New Mexico [Ph.D. Thesis]: Golden, Colorado School of Mines, 495 p.

- , 1983, Cenozoic domino-style crustal extension
in the Lemitar Mountains, New Mexico: a summary: New Mexico
Geological Society 34th Annual Field Conference, Guidebook,
p. 111-118.
- Chapin, C.E., 1979, Foreword, in Rio Grande rift:
tectonics and magmatism: American Geophysical Union, Washington,
D.C. , p. v-vii.
- Chapin, C.E., and Seager, W.R., 1975, Evolution of the
Rio Grande Rift in the Socorro and Las Cruces areas: New Mexico
Geological Society 26th Annual Field Conference, Guidebook,
p. 297-321.
- Chapin, C.E., Siemers, W.T., and Osburn, G.R., 1975,
Summary of radiometric ages of New Mexico rocks: New Mexico Bureau
of Mines and Mineral Resources Open-File Report 60.
- Clauer, N., 1981, Strontium and argon isotopes in naturally
weathered biotites, muscovites, and feldspars: Chemical Geology,
v. 31, p. 325-334.
- Coffin, G.C., 1981, Geology of the northwestern Gallinas
Mountains, Socorro County, New Mexico: New Mexico Bureau of Mines
and Mineral Resources Open-File Report 159, 214 p.

- Dallmeyer, R.D., and Van Breeman, O., 1981, Rb-Sr whole-rock and $^{40}\text{Ar}/^{39}\text{Ar}$ mineral ages of the Togus and Hallowell quartz monzonite and Three Mile Pond granodiorite plutons, south-central Maine - Their bearing on post-Acadian cooling history: Contributions to Mineralogy and Petrology, v. 78, p. 61-73.
- Dalrymple, G.B., 1979, Critical tables for conversion of K-Ar ages from old to new constants: Geology, v. 7, p. 558-560.
- Dalrymple, G.B., Alexander, E.C., Jr., Lanphere, M.A., and others, 1981, Irradiation of samples for $^{40}\text{Ar}/^{39}\text{Ar}$ dating using the Geological Survey TRIGA reactor: U. S. Geological Survey Professional Paper 1176, 55 p.
- Dalrymple, G.B., and Lanphere, M.A., 1969, Potassium-argon Dating: Principles, techniques, and application to geochronology: San Francisco, W.H. Freeman and Company, 258 p.
- , 1971, $^{40}\text{Ar}/^{39}\text{Ar}$ technique of K-Ar dating: A comparison with the conventional technique: Earth and Planetary Science Letters, v. 12, p. 300-308.
- , 1974, $^{40}\text{Ar}/^{39}\text{Ar}$ age spectra of some undisturbed terrestrial samples: Geochimica et Cosmochimica Acta, v. 38, p. 715-738.

- Deal, E.G., 1973, Geology of the northern part of the San Mateo Mountains Socorro County, New Mexico: A study of a rhyolite ash-flow tuff cauldron and the role of laminar flow in ash-flow tuffs [Ph.D. Thesis]: Albuquerque, University of New Mexico, 136 p.
- Deal, E.G., and Rhodes, R.C., 1976, Volcano-tectonic structures in the San Mateo Mountains, Socorro County, New Mexico : Cenozoic volcanism in southwestern New Mexico, New Mexico Geological Society Special Publication 5, p. 51-56.
- Eggleston, T.L., 1982, Geology of the central Chupadera Mountains, Socorro County, New Mexico [M.S. Thesis]: Socorro, New Mexico Institute of Mining and Mineral Resources, 162 p.
- Faure, G., 1977, Principles of isotope geology: New York, John Wiley and Sons, 464 p.
- Fisher, A.V., and Schmincke, H.U., 1984, Pyroclastic Rocks: New York, Springer-Verlag, 472 p.
- Fleck, R.J., Sutter, J.F., and Elliot, D.H., 1977, Interpretation of discordant $^{40}\text{Ar}/^{39}\text{Ar}$ age-spectra of Mesozoic tholeiites from Antarctica: Geochimica et Cosmochimica Acta, v. 41, p. 15-32.

- Foland, K.A., 1974, ^{40}Ar diffusion in homogeneous orthoclase and an interpretation of Ar diffusion in K-feldspars: *Geochimica et Cosmochimica Acta*, v. 38 p. 151-166.
- , 1983, $^{40}\text{Ar}/^{39}\text{Ar}$ Incremental heating plateaus for biotites with excess argon: *Isotope Geoscience*, v. 1, p. 3-21.
- Harrison, T.M., 1983, Some observations on the interpretation of $^{40}\text{Ar}/^{39}\text{Ar}$ age spectra: *Isotope Geoscience*, v. 1, p. 319-338.
- Harrison, T.M., and McDougall, I., 1982, The thermal significance of potassium feldspar K-Ar ages inferred from $^{40}\text{Ar}/^{39}\text{Ar}$ age spectrum results: *Geochimica et Cosmochimica Acta*, v. 46, p. 1811-1820.
- Huneke, J.C., and Smith, 1976, The realities of recoil: ^{39}Ar recoil out of small grains and anomalous age patterns in $^{39}\text{Ar}/^{40}\text{Ar}$ dating: *Proceedings of the 7th Lunar Science Conference*, p. 1987.
- Hurlbut, C.S., and Klein, C., 1977, *Manual of Mineralogy*, (nineteenth edition): New York, John Wiley and Sons, p. 509-510.
- Izett, G.A., 1981, Volcanic ash beds: *Recorders of upper*

Cenozoic silicic pyroclastic volcanism in the western United States: *Journal of Geophysical Research*, v. 86, no. B11, p. 10200-10222.

Kyle, P.R., and Seward, D., 1984, Dispersed rhyolitic tephra from New Zealand in deep-sea sediments of the Southern Ocean: *Geology*, v. 12, p. 487-490.

Lanphere, M.A., and Dalrymple, G.B., 1976, Identification of excess ^{40}Ar by the $^{40}\text{Ar}/^{39}\text{Ar}$ age spectrum technique: *Earth and Planetary Science Letters*, v. 32, p. 141-148.

Laroche, T.M., 1981, *Geology of the Gallinas Peak area, Socorro County, New Mexico*: New Mexico Bureau of Mines and Mineral Resources Open-File Report 128, 154 p.

Ledbetter, M.T., 1981, Tephrochronology at DSDP site 502 in the western Caribbean, in Self, S., and others, eds., *Tephra Studies*: Boston, D. Reidel Publishing Company, p. 281-288.

Lopez, D.A., and Bornhorst, T.J., 1979, *Geologic map of the Datil area, Catron County, New Mexico*: U. S. Geological Survey Miscellaneous Geologic Investigation Map I-1098, scale 1:50,000.

Massingill, G.L., 1979, *Geology of the Riley-Puertecito*

area, southeastern margin of Colorado Plateau, Socorro County, New Mexico: New Mexico Bureau of Mines and Mineral Resources Open-File Report 107, 316 p.

Mayerson, D.L., 1979, Geology of the Corkscrew Canyon-
Abbe Spring area, Socorro County, New Mexico: New Mexico Bureau of
Mines and Mineral Resources Open-File Report 112, 133 p.

McDougall, I., 1981, $^{40}\text{Ar}/^{39}\text{Ar}$ age spectra from the KBS
Tuff Koobi Fora Formation: Nature, v. 294, p. 120-124.

McDowell, F.W., 1983, K-Ar dating: Incomplete extraction of
radiogenic argon from alkali feldspar: Isotope Geoscience, v. 1,
p. 119-126.

Merrihue, C., 1965, Trace element determinations and
potassium-argon dating by mass spectroscopy of neutron- irradiated
samples [abs]: Transactions of the American Geophysical Union,
v. 46, p. 125.

Merrihue, C., and Turner, G., 1966, Potassium-argon dating
by activation with fast neutrons: Journal of Geophysical Research,
v. 71, p. 2852-2957.

Mitchell, J.G., 1968, The $^{40}\text{Ar}/^{39}\text{Ar}$ method for

potassium-argon age determination: *Geochimica et Cosmochimica Acta*, v. 32, p. 781-790.

Muller, G., 1967, *Methods in Sedimentary Petrology*: New York, Hafner Publishing Company, p. 128.

Muller, L.D., 1977, Mineral separation, in Zussman, J., ed., *Physical Methods in Determinative Mineralogy*: London, Academic Press, 720 p.

Norrish, K., and Hutton, J.T., 1969, An accurate X-ray spectrographic method for the analysis of a wide range of geologic samples: *Geochimica et Cosmochimica Acta*, v. 33, p. 431-453.

Osburn, G.R., and Chapin, C.E., 1983a, Nomenclature for Cenozoic rocks of northeast Mogollon-Datil volcanic field, New Mexico: Stratigraphic Chart 1, New Mexico Bureau Mine Mineral Resources, Socorro, New Mexico.

-----, 1983b, Ash-flow tuffs and cauldrons in the northeast Mogollon-Datil volcanic field: A summary : New Mexico Geological Society 34th Annual Field Conference, Guidebook, p. 197-204.

Osburn, G.R., Petty, D.M., and Chapin, C.E., 1981, *Geology of the Molino Peak quadrangle*: New Mexico Bureau of Mines and

Mineral Resources Open-File Report 139a, scale 1:24,000.

Ozima, M., and Saito, K., 1973, ^{40}Ar - ^{39}Ar stepwise degassing experiments on some submarine rocks: Earth and Planetary Science Letters, v. 20, p. 77-87.

Porter, S.C., 1981, Use of tephrochronology in the Quaternary geology of the United States, in Self, S., and others, eds., Tephra Studies: Boston, D. Reidel Publishing Company, p. 135-160.

Roddick, J.C., 1983, High precision intercalibration of $^{40}\text{Ar}/^{39}\text{Ar}$ standards: Geochimica et Cosmochimica Acta, v. 47, p. 887-898.

Roddick, J.C., Cliff, R.A., and Rex, D.C., 1980, The evolution of excess argon in alpine biotites - An $^{40}\text{Ar}/^{39}\text{Ar}$ analysis: Earth and Planetary Science Letters, v. 48, p. 185-208.

Ross, C.S., and Smith, R.L., 1961, Ash-flow tuffs: Their origin geologic relations and identification : U. S. Geological Survey Professional Paper 366, 81 p.

Sax, N.I., 1979, Dangerous Properties of Industrial Materials, (fifth edition): New York, Van Nostrand Reinhold Company, 1118 p.

- Sigureirsson, T., 1962, Dating recent basalt by the potassium-argon method: Report of the Physical Laboratory of the University of Iceland, 9 p.
- Sigurdsson, H., and Loebner, B., 1981, Deep-sea record of Cenozoic explosive volcanism in the north Atlantic, in Self, S., and others, eds., Tephra Studies: Boston, D.Reidel Publishing Company, p. 289-316.
- Smith, C.T., Osburn, G.R., Chapin, C.E., and others, 1983, First day road log from Socorro to Mesa del Yeso, Joyita Hills, Johnson Hill, Cerros de Amado, Lomas de Las Canas, Jornada del Muerto, Carthage, and return to Socorro: New Mexico Geological Society 34th Annual Field Conference, Guidebook, p. 1-28.
- Smith, J.V., 1974, Feldspar Minerals: 1: Crystal structures and physical properties: New York, Springer-Verlag, p. 447.
- Smith, R.L., 1960, Zones and zonal variations in welded ash flows: U. S. Geological Survey Professional Paper 354-F, 16 p.
- Smith, R.L., and Bailey, R.A., 1968, Resurgent cauldrons: Geological Society of America Memoir 116, p. 613-662.
- Spradlin, E.J., 1976, Stratigraphy of Tertiary volcanic

(196)

rocks, Joyita Hills area, Socorro County, New Mexico [M.S. Thesis]:
Albuquerque, University of New Mexico, 73 p.

Steiger, R.H., and Jager, E., 1977, Subcommission on
geochronology: Convention on the use of decay constants in geo-
and cosmochronology: Earth and Planetary Science Letters, v. 36,
p. 359-362.

Tonking, W.H., 1957, Geology of the Puertecito quadrangle,
Socorro County, New Mexico: New Mexico Bureau of Mines and Mineral
Resources, Bulletin 41, 67 p.

Turner, G., 1968, The distribution of potassium and argon in
chondrites, in L.H. Ahrens, ed., Origin and distribution of the
elements: London, Pergamon Press, p. 387-398.

-----, 1969, Thermal histories of meteorites by
the $^{40}\text{Ar}/^{39}\text{Ar}$ method, in Millman, P.M., ed., Meteorite Research:
Boston, Reidel Publishing Company, p. 407-417.

-----, 1971, $^{40}\text{Ar}/^{39}\text{Ar}$ dating: The optimization of
irradiation parameters: Earth and Planetary Science Letters,
v. 10, p. 227-234.

Villa, I.M., Huneke, J.C., and Wasserburg, G.J., 1983, ^{39}Ar

Recoil losses and presolar ages in Allende inclusions: Earth and Planetary Science Letters, v. 63, p. 1-12.

Wanke, H., and König, H., 1956, Eine neue Methode zur Kalium-Argon-Alterbestimmung und ihre Anwendung auf Steinmeteorite: Z. Naturforsch., 14a, p. 860-866.

Weber, R.H., 1971, K-Ar ages of Tertiary igneous rocks in central and western New Mexico: Isochron/West, v. 1, p. 33-45.

Weber, R.H., and Bassett, W.A., 1963, K-Ar ages of tertiary volcanic and intrusive rocks in Socorro, Catron, and Grant counties, New Mexico: New Mexico Geological Society 14th Annual Field Conference, Guidebook, p. 220-223.

Wilkinson, W.H., Jr., 1976, Geology of the Tres Montosas-Cat Mountain area, Socorro County, New Mexico: New Mexico Bureau of Mines and Mineral Resources Open-File Report 39, 169 p.

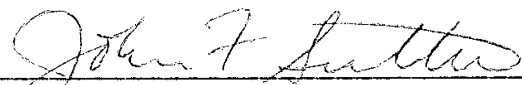
Williams, H., and McBirney, A.R., 1979, Volcanology, San Francisco, Freeman, Cooper, and Company, 397p.

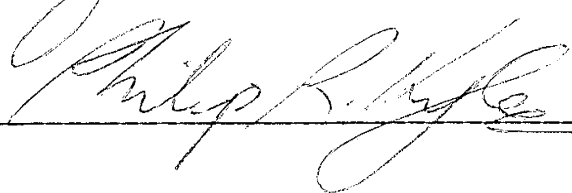
York, D., 1969, Least squares fitting of a straight line with correlated errors: Earth and Planetary Science Letters, v. 5, p. 320-324.

This thesis is accepted on behalf of the faculty
of the Institute by the following committee:



Adviser







Date